Electronic Supplementary Material (ESI) for Organic Chemistry Frontiers.


Supplementary Information

# Diverse binding of cationic guests by highly substituted [3+3] Schiff-base macrocycles

Mohammad T. Chaudhry,[+a] Miguel A. Soto,[+a] Francesco Lelj,*[b] and Mark J. MacLachlan*[a,c,d]

[a]Department of Chemistry, University of British Columbia, 2036 Main Mall, Vancouver, British Columbia, Canada V6T 1Z1.

[b]La.M.I. and LaSSCAM INSTM Sezione Basilicata, Dipartimento di Chimica Università della Basilicata Via dell'Ateneo Lucano 10, 85100 Potenza, Italy.

[c]Stewart Blusson Quantum Matter Institute, University of British Columbia, 2355 East Mall, Vancouver, British Columbia, Canada V6T 1Z4.

[d]WPI Nano Life Science Institute, Kanazawa University, Kanazawa, Japan 920-1192.

[+]These authors contributed equally to this work

# *Contents*

## *Materials and Equipment*

All solvents and reagents were used as received, unless otherwise stated. **DBA**·$PF_6$,[1] **DXA**·$PF_6$,[2] **7**,[3] **8**,[3] **9**,[1] **10**,[4] were all prepared following previously published methodologies.

Chloroform-$d_1$ (C*D*$Cl_3$) and 1,1,2,2-tetrachloroethane-$d_2$ (1,1,2,2-TCE-$d_2$) were purchased from Cambridge Isotope Laboratories; acetonitrile-$d_3$ (MeCN-$d_3$), dichloromethane-$d_2$ (DCM-$d_2$), dimethyl sulfoxide-$d_6$ (DMSO-$d_6$), tetrahydrofuran-$d_8$ (THF-$d_8$) were purchased from Sigma-Aldrich. Matrix compound *trans*-2-[3-(4-*tert*-butylphenyl)-2-methyl-2-propenylidene]malononitrile (dctb), was purchased from Sigma-Aldrich. All reactions were conducted under air unless explicitly stated. Dry tetrahydrofuran (THF) was obtained from an Inert PureSolv MD5 Solvent Purification System.

Nuclear magnetic resonance (NMR) spectra were recorded on Bruker AV-300 or AV-400 MHz spectrometers and chemical shifts ($\delta$) were referenced to residual proton signal of the employed deuterated solvent. Mass spectra (MS) were obtained using electrospray ionization (ESI) on a Bruker Esquire-LC ion trap mass spectrometer equipped with an electrospray ion source. High-resolution mass spectra were obtained using an ESI-TOF Waters Micromass LCT spectrometer. Ultraviolet-visible (UV-vis) spectra were obtained on a Varian Cary 5000 UV-vis-near-IR spectrophotometer using a 1 cm pathlength quartz cuvette.

## *Synthesis of compounds*

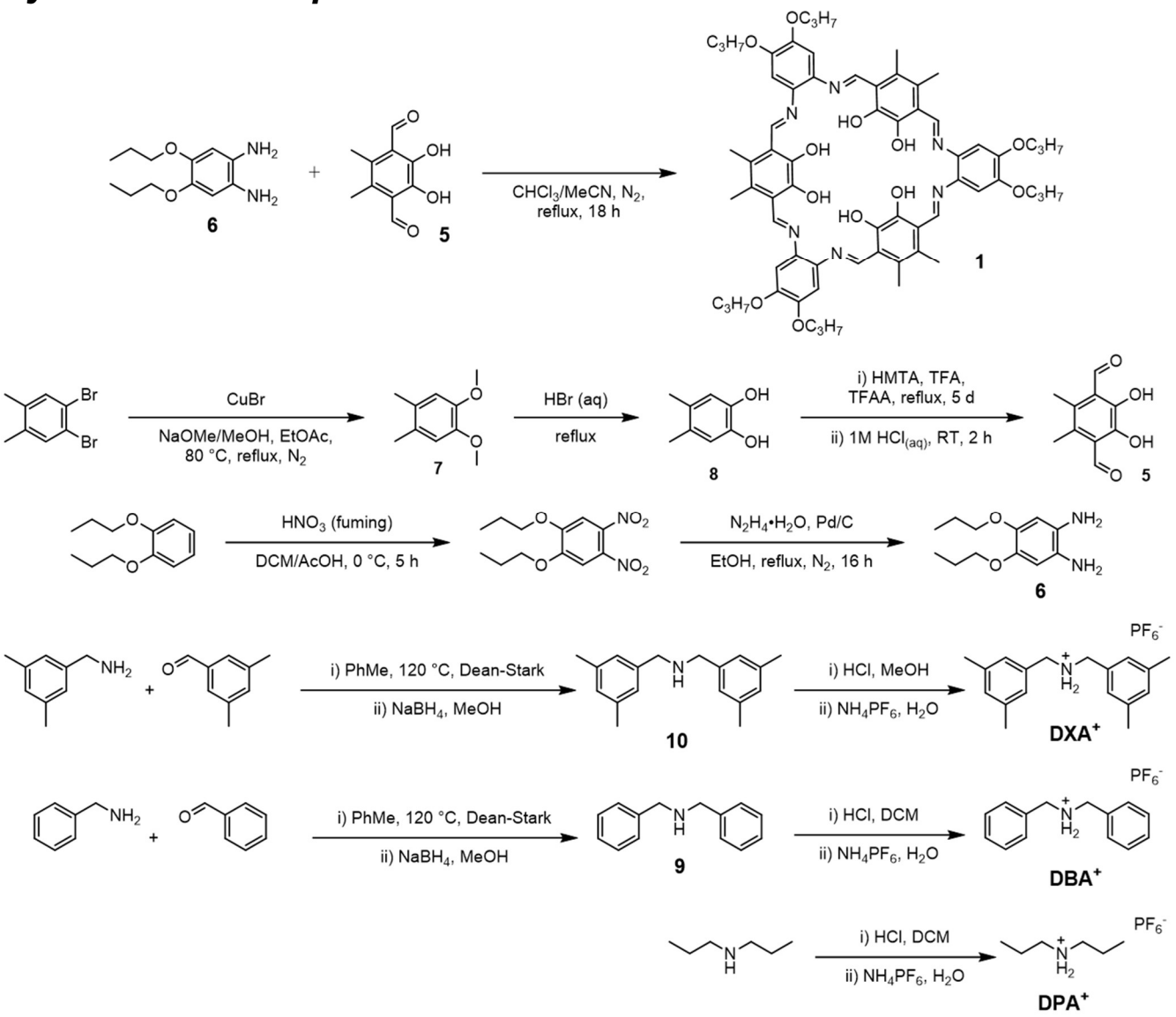


**Scheme S1.** Preparation of host **1** and guests **DBA**$^+$, **DXA**$^+$, and **DPA**$^+$.

**Improved method for the synthesis of 5**

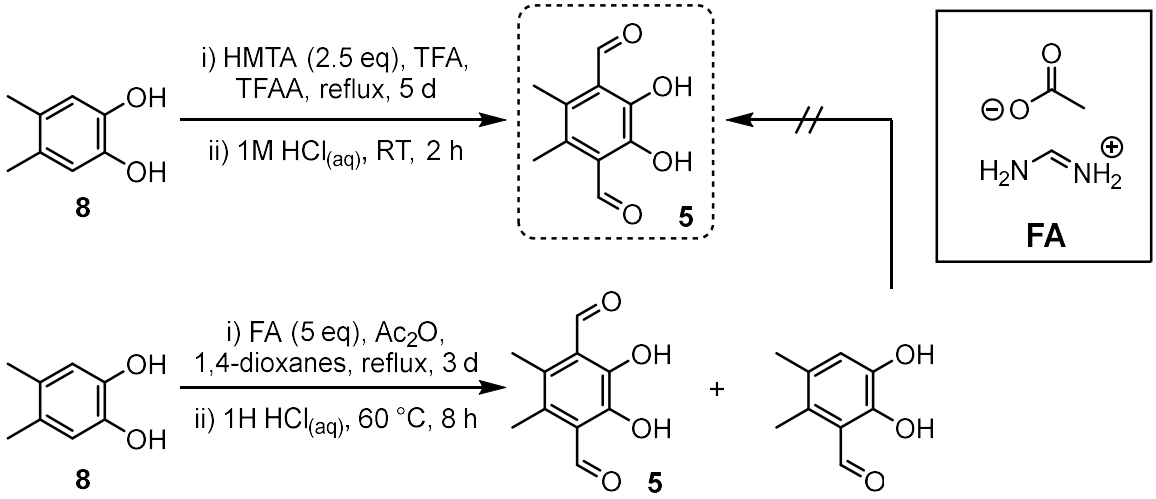


**Scheme S2.** Synthesis of **5** using the modified approach (top), and previously published methodology (bottom).

We first attempted the synthesis of **5** using a previously published methodology utilizing formamidine acetate (FA) as the formylating agent, but found that it yielded a significant amount of mono-substituted product.[3,5] The 2,3-dihydroxy-5,6-dimethylbenzaldehyde product, obtained in high yields with this method, could not be further reacted to give **5**, and was difficult to separate.

The Duff formylation using hexamethylenetetramine (HMTA), trifluoroacetic acid (TFA), and trifluoroacetic anhydride (TFAA, dehydrating agent) worked well, yielding the target molecule **5** in 26% yield.

**Synthesis of 5**

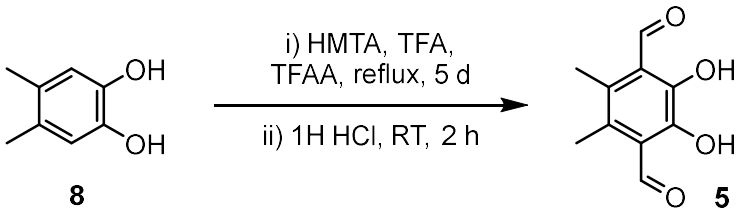


Compound **8** (500 mg, 2.57 mmol, 1 eq) and hexamethylenetetramine (1.10 g, 7.85 mmol, 3 eq) were added to a Schlenk flask equipped with a condenser. The solids were backfilled with $N_2$ (× 3), followed by the addition of trifluoroacetic acid (11.5 mL) and trifluoroacetic anhydride (800 µL, 5.75 mmol, 2.2 eq) *via* syringe. The mixture turned red-brown and was heated to 85 °C for 5 d. The resulting brown-black solution was cooled to room-temperature and $HCl_{(aq)}$ (1 M, 30 mL) was added. The solution was stirred under air for 2 h. Product was extracted with DCM (5 x 30 mL), dried with $MgSO_4$, filtered, and solvent removed *in vacuo*. The resulting brown solid was recrystallized from EtOH/$H_2O$ (1:1, v/v, 30 mL), yielding compound **5** as an orange solid (124 mg, 0.67 mmol, 26%).

Spectral data matched previously published reports. **$^1$H NMR** (400 MHz, DCM-$d_2$, 25 °C) δ (ppm): 11.85 (s, 2H), 10.46 (s, 2H), 2.48 (s, 6H).[3,5]

**Synthesis of 6**

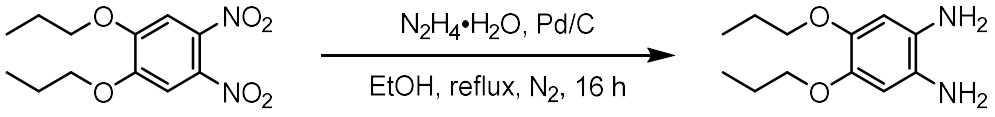


**6**

1,2-Dinitro-4,5-dipropyloxybenzene (1.00 g, 3.52 mmol, 1 eq) and ethanol (25 mL) were added to a Schlenk flask equipped with a reflux condenser. The mixture was then sparged with $N_2$ for *ca*. 1 h, followed by the addition of Pd/C (10 wt%, 200 mg), and then, previously degassed hydrazine monohydrate (2 mL, 41.3 mmol mmol) was added dropwise. The mixture was then heated to reflux overnight. After the suspension cooled to room temperature, Raney Nickel (100 mg) was added. The mixture was stirred for 1 h, then passed through a plug of Celite. Solvent was removed *in vacuo*, and the product was washed with cold diethyl ether (15 mL) to yield **6** as a white-yellow solid (663 mg, 2.96 mmol, 84%). The product was used right away, to prevent decomposition. Spectral data matched previously published reports. **$^1$H NMR** (400 MHz, DMSO-$d_6$, 25 °C) δ (ppm): 6.23 (s, 2H), 4.08 (s, 4H), 3.71 (t, $^3J$ = 6.5 Hz, 4H), 1.61 (m, 4H), 0.94 (t, $^3J$ = 7.4 Hz, 6H).[5]

*Note. Dialkoxy diaminobenzenes are highly oxygen sensitive and should be stored under $N_2$ or Ar in a freezer. Under these conditions the compounds are often stable for weeks. In solution, however, appearance of a green colour is indicative of decomposition.*

**Synthesis of 7**

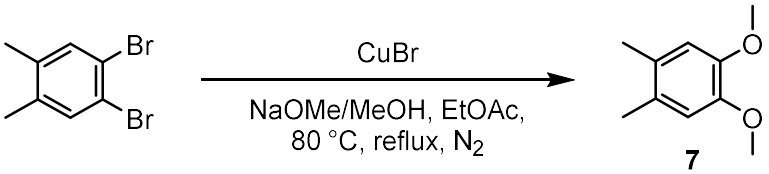


**7**

1,2-Dibromo-4,5-dimethylbenzene (10.0 g, 37.9 mmol, 1 eq), NaOMe/MeOH (25 wt%, 300 mL), and ethyl acetate (3 mL) were added to a two-neck round-bottom flask. The mixture was sparged with $N_2$ for *ca.* 30 mins, followed by the addition of CuBr (250 mg, 1.74 mmol, 4.6 mol%) under a strong flow of $N_2$. The deep-blue solution was then heated at 80 °C overnight. The solution was cooled to room temperature, poured into $H_2O$ (300 mL), and extracted with diethyl ether (3 x 100 mL). The combined organic layers were dried with $Na_2SO_4$ and then solvent was removed *in vacuo*, yielding a white solid. Recrystallization from ethanol and water (1:1, v/v) yielded **7** as a white crystalline solid (5.2 g, 31.4 mmol, 83%). Spectral data matched previously published reports. **$^1$H NMR** (400 MHz, C*D*Cl$_3$, 25 °C) δ (ppm): 6.67 (s, 2H), 3.85 (s, 6H), 2.21 (s, 6H).[3]

**Synthesis of 8**

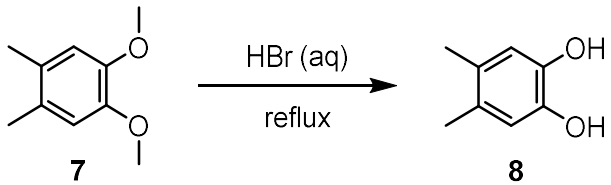


**7** **8**

HBr (48 wt% in $H_2O$, 10 mL) and **7** (1.04 g, 6.26 mmol, 1 eq) were added to a round-bottom flask. The mixture was then heated to reflux for 19 h, and monitored by TLC (1:1, v/v, DCM/EtOAc). The black-red solution was cooled to room temperature and poured into cold $H_2O$ (50 mL). The suspension was extracted with diethyl ether (3 x 50 mL), dried with $MgSO_4$, filtered, and the solvent was removed *in vacuo*, yielding a brown-black solid. Recrystallization from DCM yielded **8** as a tan-coloured solid (760 mg, 5.51 mmol, 88%). Spectral data matched previously published reports. **$^1$H NMR** (400 MHz, C*D*$Cl_3$, 25 °C) δ (ppm): 6.66 (s, 2H), 4.83 (s, 2H), 2.14 (6H).[3]

**Synthesis of 9 and DBA**[$PF_6$]

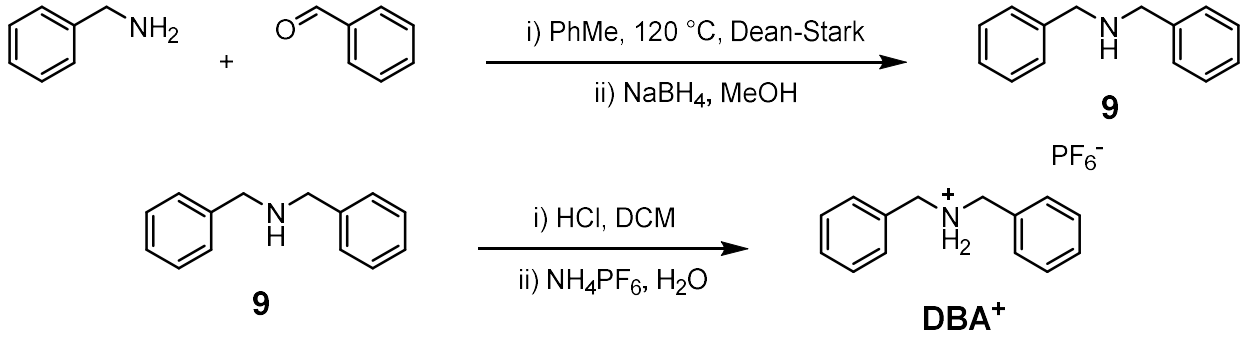


Benzaldehyde (1.00 g, 9.42 mmol, 1 eq), benzylamine (1.01 g, 9.42 mmol, 1 eq) and toluene (120 mL) were added to a round-bottom flask equipped with a Dean-Stark trap. The mixture was heated to 120 °C for *ca*.16 h. After the mixture cooled to room temperature, solvent was removed *in vacuo*. The crude product was redissolved in MeOH (60 mL), and $NaBH_4$ (2.10 g, 56.6 mmol, 1.05 eq) was added slowly. The mixture was stirred at room temperature overnight and quenched with HCl (2 M, 10 mL), followed by removal of solvent *in vacuo*. The crude product was suspended in NaOH (8 M, 30 mL) and extracted with $CHCl_3$ (3 x 60 mL). Combined organic fractions were dried with $MgSO_4$, filtered, and the solvent was removed *in vacuo*, yielding compound **9**. This crude product was used in the following reaction.

HCl (12 M, 10 mL) was added dropwise to a solution of compound **9** in DCM (25 mL) with vigorous stirring. The solvent and remaining HCl was then removed *in vacuo*, yielding a white solid. The crude product was redissolved in $H_2O$ (200 mL) and MeOH (130 mL), then a saturated solution of $NH_4PF_6$ (4.55 M, 5 mL) was added. The resulting white crystalline precipitate was filtered, washed with a small portion of $H_2O$, and dried *in vacuo* yielding **DBA**[$PF_6$] (1.63 g, 4.71 mmol, 50%). Spectral data matched previously published reports.[1] **$^1$H NMR** (400 MHz, THF-$d_8$, 25 °C) δ (ppm): 8.24 (s, 2H), 7.72 – 7.48 (m, 5H), 7.49 – 7.20 (m, 5H), 4.37 (s, 4H). **$^{13}$C{$^1$H} NMR** (101 MHz, THF-$d_8$, 25 °C) δ (ppm): 132.4, 131.1, 130.4, 123.0, 52.1.[1]

**Synthesis of 10**

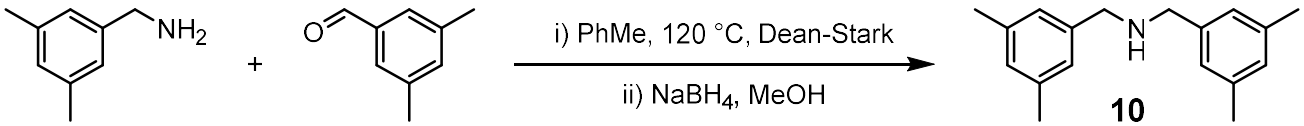


3,5-Dimethylbenzaldehyde (250 mg, 1.86 mmol, 1 eq), (3,5-dimethylphenyl)methanamine (251 mg, 1.86 mmol, 1 eq), and toluene (10 mL) were added to a round-bottom flask equipped with a Dean-Stark trap. The mixture was heated to 120 °C for *ca*. 18 h. After the mixture cooled to room temperature, solvent was removed *in vacuo*. The crude product was redissolved in MeOH (10 mL) and cooled to 0 °C. $NaBH_4$ (352 mg, 9.30 mmol, 5 eq) was slowly added, then the mixture was warmed to room

temperature. After *ca.* 18 h of stirring, the mixture was quenched with $H_2O$ (*ca.* 2 mL). The mixture was dissolved in DCM (100 mL) and washed with $H_2O$ (3 x 75 mL), then dried with $MgSO_4$. Solvent was removed *in vacuo* to yield **10** (388 mg, 7.63 mmol, 82%), with no further purification required.

**$^1$H NMR** (400 MHz, MeCN-$d_3$, 25 °C) δ (ppm): 7.11 (s, 2H), 7.05 (s, 4H), 4.11 (s, 4H), 2.32 (s, 12H).[4]

**Synthesis of DXA**[$PF_6$]

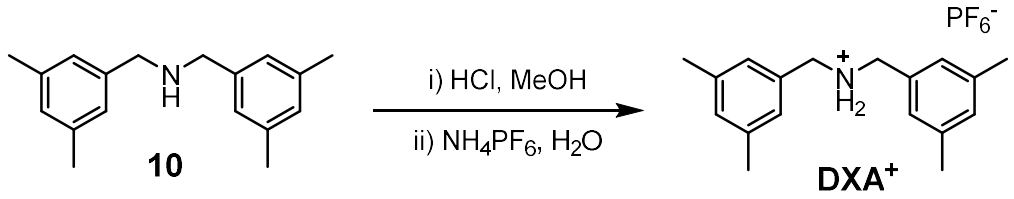


Compound **10** (1 eq, 338 mg, 1.33 mmol) and MeOH (5 mL) were combined in a round-bottom flask. HCl (37%, aq) was added dropwise until the pH of the mixture was *ca*. 2. Solvent and excess acid were removed *in vacuo*, and water (5 mL) was added to the crude mixture. $NH_4PF_6$ (650 mg, 3.99 mmol, 3 eq) dissolved in minimal water was added dropwise to the mixture with vigorous stirring. After 5 mins of stirring, the white precipitate was isolated by filtration, washed with $H_2O$, and dried *in vacuo* to yield **DXA**[$PF_6$] (530 mg, quant.).

**$^1$H NMR** (400 MHz, THF-$d_8$, 25 °C) δ (ppm): 7.99 (s, 2H), 7.13 (s, 4H), 7.06 (s, 2H), 4.24 (s, 4H), 2.30 (s, 12H). **$^{13}$C{$^1$H} NMR** (101 MHz, THF-$d_8$, 25 °C) δ (ppm): 139.64, 132.1, 131.8, 128.7, 52.0, 21.2.

**Synthesis of DPA**[$PF_6$]

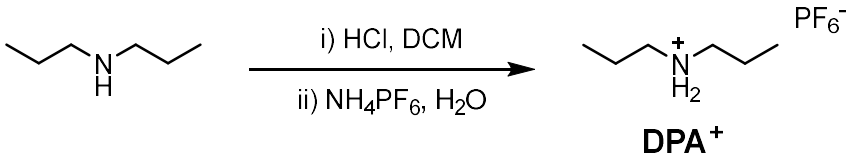


Dipropylamine (1.00 mL, 7.80 mmol) was dissolved in DCM (5 mL), followed by slow addition of HCl (37 wt.%, aq, 2 mL). The resulting suspension was evaporated to dryness *in vacuo*, and the product redissolved in water (10 mL) and filtered to remove any particulates. $NH_4PF_6$ (1.40 g, 8.3 mmol, 1.05 eq) was added, and the resulting suspension was cooled to 4 °C for 10 min. The suspension was then filtered and washed with water, followed by DCM, to isolate **DPA[$PF_6$]** (270 mg, 1.17 mmol, 15%) as a white-yellow solid.

**$^1$H NMR** (400 MHz, THF-$d_8$, 25 °C) δ (ppm): 7.32 (s, 2H), 3.05 (t, $^3J$ = 8.0 Hz, 4H), 1.85 – 1.69 (m, 4H), 1.00 (t, $^3J$ = 7.4 Hz, 6H). **$^{13}$C{$^1$H} NMR** (101 MHz, THF-$d_8$, 25 °C) δ (ppm): 50.5, 20.4, 11.1.

**Synthesis of 1**

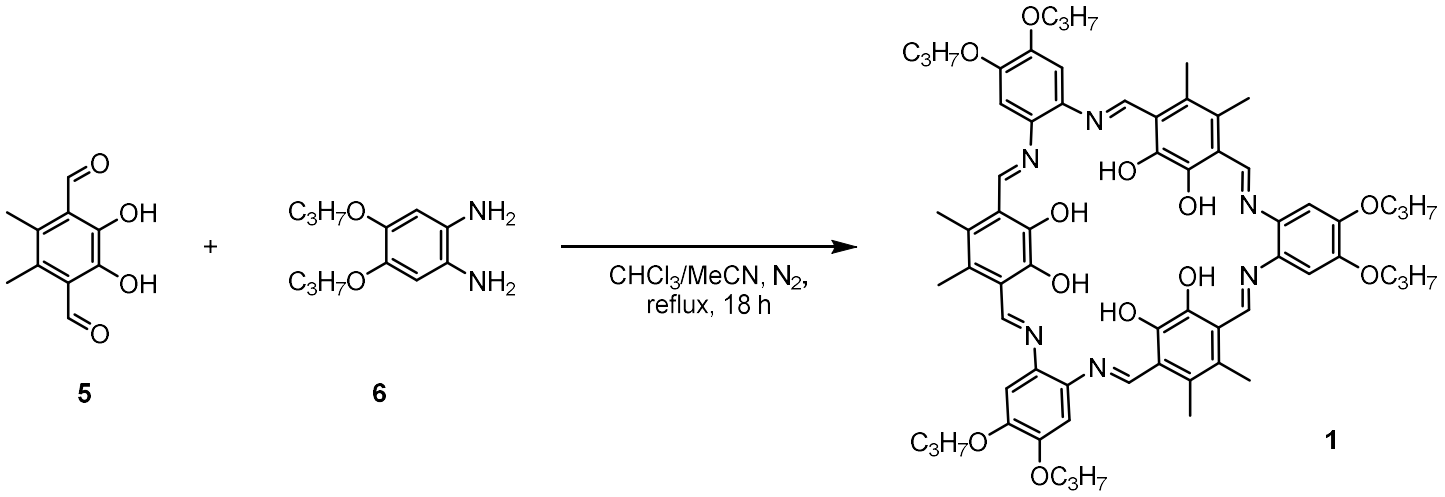


Compound **5** (95 mg, 0.49 mmol, 1 eq) was added to a Schlenk-flask equipped with a reflux condenser and was backfilled with $N_2$ (× 3). Previously degassed $CHCl_3$/MeCN (1:1, v/v, 10 mL) was added *via* syringe under a strong flow of nitrogen, then diamine **6** (109 mg, 49 mmol, 1 eq) was added quickly. The intense red solution was heated to reflux (90 °C) for 18 h. The mixture was cooled to room temperature, following which solvent was removed *in vacuo*. The crude mixture was redissolved in minimal $CHCl_3$/MeCN (1:1, v/v) and recrystallized at -10 °C, yielding **1** as a brown solid (80 mg, 0.21 mmol, 42%)

**$^1$H NMR** (400 MHz, C*D*$Cl_3$, 25 °C) δ (ppm): 14.03 (s, 6H), 8.99 (s, 6H), 6.78 (s, 6H), 4.02 (t, $^3J$ = 6.5 Hz, 12H), 2.37 (s, 18H), 1.88 (m, 12H), 1.08 (t, $^3J$ = 7.4 Hz, 18 H).**$^{13}$C{$^1$H} NMR** (101 MHz, C*D*$Cl_3$, 25 °C): 161.2, 150.9, 149.1, 136.1, 125.0, 119.2, 106.1, 71.6, 22.9, 14.7, 10.7. **ESI-MS** (MeOH/$CHCl_3$, *m/z*): exp. 1147.5748 [**1**+H]$^+$, calc. 1147.5756. **UV-Vis $\lambda_{max}$** (ε / $M^{-1}cm^{-1}$) in THF: 415 nm (1.50 x $10^5$), 340 nm (1.07 x $10^5$).

## *Acid sensitivity of 1*

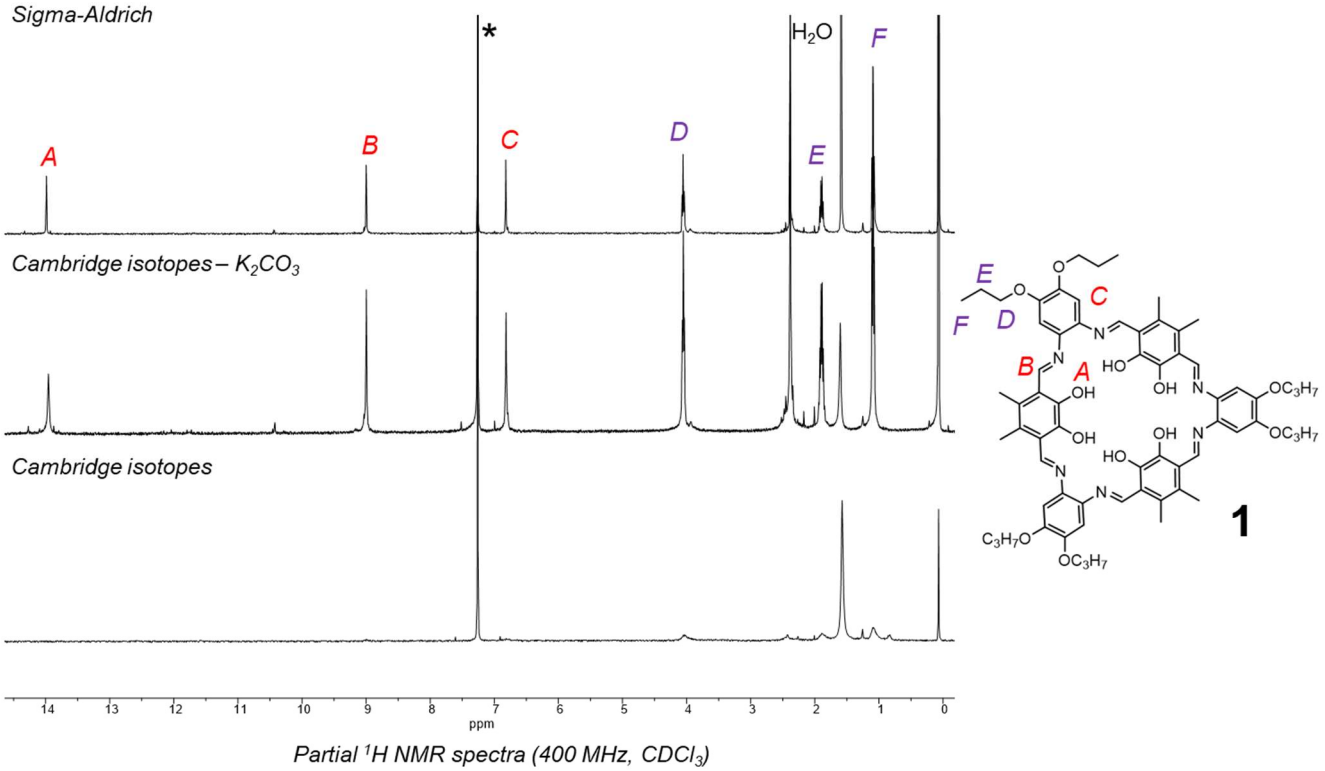


*Partial $^1$H NMR spectra (400 MHz, $CDCl_3$)*

**Figure S1.** Stacked $^1$H NMR spectra (400 MHz, 25 °C) of **1** in different commercially available C*D*Cl$_3$ solvents. Top) Sigma-Aldrich, middle) Cambridge Isotopes neutralized over $K_2CO_3$, bottom) Cambridge Isotopes untreated.

The acidity of the chosen deuterated and chlorinated solvents has a drastic effect on the resulting $^1$H NMR spectrum of **1**. If Cambridge Isotopes C*D*Cl$_3$ is used, most signals for the macrocycle are not seen, which is explained by the increased acidity of the untreated solvent. However, if potassium carbonate ($K_2CO_3$) is used to neutralize the solvent, all of the expected signals for the compound can be seen (**Figure S1**, middle). Sigma-Aldrich $CDCl_3$ does not need to be neutralized prior to use. This is one reason for the use of DCM-$d_2$ within this work.

*Note: the same trend is seen for diamino compound **6**, where NMR spectra of the compound in acidic $CDCl_3$ shows almost no signals, but the same sample dissolved in acid-free $CDCl_3$ shows the expected product.*

## *NMR spectra of 5*

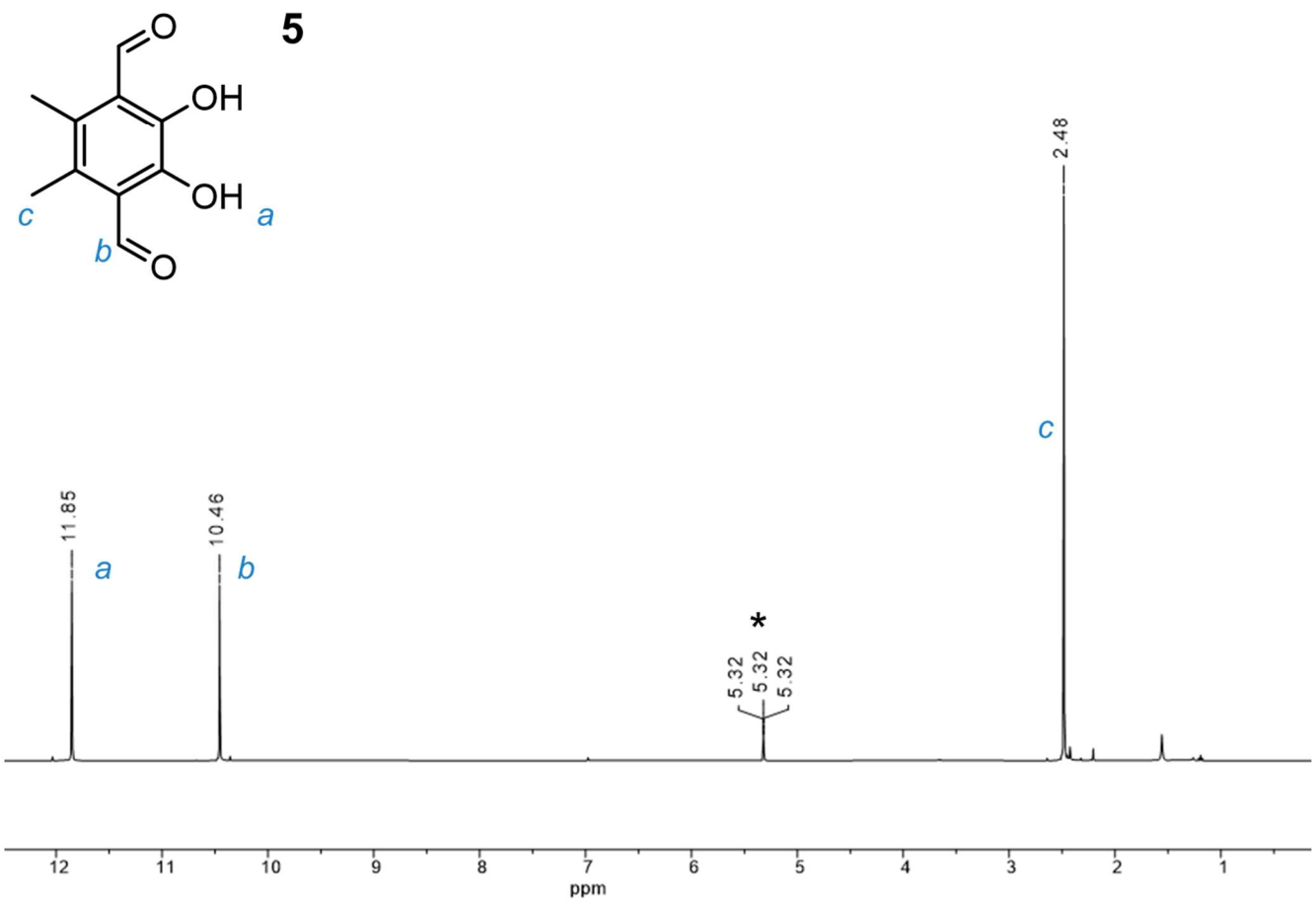


**Figure S2.** $^{1}$H NMR spectrum (400 MHz, DCM-$d_2$, 25 °C) of compound **5**. * = $CDHCl_2$.

## *NMR spectra for 6*

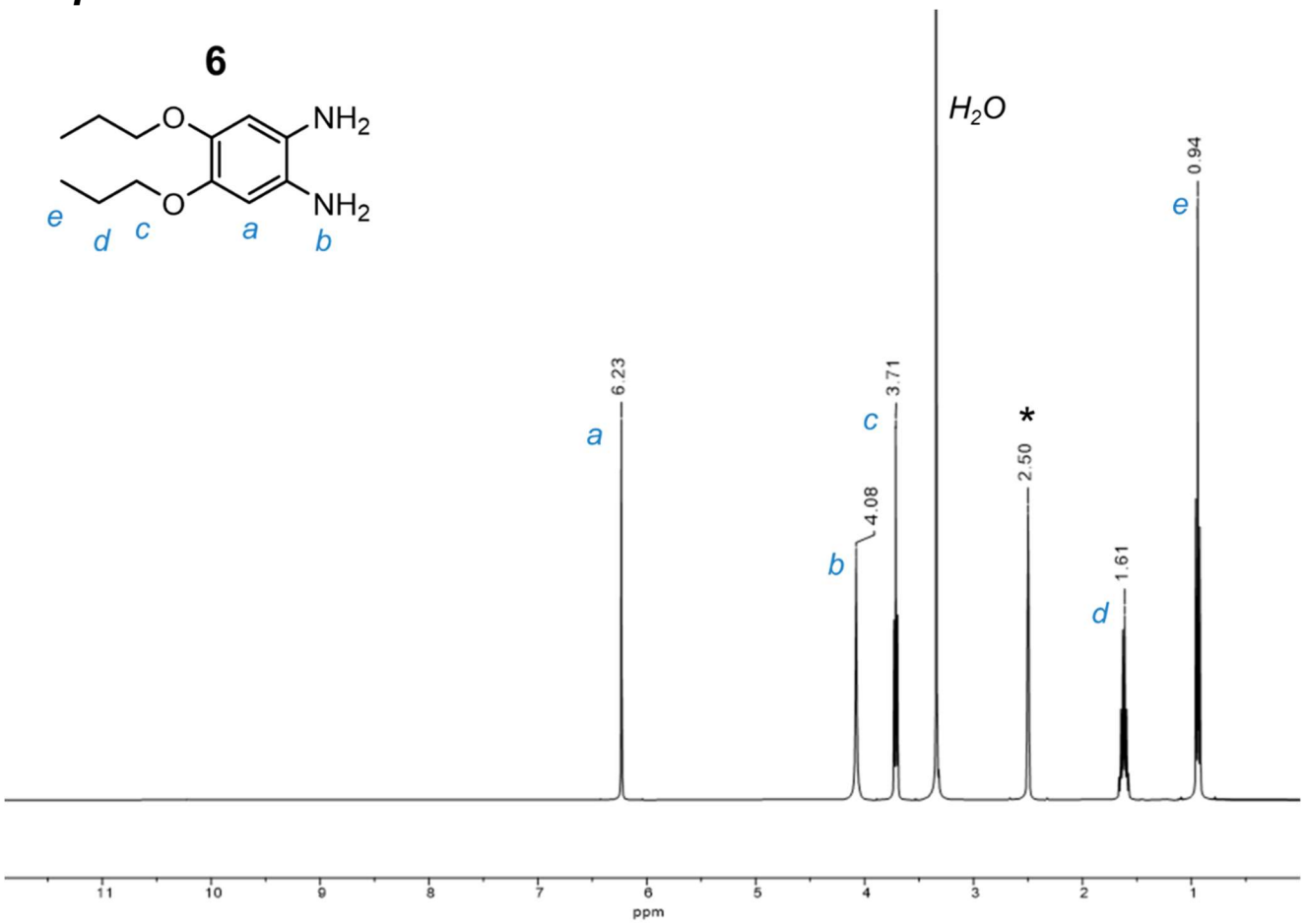


**Figure S3.** $^{1}$H NMR spectrum (400 MHz, DMSO-$d_6$, 25 °C) of compound **6**. * = $SO(CD_3)(CD_2H)$.

## *NMR spectrum for 7*

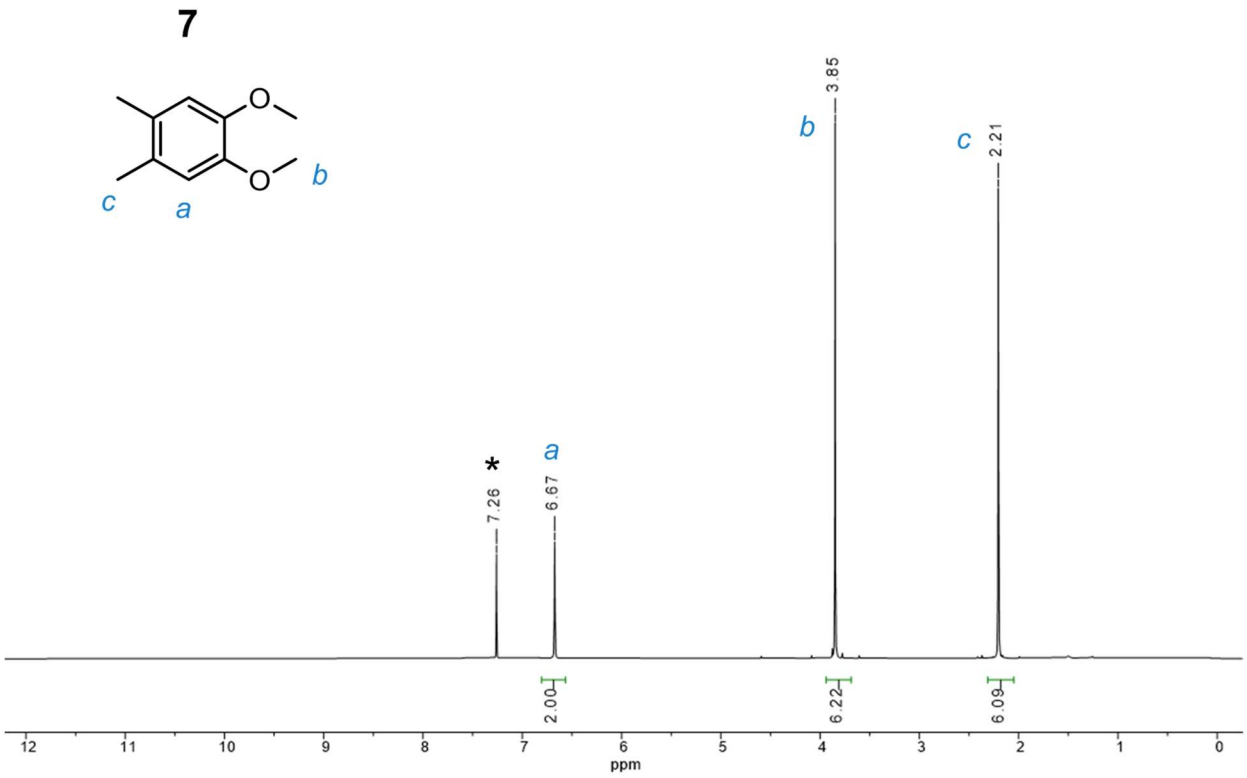


**Figure S4.** $^{1}$H NMR spectrum (400 MHz, C*D*Cl$_3$, 25 °C) of compound **7**. *= CHCl$_3$.

## *NMR spectrum for 8*

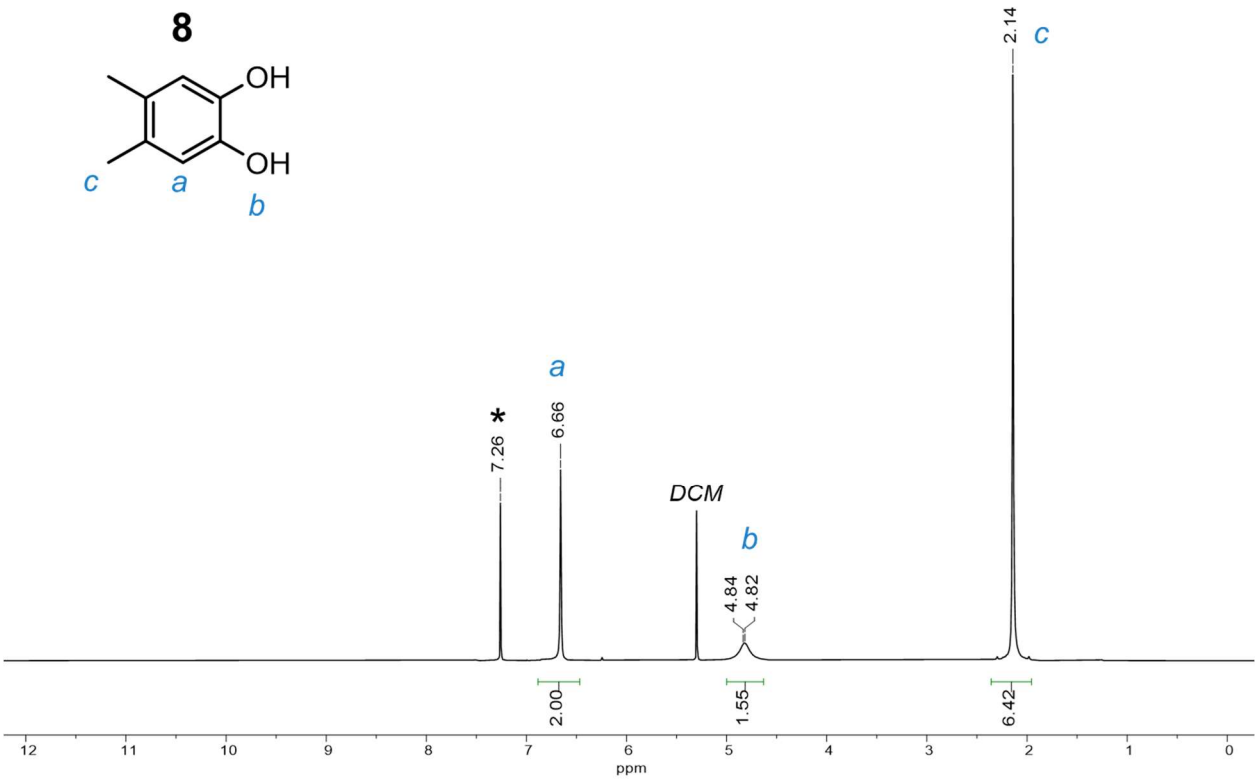


**Figure S5.** $^{1}$H NMR spectrum (400 MHz, C*D*Cl$_3$, 25 °C) of compound **8**. * = CHCl$_3$.

## *NMR spectrum for DBA[$PF_6$]*

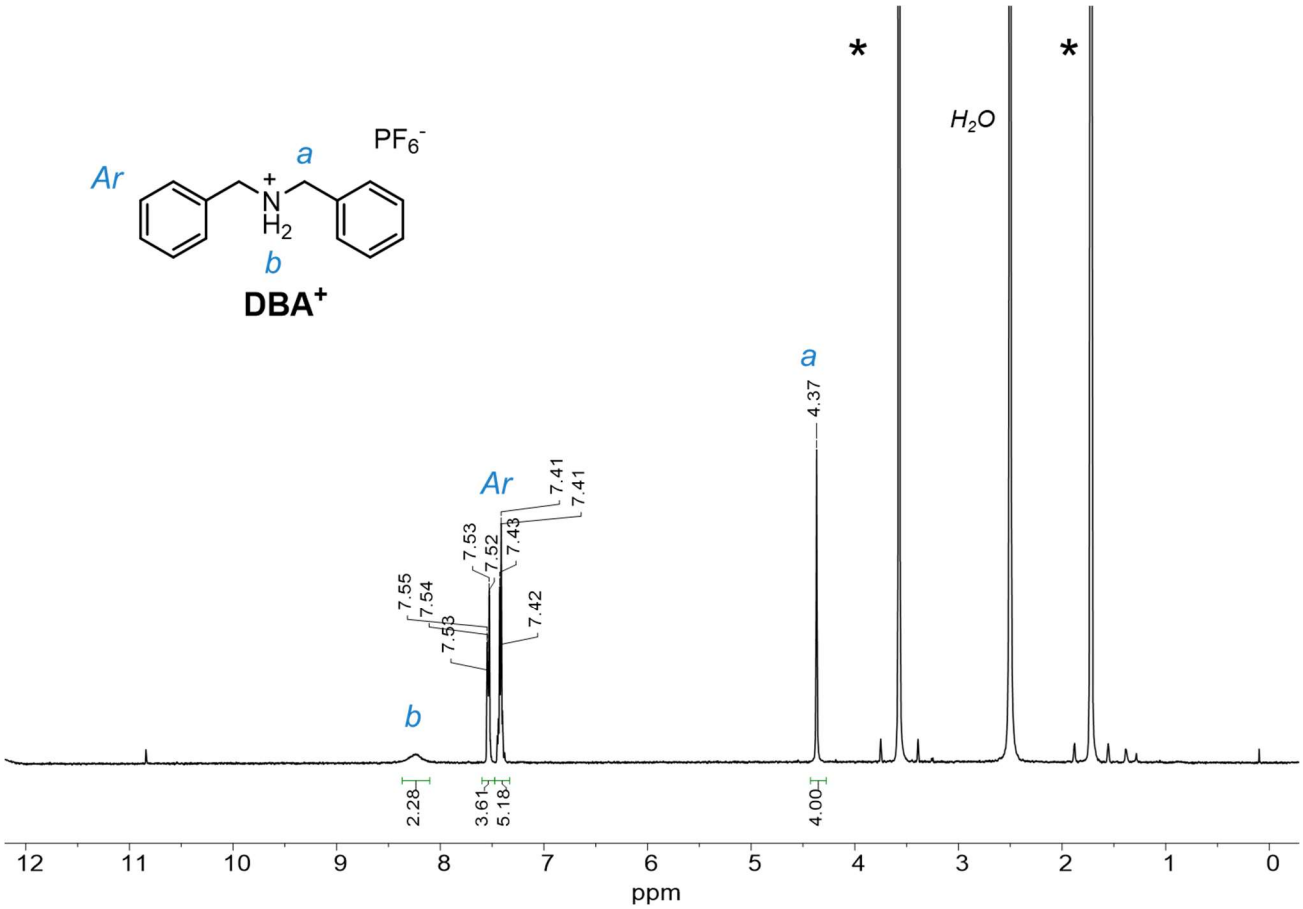


**Figure S6.** $^1$H NMR spectrum (400 MHz, THF-$d_8$, 25 °C) of compound **DBA**[$PF_6$]. * = $O(CD_2)_3(CDH)$.

## *NMR spectrum for DXA*[$PF_6$]

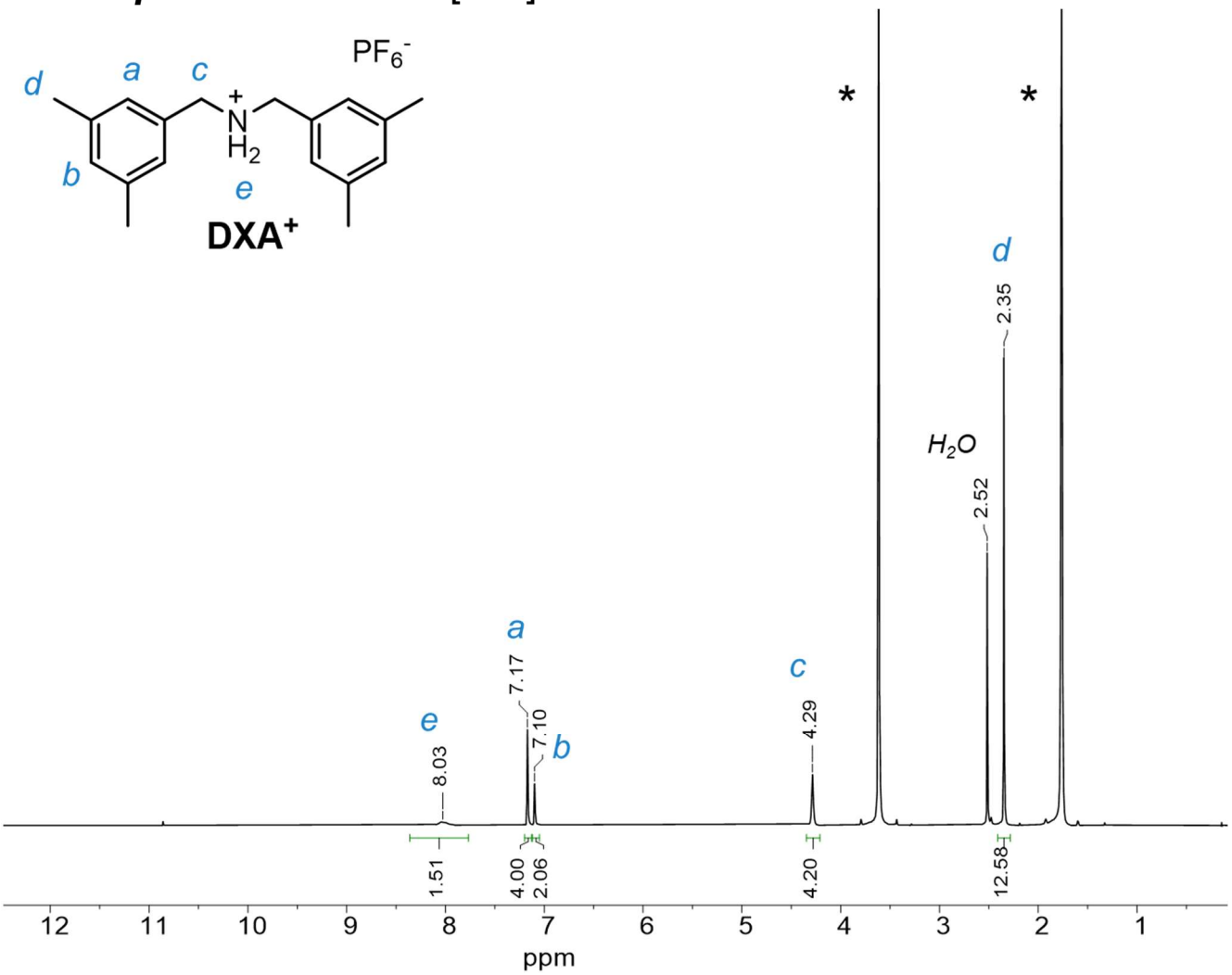


**Figure S7.** $^1$H NMR spectrum (400 MHz, THF-$d_8$, 25 °C) of compound **DXA**[$PF_6$]. * = $O(CD_2)_3(CDH)$.

## *NMR spectra for DPA[$PF_6$]*

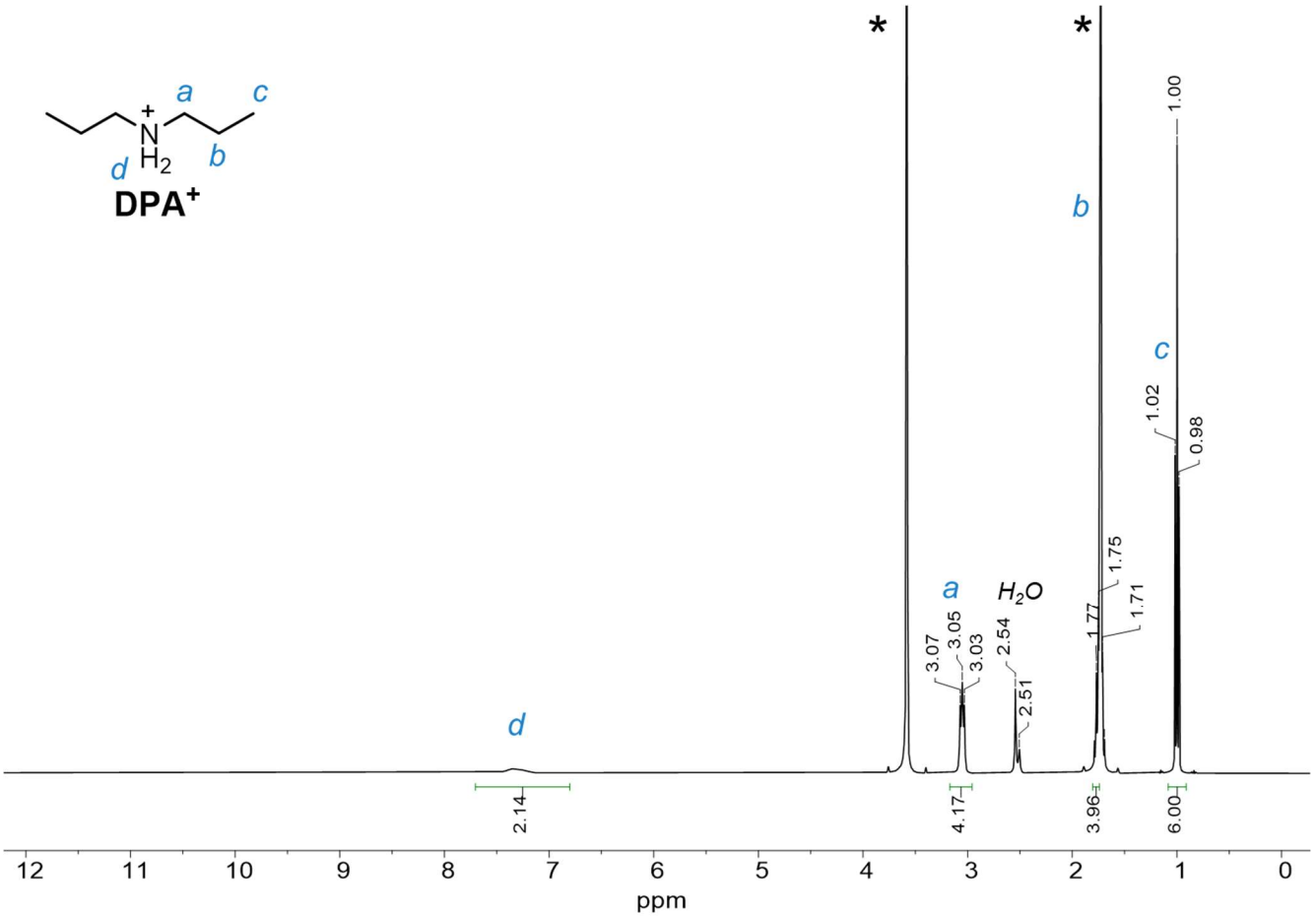


**Figure S8.** $^1$H NMR spectrum (400 MHz, THF-$d_8$, 25 °C) of compound **DPA**[$PF_6$]. * = $O(CD_2)_3(CDH)$.

## *NMR spectra for 1*

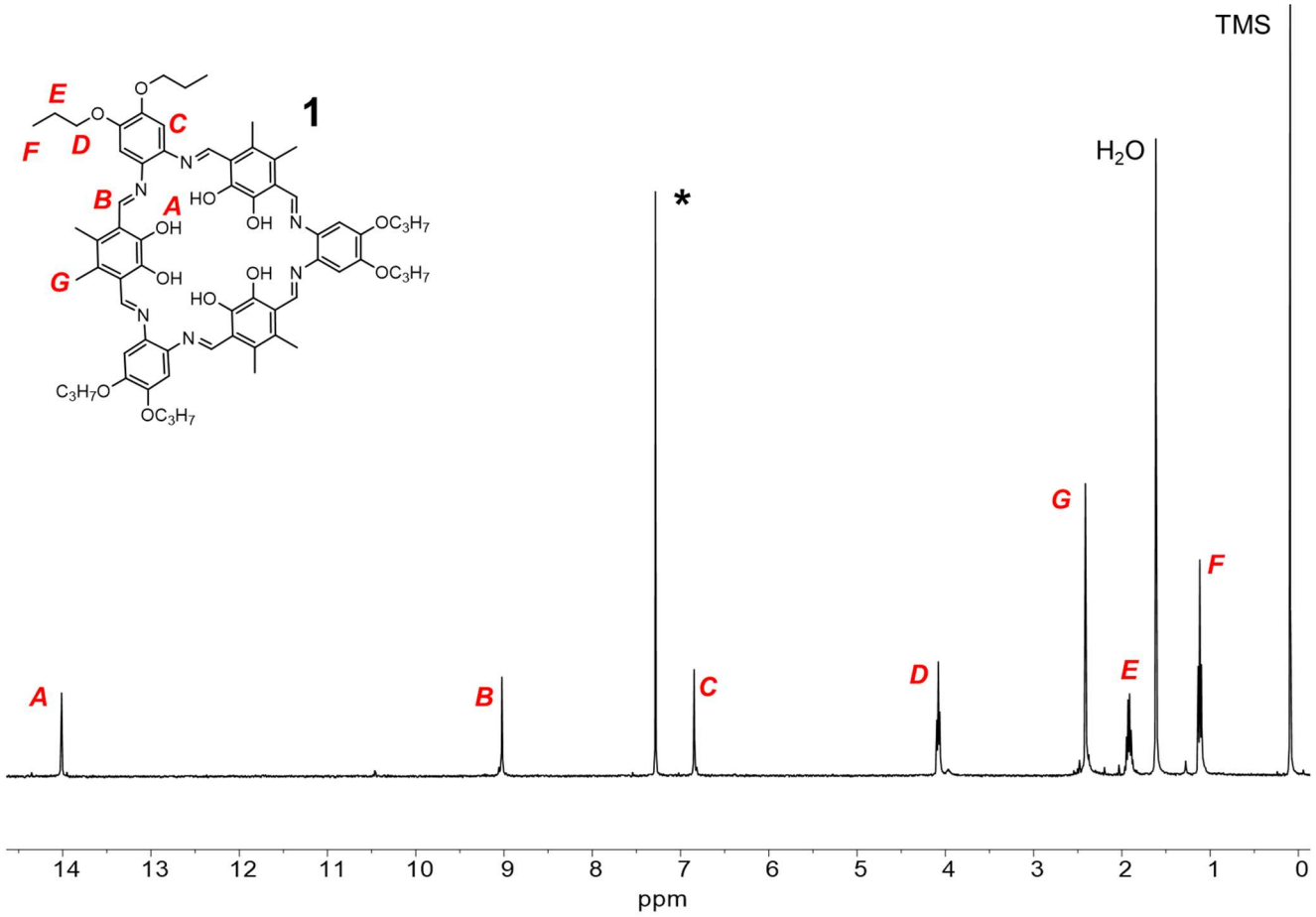


**Figure S9.** $^{1}$H NMR spectrum (400 MHz, C*D*Cl$_3$, 25 °C) of compound **1**. * = CHCl$_3$.

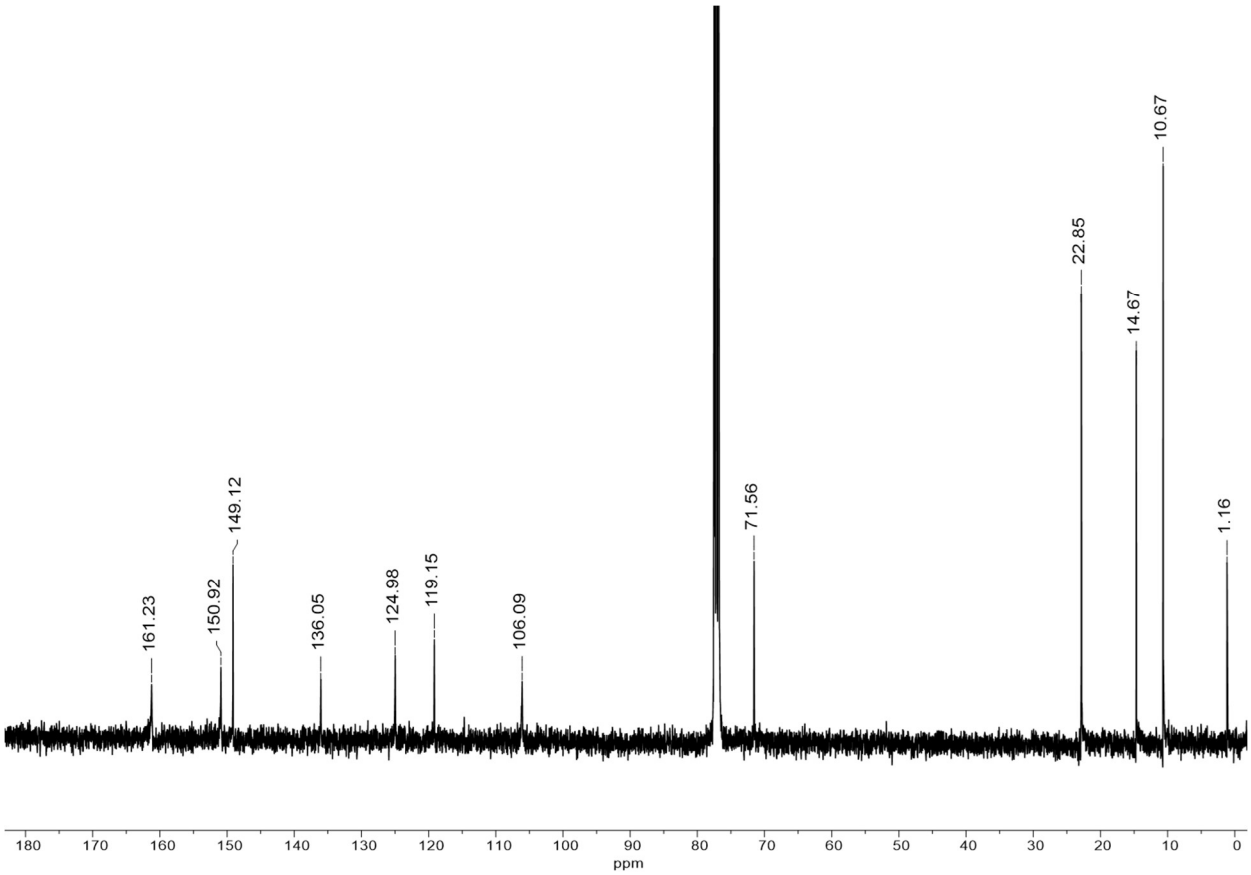


**Figure S10.** $^{13}C\{^{1}H\}$ NMR spectrum (101 MHz, C*D*Cl$_3$, 25 °C) of compound **1**.

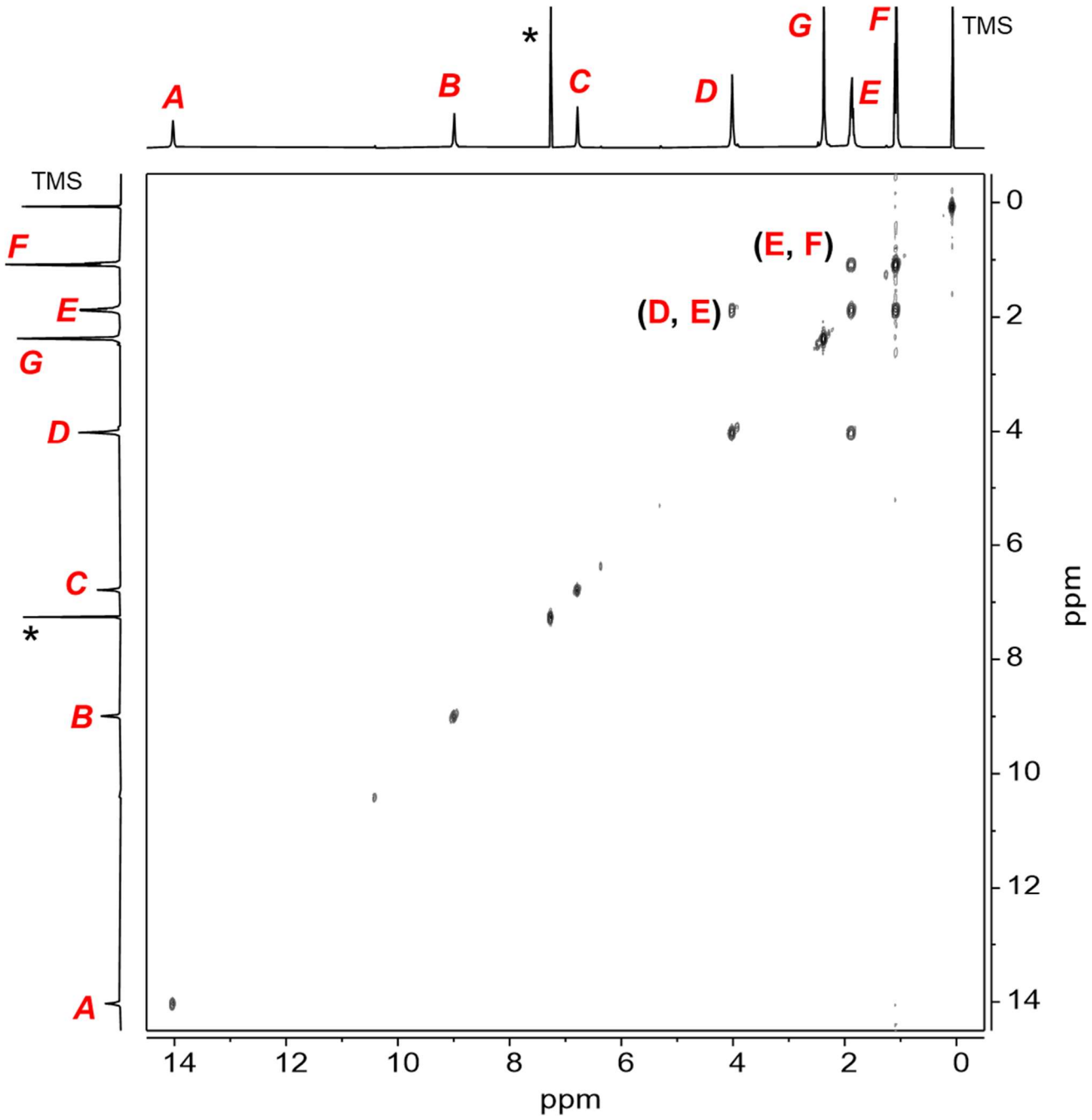


**Figure S11.** $^{1}$H-$^{1}$H COSY NMR spectrum (400 MHz, C*D*Cl$_3$, 25 °C) of compound **1**. * = CHCl$_3$.

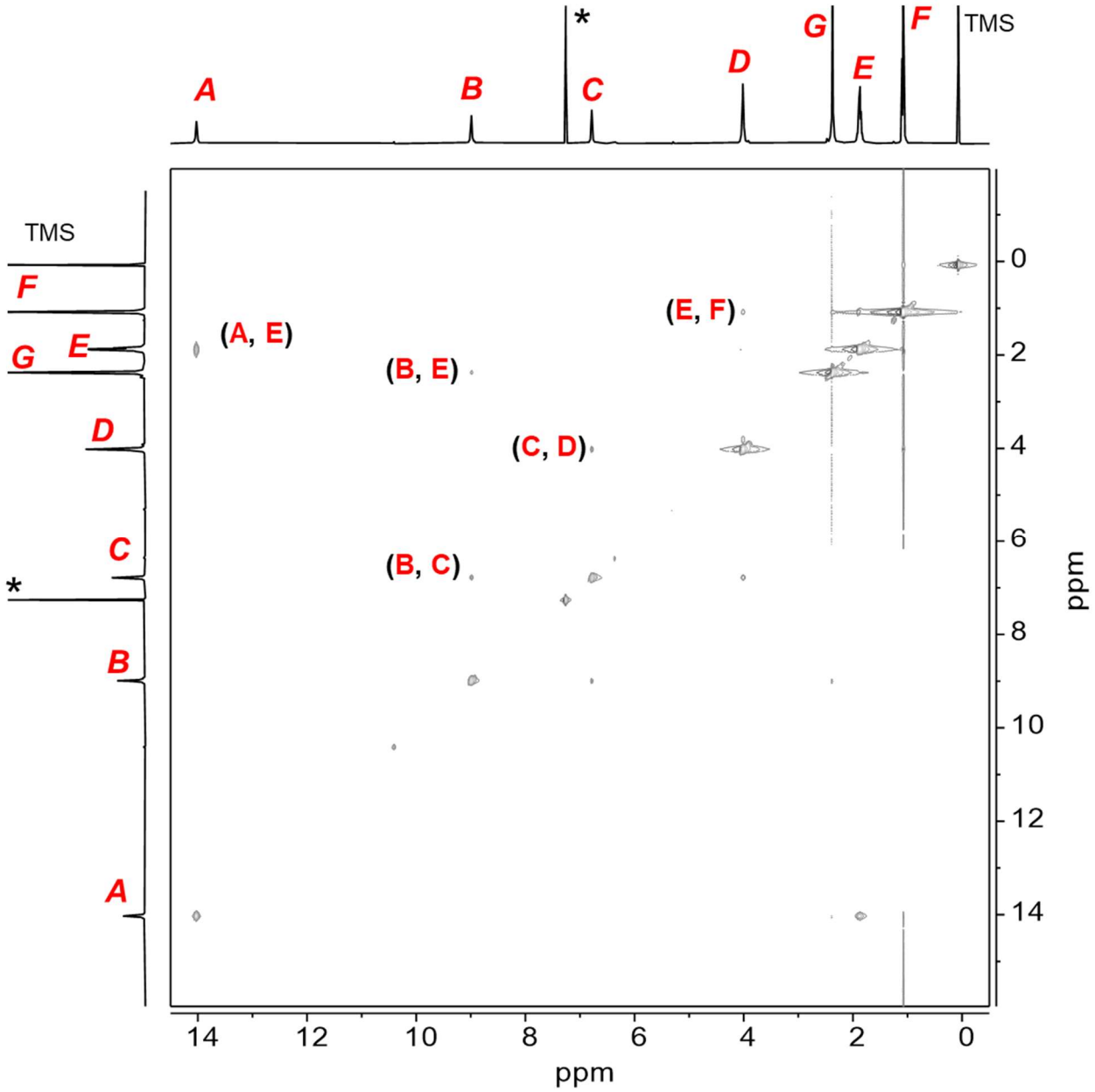


**Figure S12.** $^{1}$H-$^{1}$H NOESY NMR spectrum (400 MHz, C*D*Cl$_3$, 25 °C) of compound **1**. * = CHCl$_3$.

## *Evidence of 1⊃DBA⁺ not being purely enol-imine*

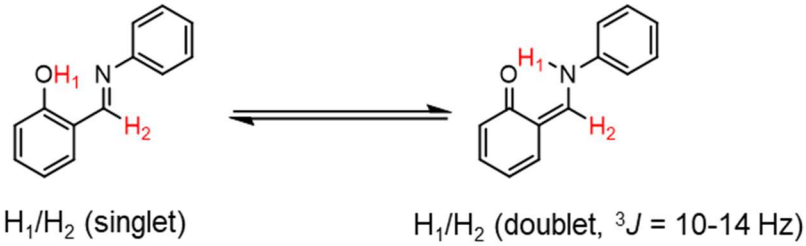


**Scheme S3.** Interconversion of a simple enol-imine (left) with the keto-enamine (right) tautomer. *H₁* is the acid proton that changes between the oxygen and nitrogen atoms.

In **1+DBA⁺** we saw two complexes, **1⊃DBA⁺** and **1·DBA⁺**, which have different splitting patterns for phenolic protons *A* (Figure S13). External complex **1⊃DBA⁺** displays doublets for $A^t$ and $B^t$ respectively. This arises due to tautomerization between the two imine forms, the keto-enamine form allows for efficient $^3J$ coupling to be possible ($J$ = 3.6 Hz). Although keto-enamine groups generally have $^3J$ coupling constants of 10-14 Hz, lower values can be present for weakly coupling species and have been seen in tautomerically labile Schiff-base macrocycles.[6,7] Also, if only some of the imine groups are in the keto-enamine form, with the other existing in the enol-imine tautomer, the coupling constant could be smaller than the expected 10-14 Hz.

For compound **1⊃DBA⁺** we saw $A^{ut}$ and $B^{ut}$ appearing as singlets in the $^1$H NMR spectrum. However, in the $^1$H-$^1$H COSY spectrum (Figure S13) the cross-peaks for $A^{ut}$/$B^{ut}$ and $A^t$/$B^t$ both appear as doublets, even for external complex **1·DBA⁺**.This implies that although $A^{ut}$/$B^{ut}$ appear as singlets, the complex is in a mixed tautomeric form. Likely **1·DBA⁺** has more enol-imine character than keto-enamine.

Through computational analysis the most stable tautomers for internal and external complexes, **$1_{Me}$⊃DBA⁺** and **$1_{Me}$·DBA⁺** respectively, are mixtures of enol-imine and keto-enamine groups. See computational discussion for more information.

For pure macrocycle **1** (Figure S14B-C) we saw no cross-peaks in the $^1$H-$^1$H COSY or NOESY NMR spectra for protons *A* and *B*; this lack of through-bond coupling is consistent with macrocycles in the enol-imine form.[8]

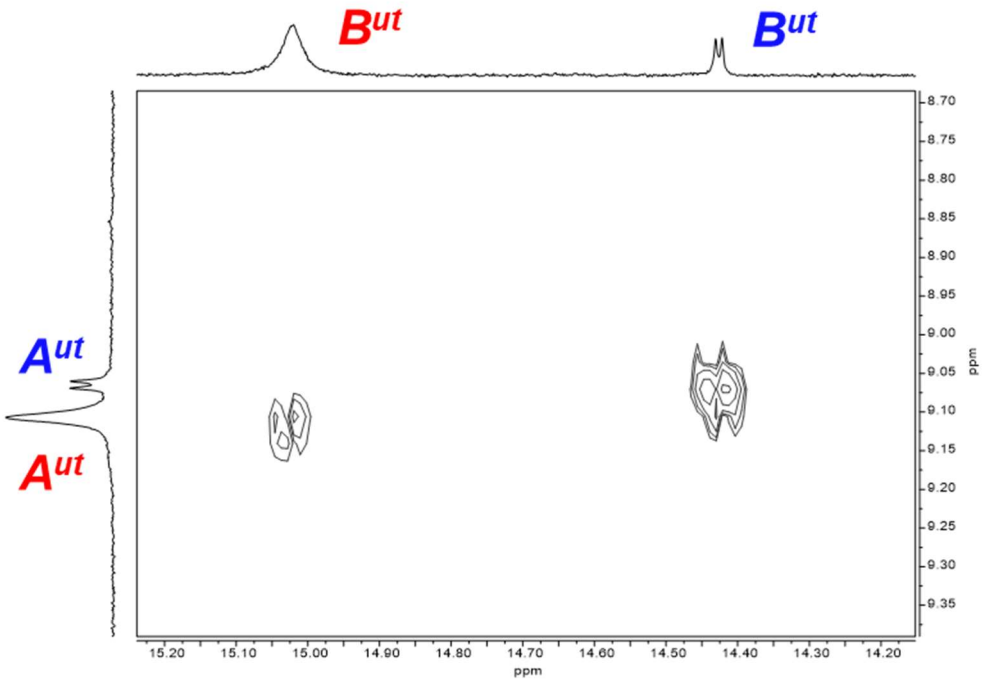


**Figure S13.** Partial $^{1}$H-$^{1}$H COSY NMR spectrum (400 MHz, THF-$d_8$, 25 °C) for **1+DBA**$^{+}$.

The full $^{1}$H-$^{1}$H COSY NMR spectrum is given below in Figure S16, the above spectrum highlights the coupling between $A^{ut}$/$B^{ut}$ and $A^{t}$/$B^{t}$, respectively, with a coupling pattern of a doublet.

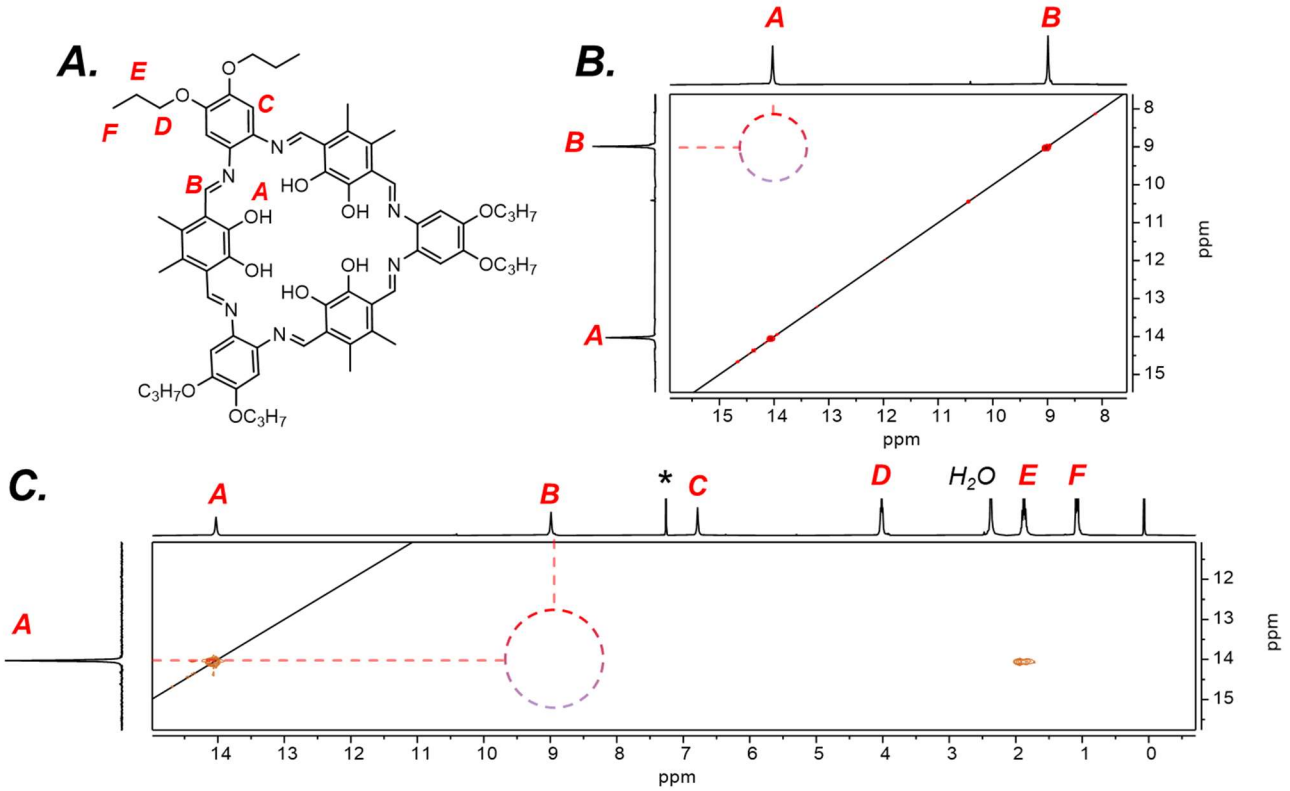


**Figure S14.** A) Proton assignment for **1**, B) partial $^{1}$H-$^{1}$H COSY NMR spectrum (400 MHz, C*D*Cl$_3$, 25 °C), and c) partial $^{1}$H-$^{1}$H NOESY spectrum (400 MHz, C*D*Cl$_3$, 25 °C). * = CHCl$_3$.

## *NMR spectra for 1+DBA⁺*

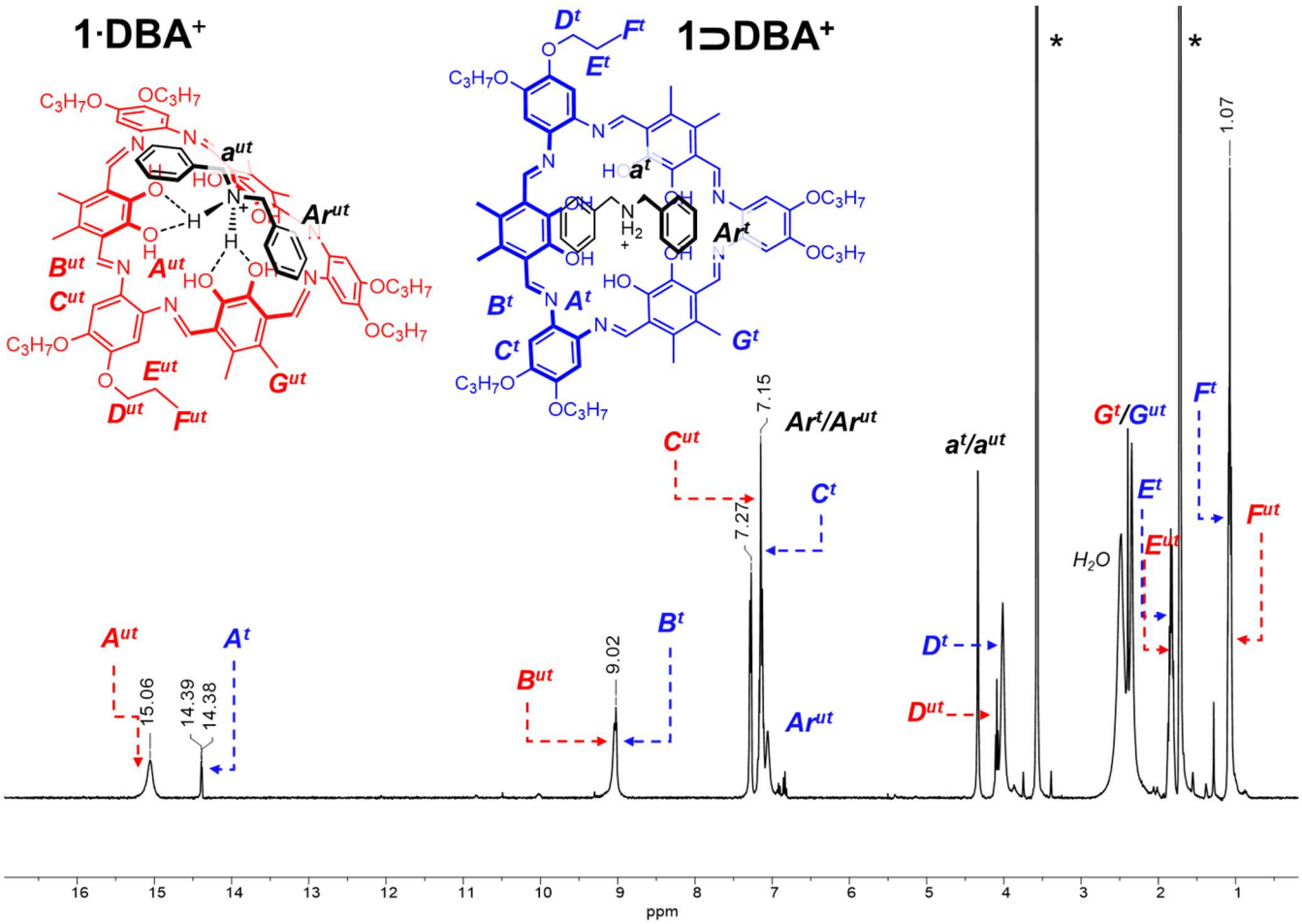


**Figure S15.** $^{1}$H NMR spectrum (400 MHz, THF-$d_8$, 25 °C) for **1+DBA⁺**. * = $O(CD_2)_3(CDH)$.

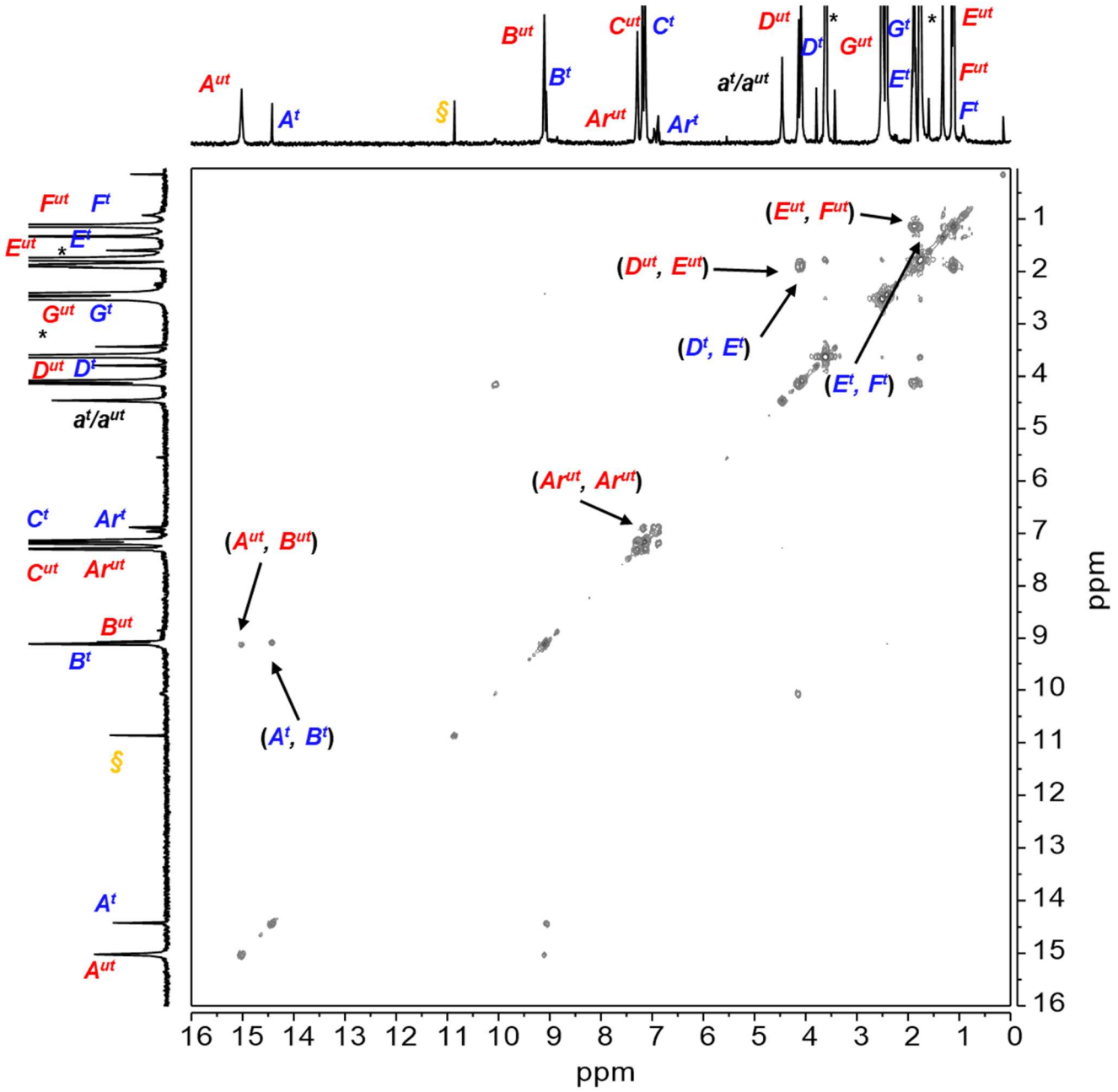


**Figure S16.** $^{1}$H-$^{1}$H COSY NMR spectrum (400 MHz, THF-$d_8$, 25 °C) for **1+DBA**$^{+}$. § denotes peroxide present in this sample of THF-$d_8$. * = O(CD$_2$)$_3$(CDH).

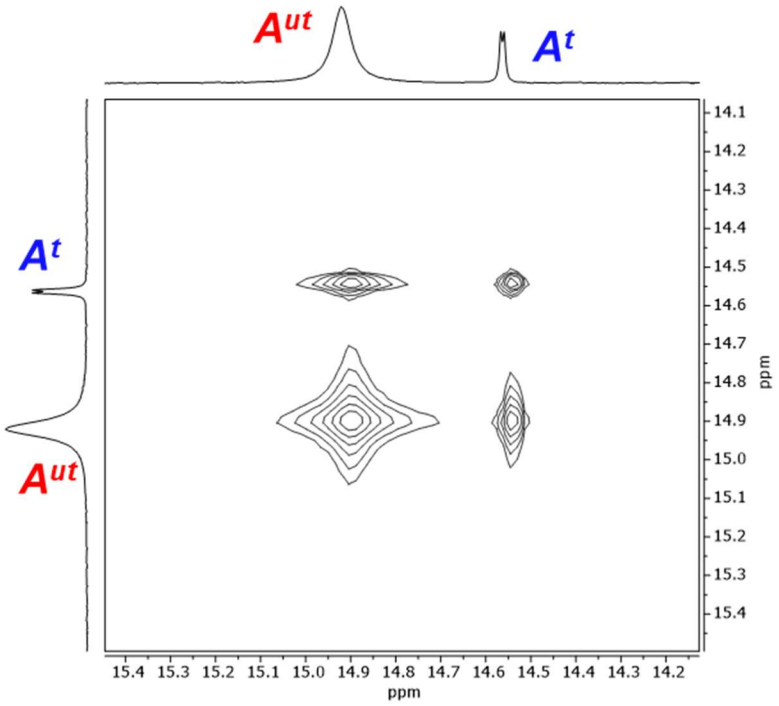


**Figure S17.** Partial $^{1}$H-$^{1}$H EXSY NMR spectrum (400 MHz, THF-$d_8$, 25 °C) for **1+DBA$^{+}$**.

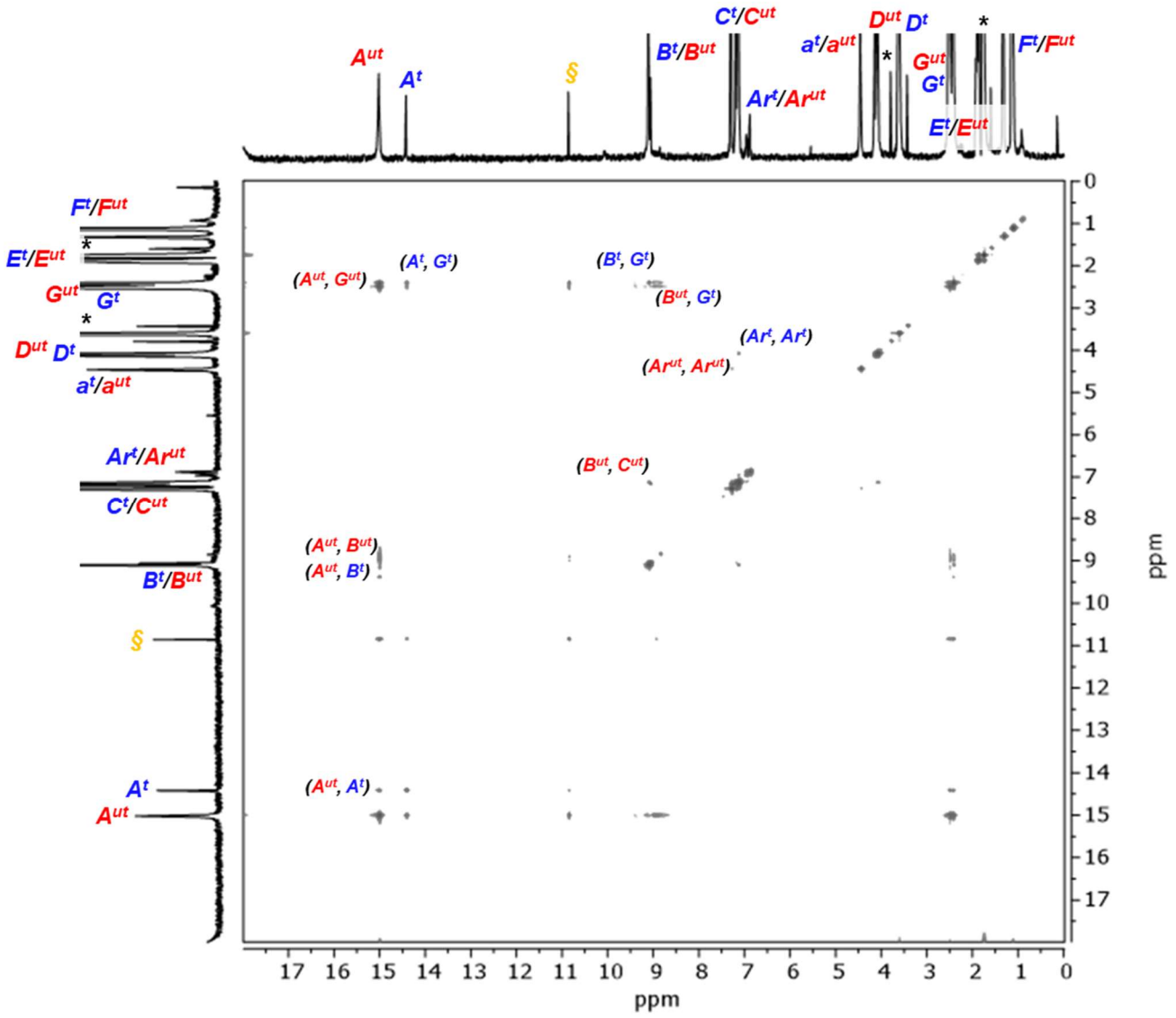


**Figure S18.** $^{1}$H-$^{1}$H NOESY NMR spectrum (400 MHz, THF-$d_8$, 25 °C) for **1+DBA**$^{+}$. § denotes peroxide present in some samples of THF-$d_8$. * = $O(CD_2)_3(CDH)$.

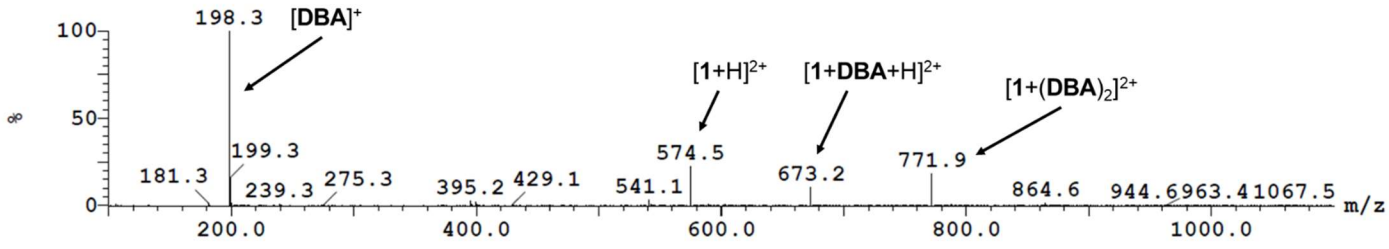


**Figure S19**. LR-ESI mass spectrum of **1**+**DBA**$^{+}$.

## *NMR spectra for 1+DXA⁺*

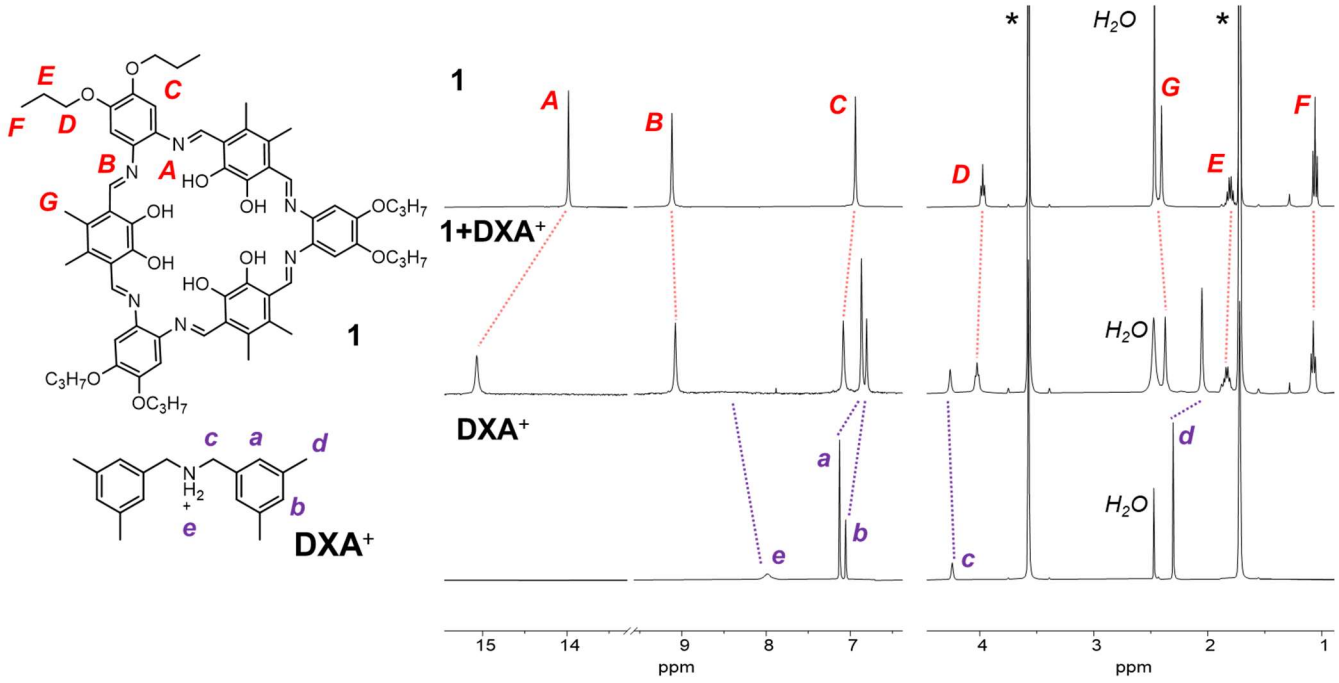


**Figure S20.** Molecular structures of **1** and **DXA⁺** with proton assignment along with stacked $^{1}$H NMR spectra (400 MHz, THF-$d_8$, 25 °C) of **1+DXA⁺**.* = $O(CD_2)_3(CDH)$.

The same type of stacked $^{1}$H NMR spectra for **1**+**DBA⁺** can be seen in the main text (Figure 2).

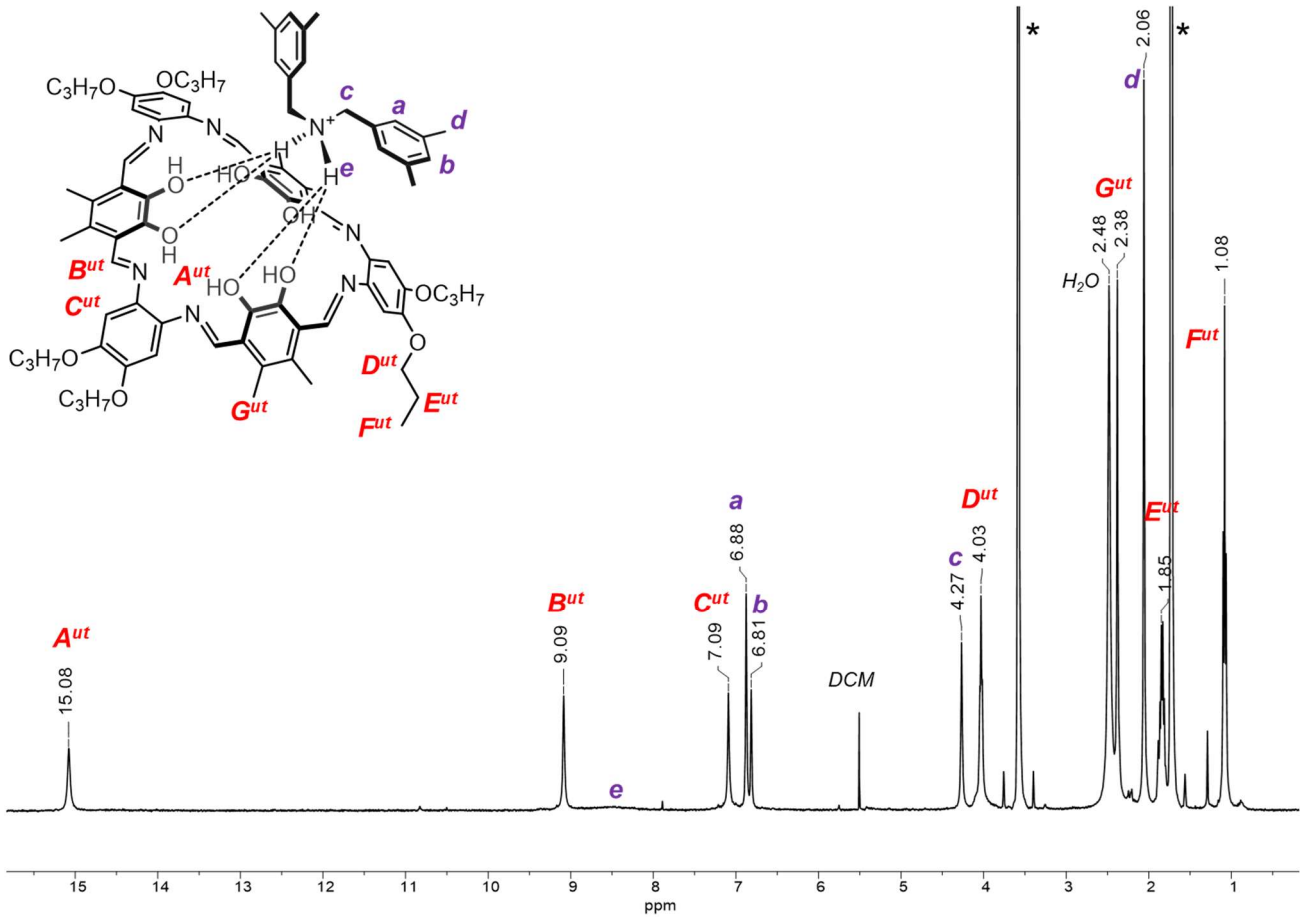


**Figure S21.** $^{1}$H NMR spectrum (400 MHz, THF-$d_8$, 25 °C) of **1+DXA**$^{+}$. * = $O(CD_2)_3(CDH)$.

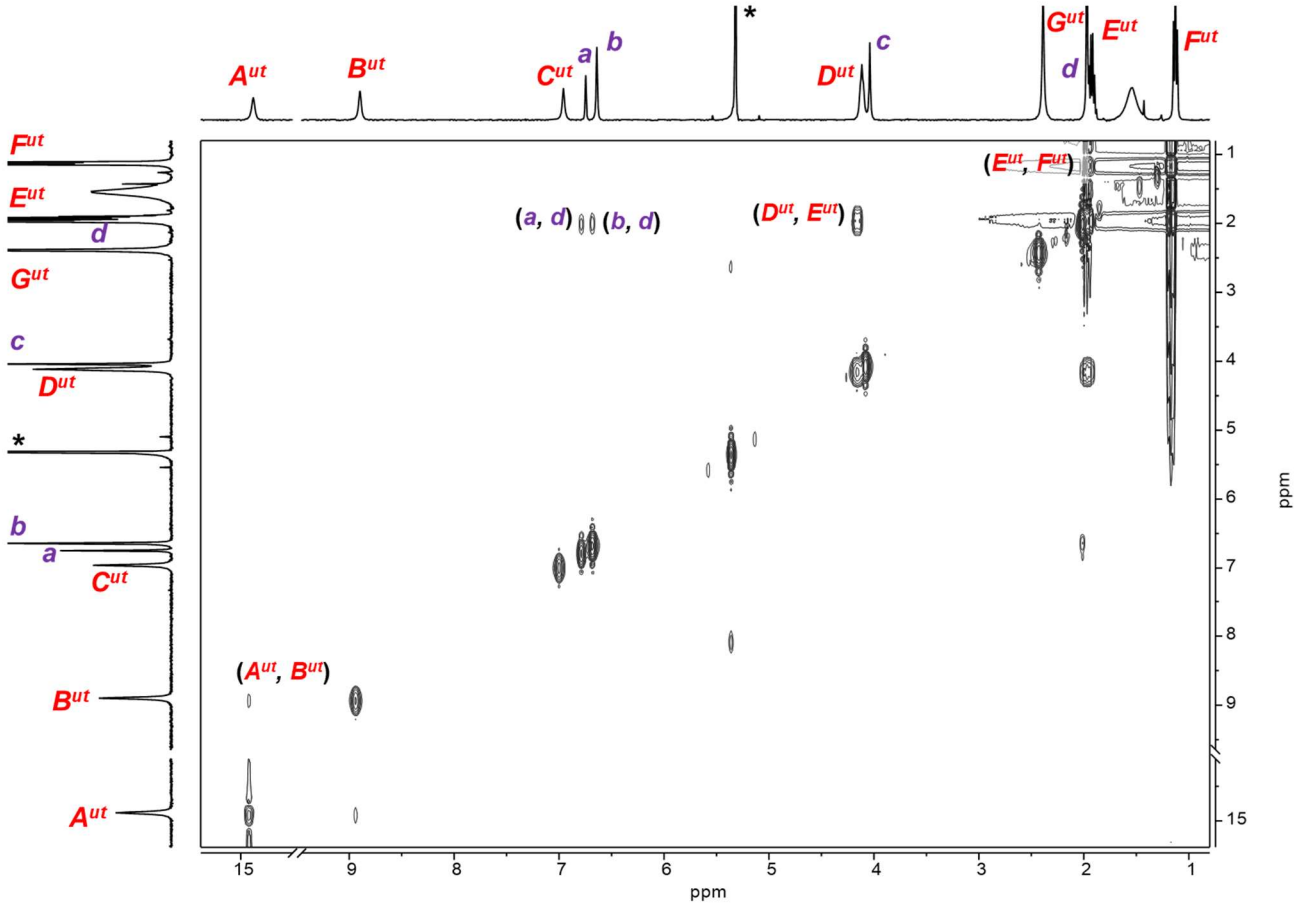


**Figure S22.** Partial $^{1}$H-$^{1}$H COSY NMR spectrum (400 MHz, DCM-$d_2$, 25 °C) of **1+DXA**$^{+}$. * = $CDHCl_2$.

## *Formation of 1⊃DXA⁺ over time from a solution of 1·DXA⁺*

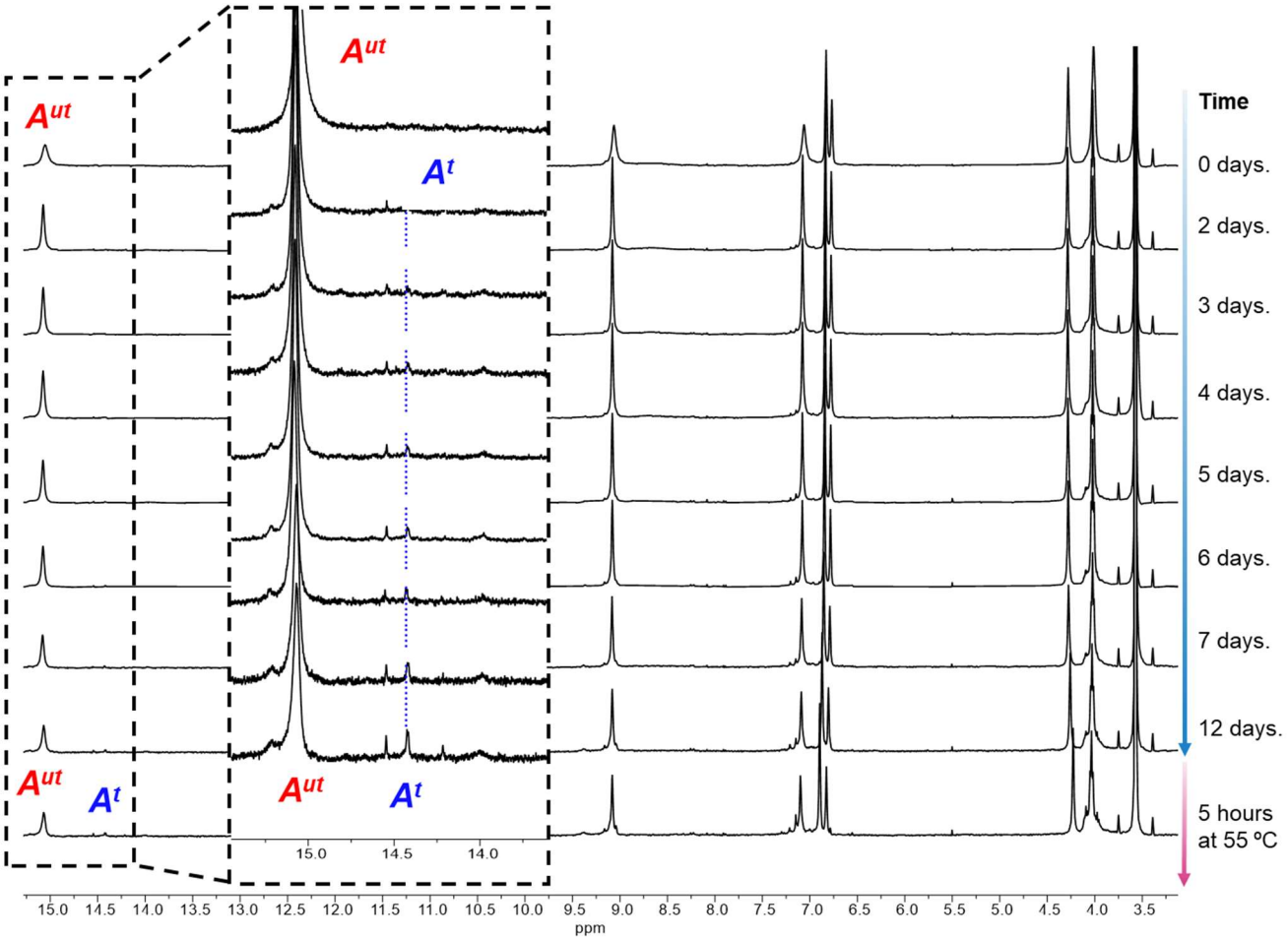


**Figure S23.** Stacked partial $^{1}$H NMR spectra (400 MHz, THF-$d_8$, 25 °C) of **1+DXA**$^{+}$ over time.

Although only the unthreaded complex (**1·DXA**$^{+}$) was initially detected in a mixture of **1** and **DXA**$^{+}$ in THF-$d_8$, a small doublet appeared at *ca.* 14.4 ppm over time, which corresponds to the threaded complex (**1⊃DXA**$^{+}$). In this medium, however, the macrocycle slowly decomposed, which made it impossible for us to determine the thermodynamic and kinetic parameters for the formation of complex **1⊃DXA**$^{+}$.

## *NMR spectra for 1+DPA⁺*

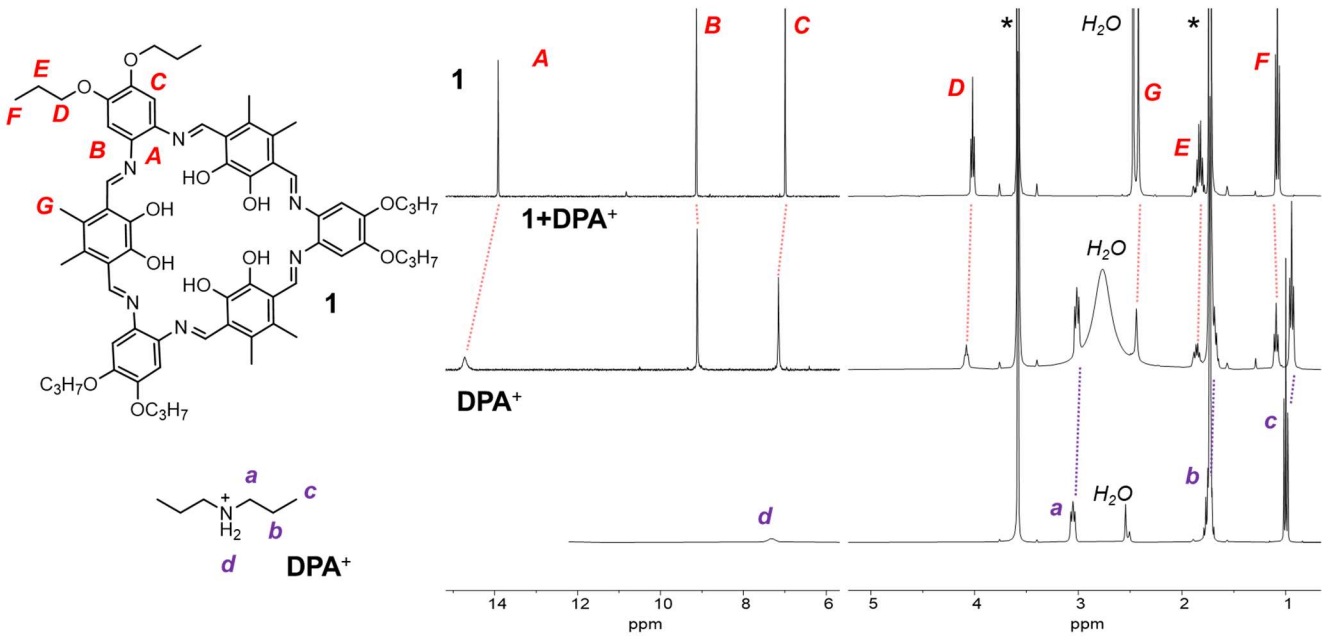


**Figure S24.** Molecular structures of **1** and **DPA⁺** with proton assignments along with stacked $^{1}$H NMR spectra (400 MHz, THF-$d_8$, 25 °C) for **1+DPA⁺**.* = $O(CD_2)_3(CDH)$.

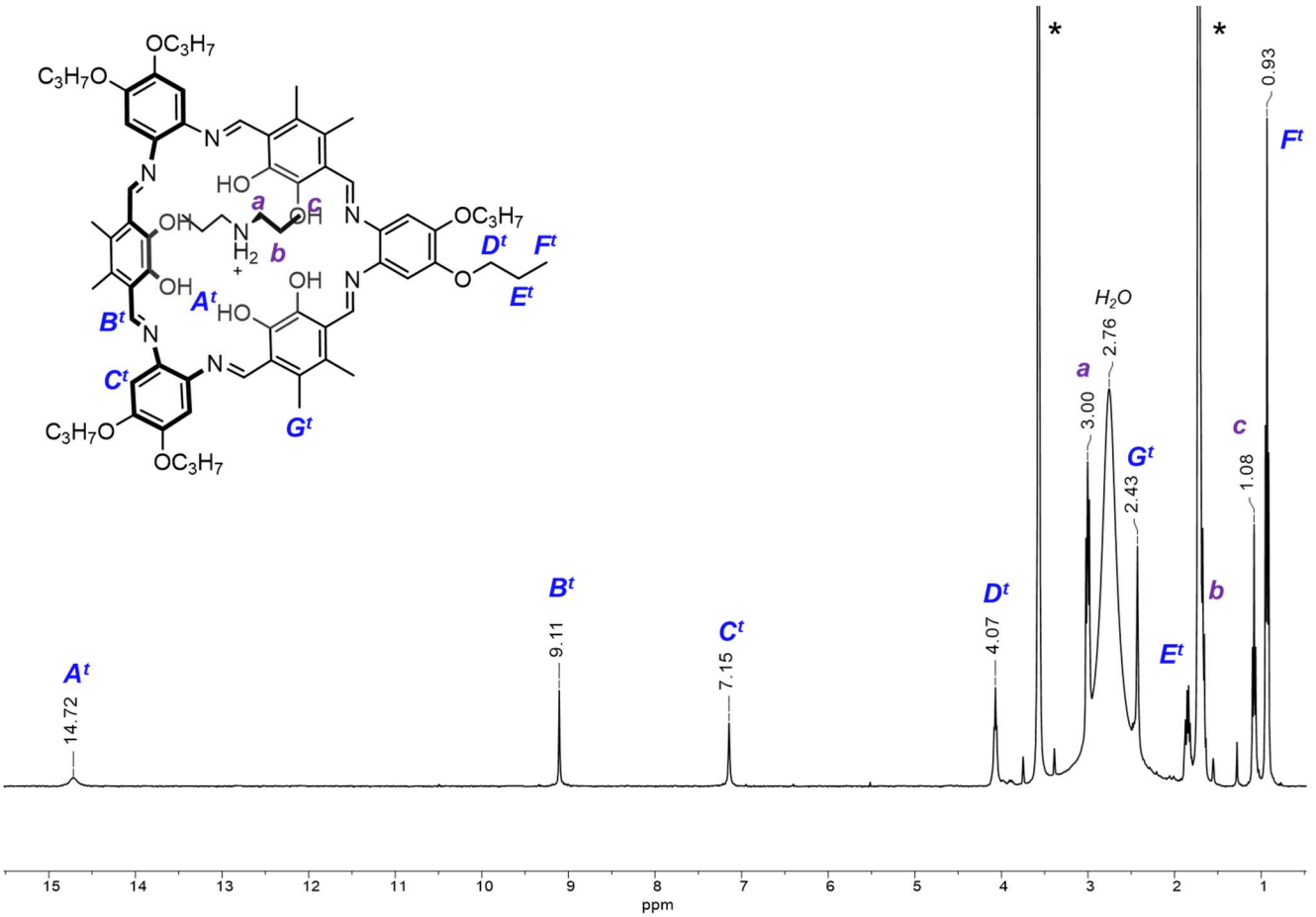


**Figure S25.** $^{1}$H NMR spectrum (400 MHz, THF-$d_8$, 25 °C) for **1+DPA**$^{+}$. * = O(CD$_2$)$_3$(CDH).

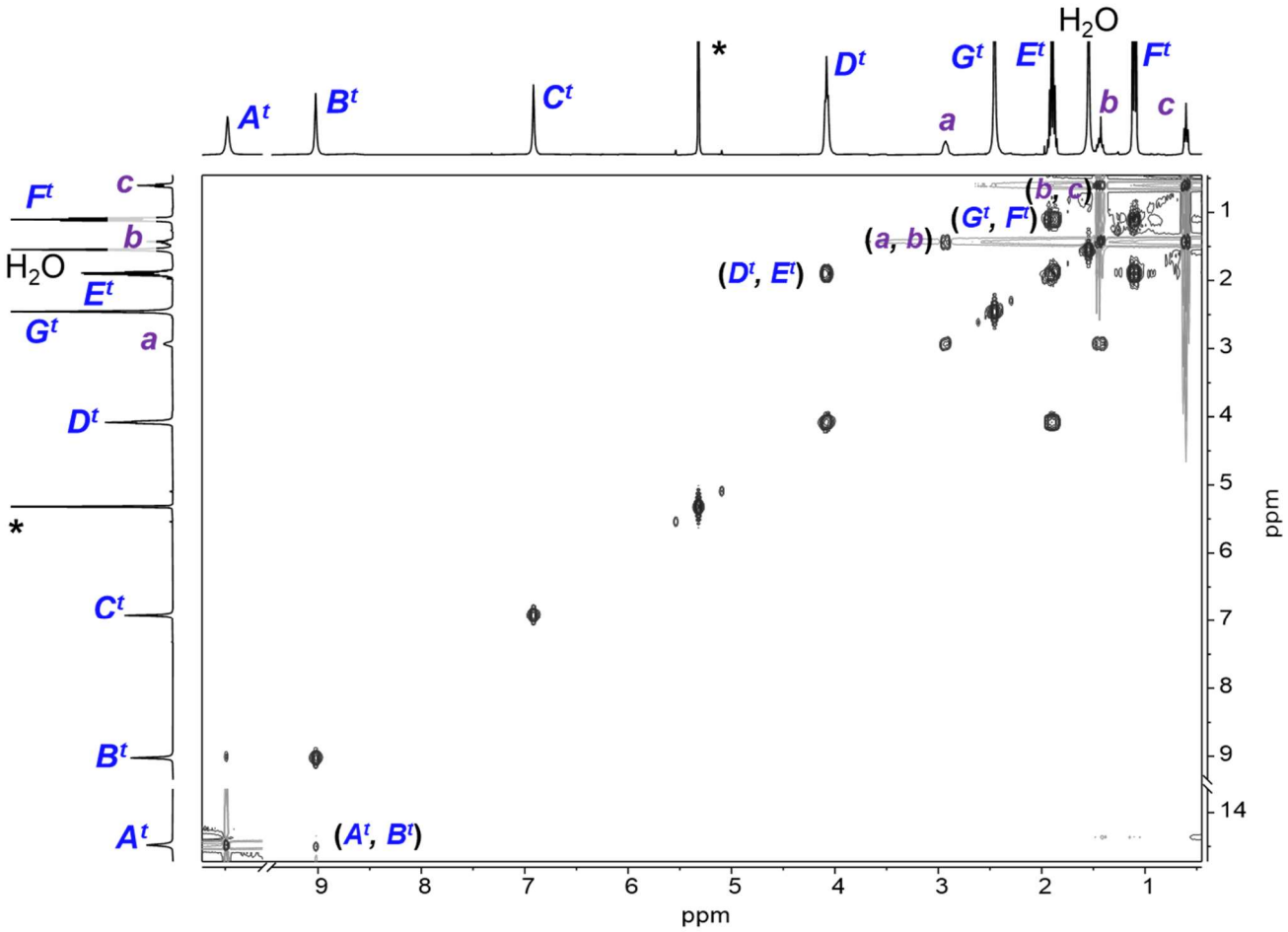


**Figure S26.** Partial $^{1}$H-$^{1}$H COSY NMR spectrum (400 MHz, DCM-$d_2$, 25 °C) of **1+DPA**$^{+}$. * = $CDHCl_2$.

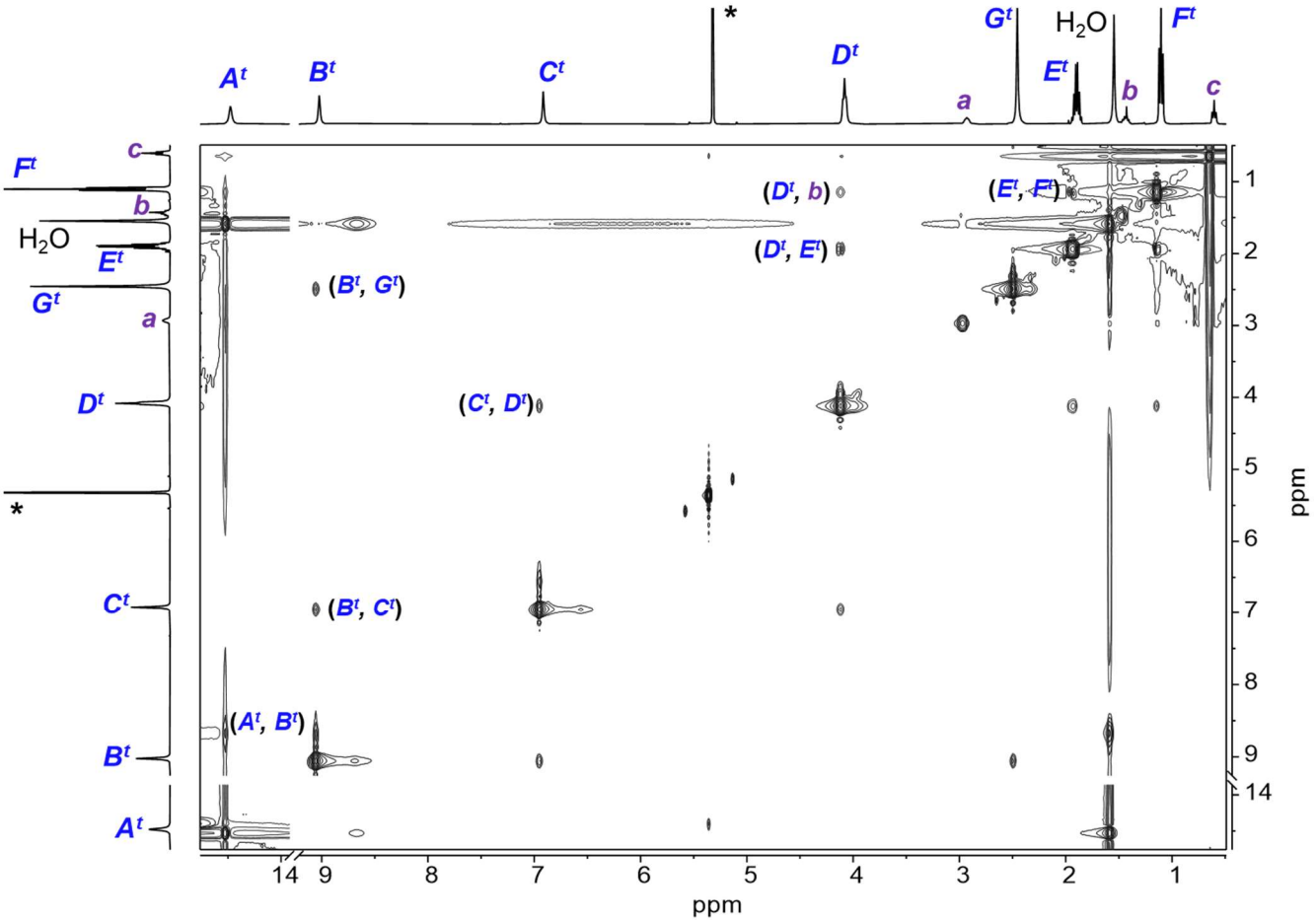


**Figure S27.** $^1$H-$^1$H NOESY NMR spectrum (400 MHz, DCM-$d_2$, 25 °C) of **1+DPA**$^+$. * = $CDHCl_2$.

## *VT-NMR Experiments*

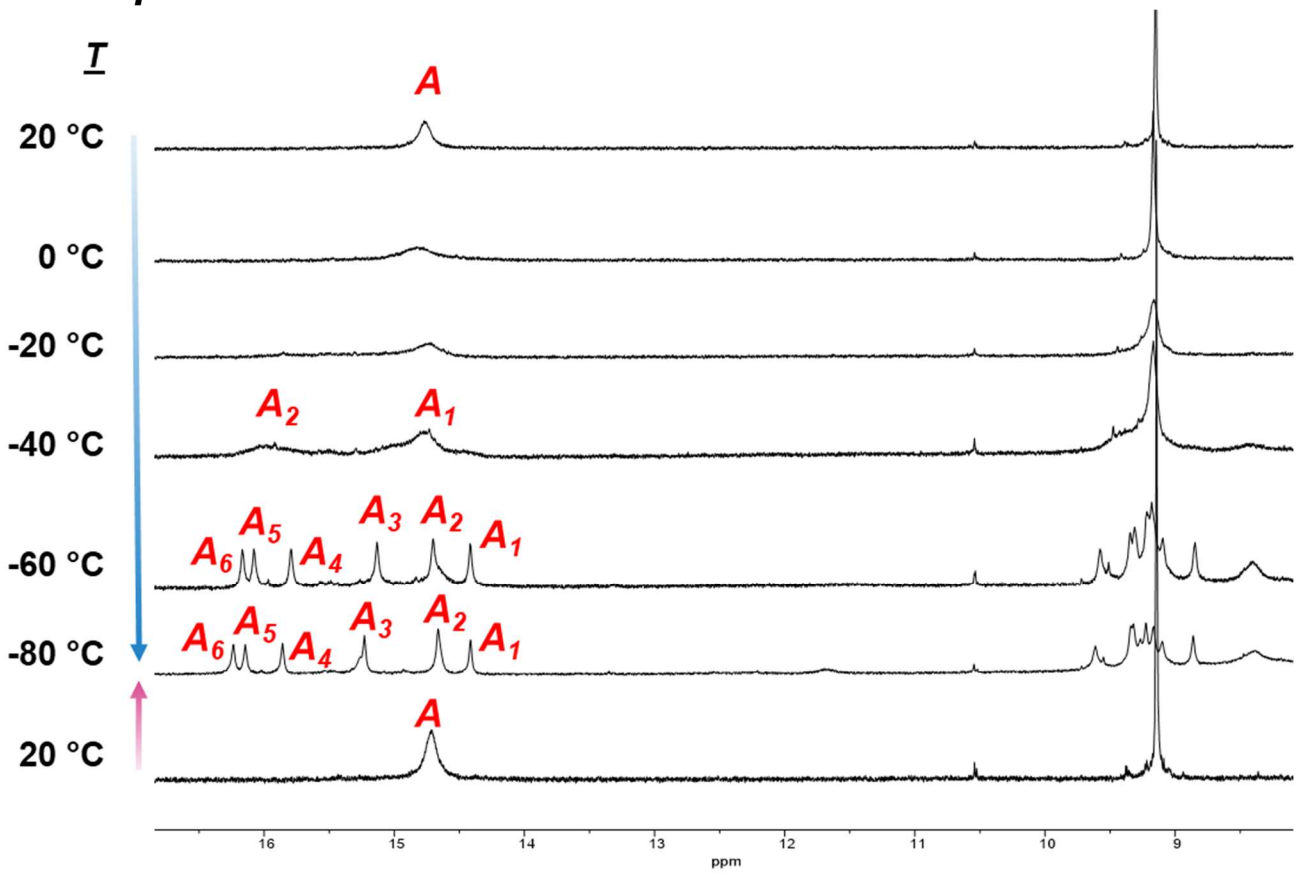


**Figure S28.** Stacked VT $^{1}$H NMR spectra (400 MHz, THF-$d_8$) for **1+DPA**$^{+}$ cooled from 20 to -80 °C, then warmed back to 20 °C.

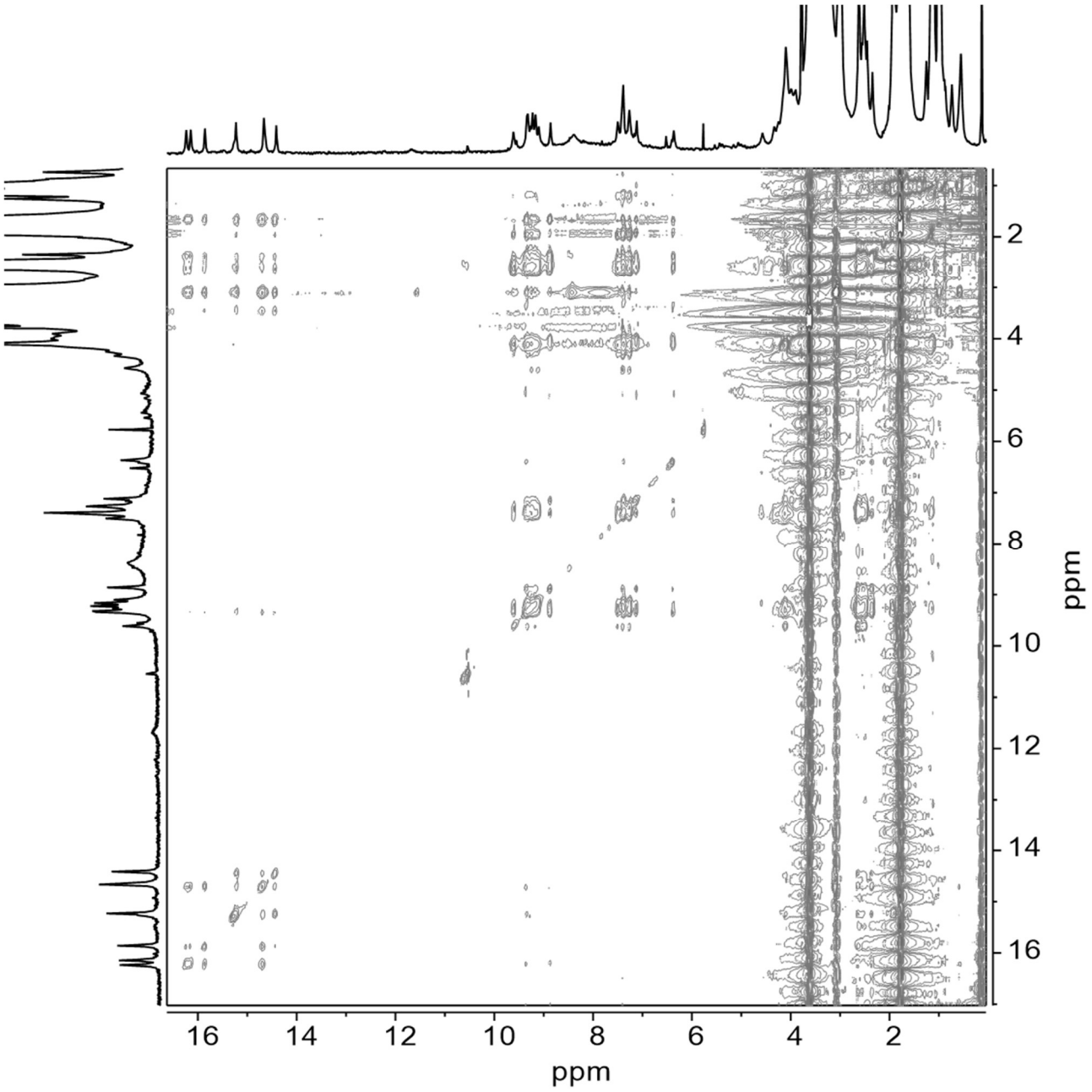


**Figure S29.** Partial $^{1}$H-$^{1}$H NOESY NMR spectrum (400 MHz, THF-$d_8$) of **1+DPA**$^{+}$ taken at -80 °C. Due to large number of overlapping signals, assignment was not possible.

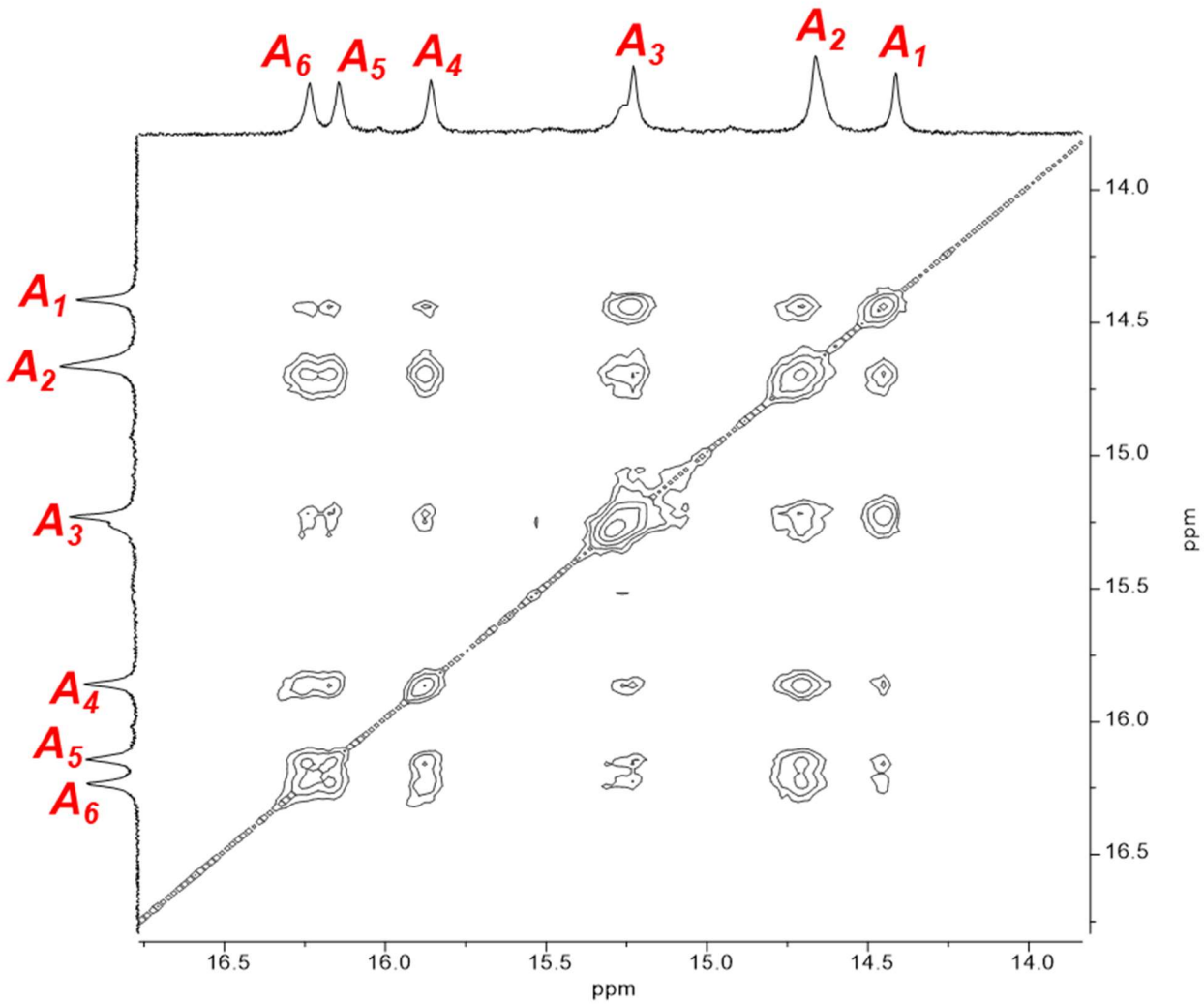


**Figure S30.** Partial $^{1}$H-$^{1}$H NOESY NMR spectrum (400 MHz, THF-$d_8$) for **1+DPA**$^{+}$ taken at –80 °C.

At -40 °C a new peak is observed ($A_{2'}$), which is likely the external complex, because of its similarity in chemical shift to those seen for other external guests (**DBA**$^{+}$ and **DXA**$^{+}$). Once the system is further cooled (-60 °C) these two signals split into at least six distinguishable signals, all with equal integration. $^{1}$H-$^{1}$H EXSY NMR shows cross peaks between all signals, implying the chemical species slowly interconvert at -60 °C; from computational analysis it seems these compounds are different tautomers of **1⊃DBA**$^{+}$.

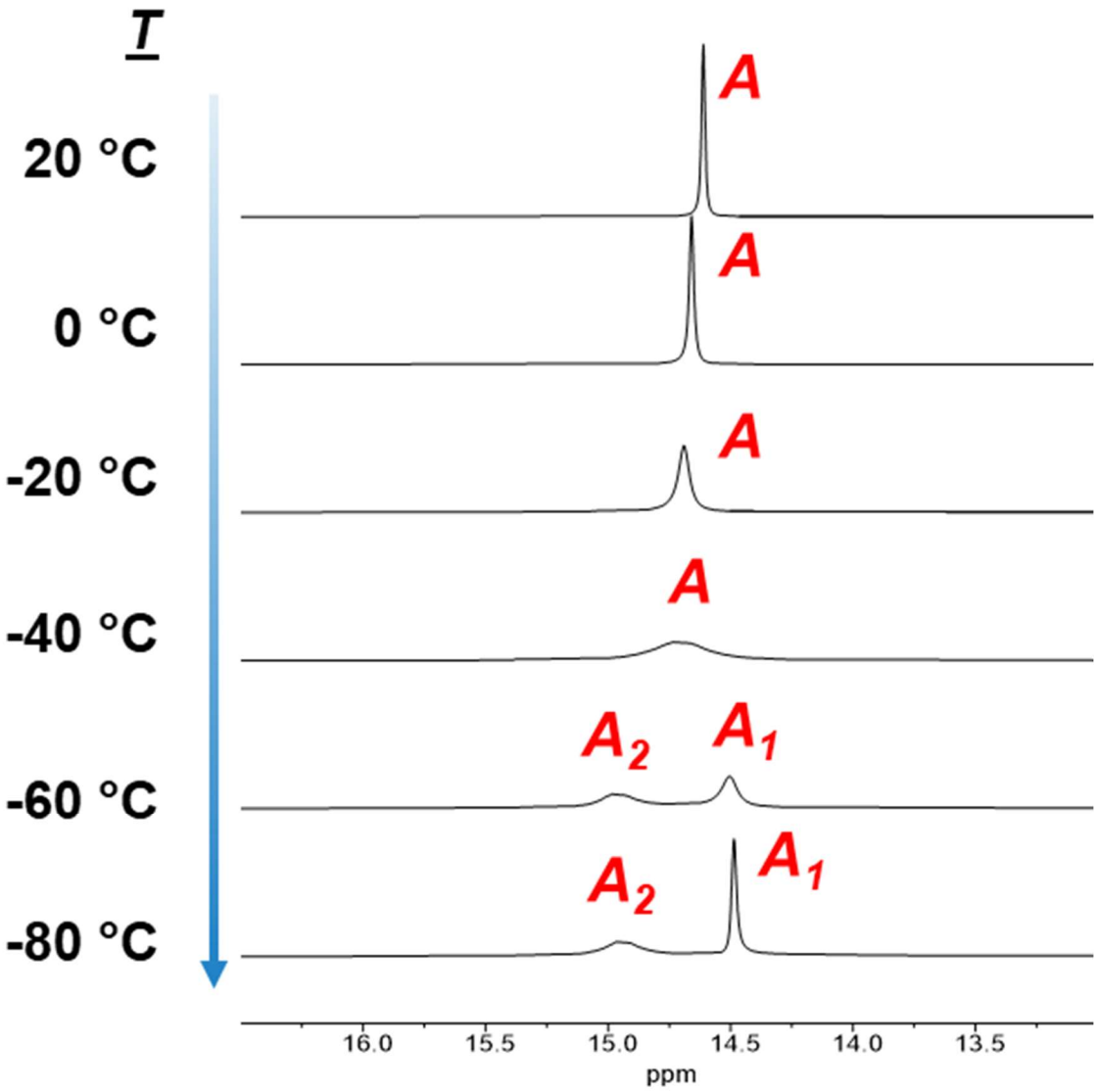


**Figure S31.** Stacked partial VT $^{1}$H NMR spectra (400 MHz, DCM-$d_2$) for **1+DPA**$^{+}$ from 20 to -80 °C.

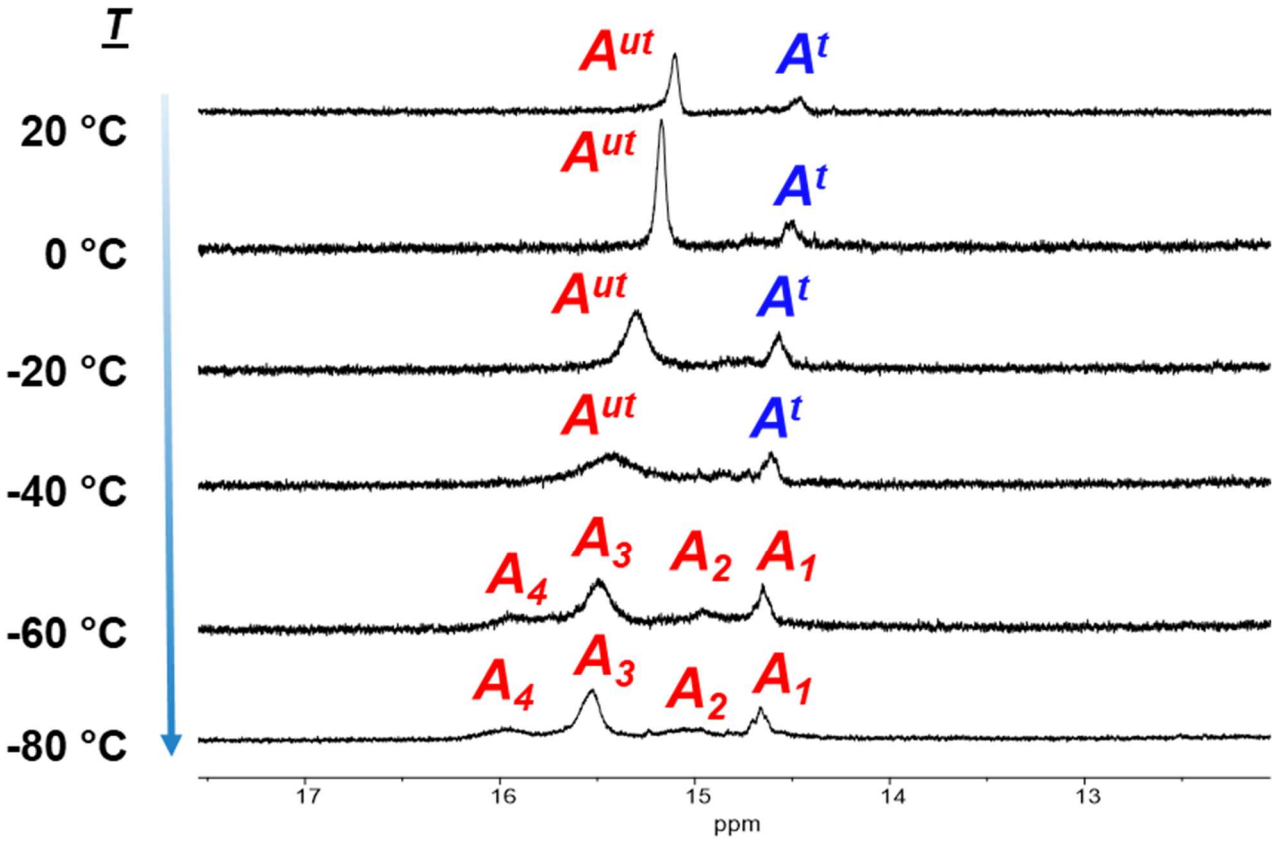


**Figure S32.** Stacked partial VT $^{1}$H NMR spectra (400 MHz, THF-$d_8$) for **1+DBA**$^{+}$ from 20 to -80 °C.

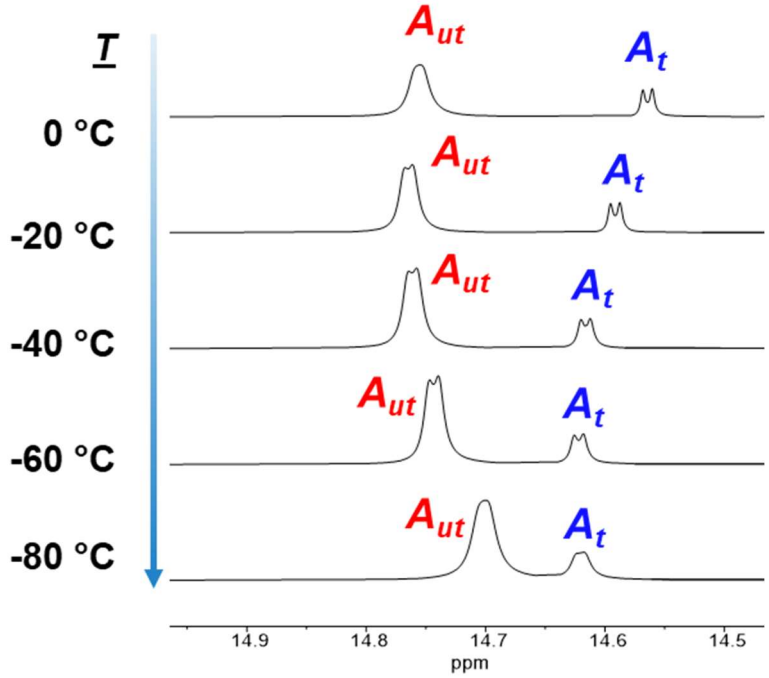


**Figure S33.** Stacked partial VT $^{1}$H NMR spectra (400 MHz, DCM-$d_2$) for **1+DBA**$^{+}$ from 0 to -80 °C.

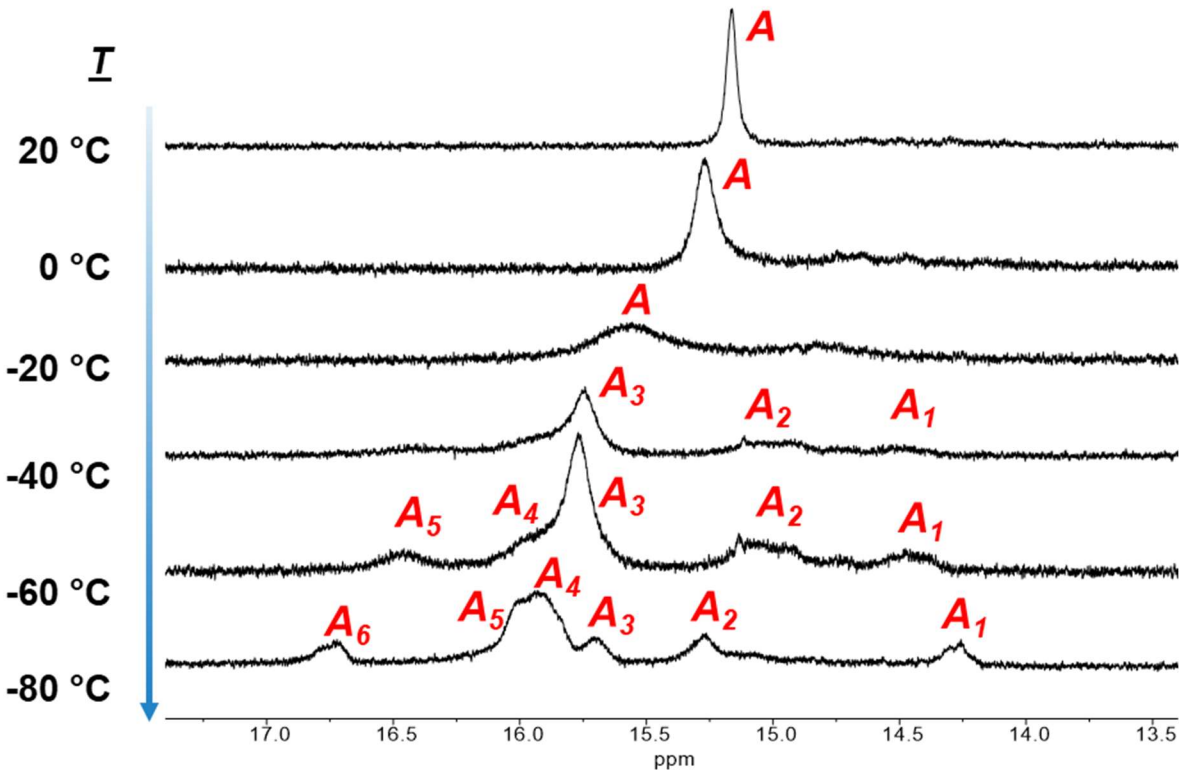


**Figure S34.** Stacked partial VT $^{1}$H NMR spectra (400 MHz, THF-$d_8$) for **1+DXA**$^{+}$ from 20 °C to -80 °C.

## *NMR titrations*

The association constant ($K_{asso}$) for **1+DPA**$^{+}$ was calculated from the binding isotherm using the titration method outlined by Thordarson.[9] Originally, we attempted the titration experiments with THF-$d_8$ but due to precipitation even at very low concentrations (0.5 mM), we could not calculate an accurate $K_{asso}$. Because guest molecules **DPA**·$PF_6$ and **DXA**·$PF_6$ are only sparingly soluble in DCM-$d_2$, we opted to use minimal amounts of MeCN-$d_3$ to dissolve the guest.

Based on the results of the titration, many different stoichiometries are possible. With the low solubility of these complexes making the continuous variation method not feasible (See below on page 49) we used tools provided by supramolecular.org to fit obtained titration data with mathematical models for 1:1, 1:2, and 2:1 complexes. Those that resulted in the lowest error (%) were considered the dominant host-guest complexes, which are discussed below. However, these data are not relevant in determining the $K_{asso}$, as these systems assume just one type of host-guest complex is present in solution.

**1+DPA$^+$ NMR titration in DCM-$d_2$**

A solution of **1** (5.82 x $10^{-4}$ mmol, 1.46 mM) in DCM-$d_2$ (400 µL), contained in an NMR tube, was titrated with **DPA**·$PF_6$ (50 mM, MeCN-$d_3$). NMR data was collected at 25 °C. Calculated association constants and the respective errors are shown below in Table S1. From all tested models, the data set fits well to a 2:1 (non-cooperative) system. However, we discarded this result; such stoichiometry is unlikely given the number of recognition sites present in the guest's structure.

**Table S1.** Association constants with binding stoichiometries found for **1+DPA$^+$.**

| Type of binding (host/guest) | Association constant ($K_{asso}$, $M^{-1}$) | Error (%) |
|---|---|---|
| 1:1 (none) | 4.46 x $10^6$ | ± 2824 |
| 1:2 (none) | Fit failed | N.A. |
| 1:2 (non-cooperative) | Fit failed | N.A. |
| 1:2 (additive) | $K_{11}$ = 1.46 x $10^6$<br>$K_{12}$ = -2.87 | $K_{11}$ = ± 1237<br>$K_{12}$ = ± -224 |
| 1:2 (statistical) | 3.39 x $10^5$ | ± 986 |
| 2:1 (none) | Fit failed | N.A. |
| **2:1 (non-cooperative)** | **2.59 x $10^4$** | **± 19** |
| 2:1 (additive) | $K_{11}$ = 6.74 x $10^4$<br>$K_{12}$ = 338 | $K_{11}$ = ± 207<br>$K_{12}$ = ± 17 |
| 2:1 (statistical) | Fit failed | N.A. |

All calculations were done using the Nelder-Mead method.

A double reciprocal plot of these collected data (Figure S44) reveals that there are more than two species coexisting in the media, which precludes the estimation of a $K_{asso}$ under these experimental conditions.

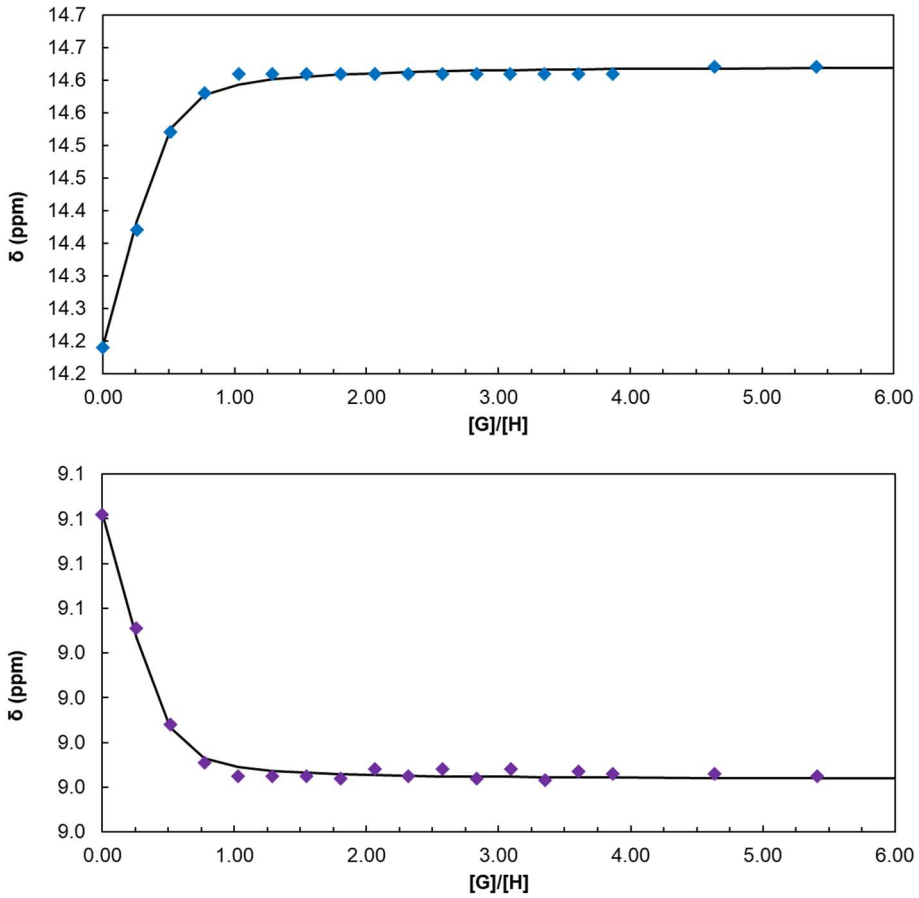


**Figure S35.** Binding isotherm of **1+DPA**$^{+}$ using protons *A* and *B* in DCM-$d_2$ 2:1 (host/guest) non-competitive.

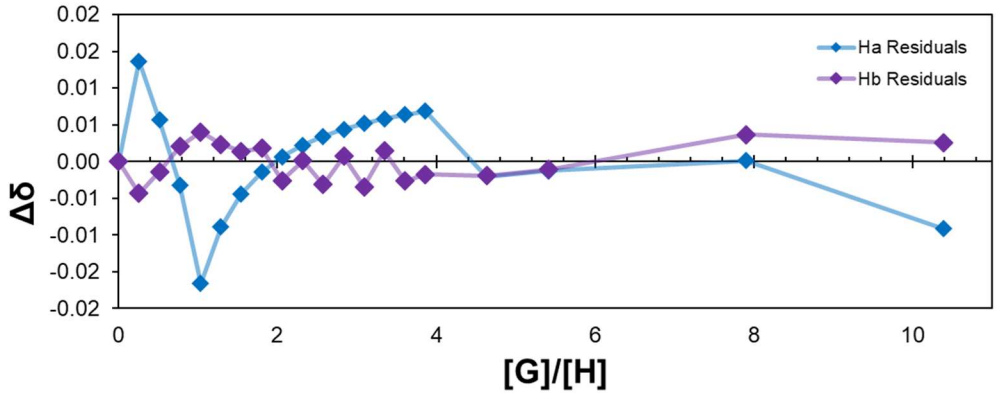


**Figure S36.** Residuals for the binding isotherm of **1+DPA**$^{+}$ using protons *A* and *B* in DCM-$d_2$.

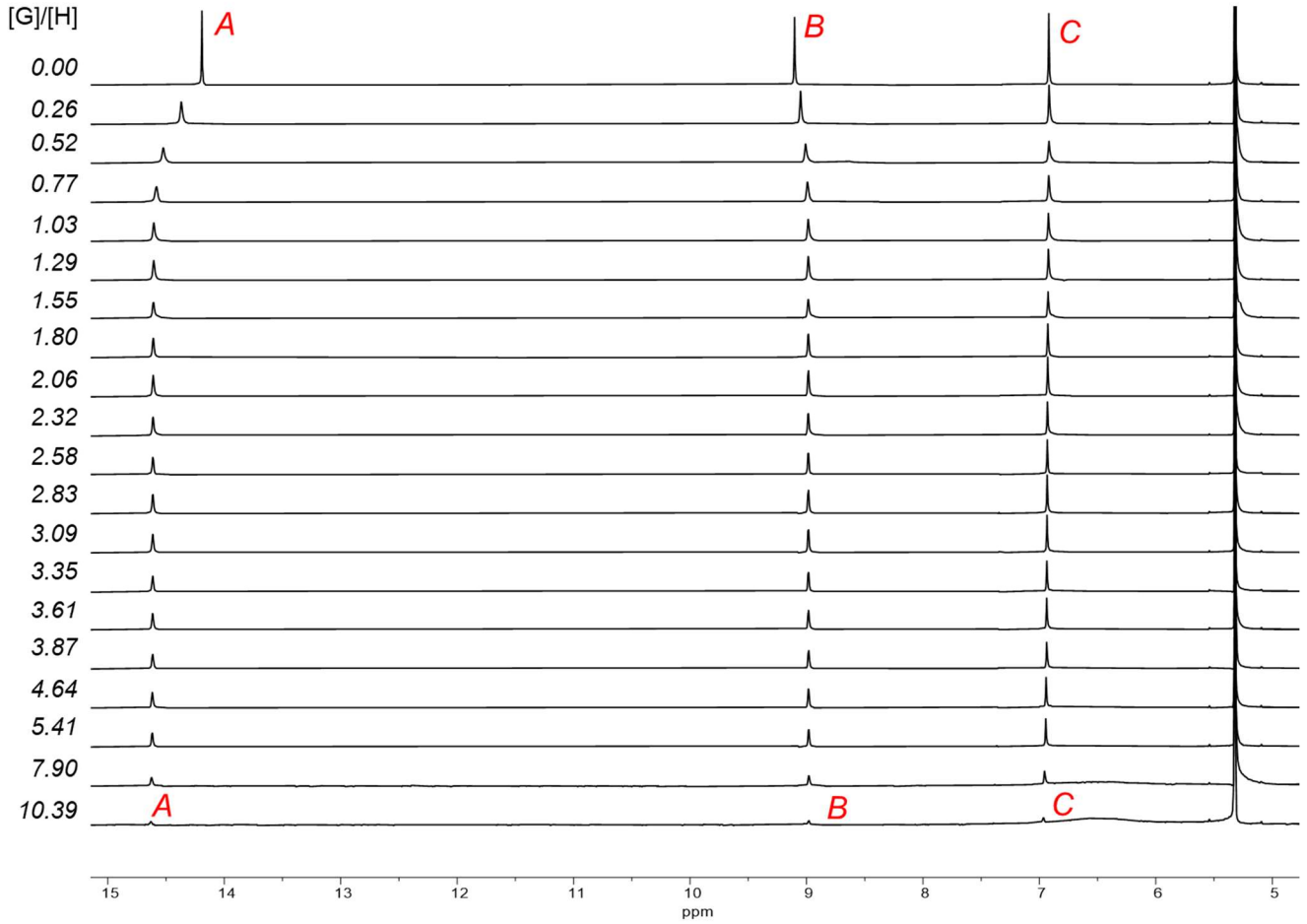


**Figure S37.** Stacked $^{1}$H NMR (400 MHz, DCM-$d_2$, 25 °C) showing the titration of **1** with **DPA**$^{+}$.

### 1+DXA$^+$ NMR titration in DCM-$d_2$

To an NMR tube containing **1** (5.82 x $10^{-4}$ mmol, 1.46 mM) in DCM-$d_2$ (400 µL) was titrated **DXA**·$PF_6$ (50 mM, MeCN-$d_3$). NMR data were collected at 25 °C. Calculated association constants and the respective errors are shown below in Table S2, with $K_{asso}$ = 4.11 x $10^3$ $M^{-1}$ ± 10.3 % being the dominant stoichiometry.

**Table S2.** Association constants with binding stoichiometries found for **1+DXA$^+$.**

| Type of binding (host/guest) | Association constant ($K_a$, $M^{-1}$) | Error (%) |
|---|---|---|
| **1:1 (none)** | **4.11 x $10^3$** | **± 10** |
| 1:2 (none) | $K_{11}$ = 1.53 x $10^4$<br>$K_{12}$ = 104 | $K_{11}$ = ± 17<br>$K_{12}$ = ± 15 |
| 1:2 (non-cooperative) | 4.32 x $10^3$ | ± 17 |
| 1:2 (additive) | $K_{11}$ = 9.93 x $10^3$<br>$K_{12}$ = 20.2 | $K_{11}$ = ± 17<br>$K_{12}$ = ± 20 |
| 1:2 (statistical) | 4.22 x $10^3$ | ± 120 |
| 2:1 (none) | Fit failed | N.A. |
| 2:1 (non-cooperative) | 1.37 x $10^5$ | ± 21 |
| 2:1 (additive) | $K_{11}$ = 2.66 x $10^3$<br>$K_{12}$ = 56.3 | $K_{11}$ = ± 26<br>$K_{12}$ = ± 80 |
| 2:1 (statistical) | Fit failed | N.A. |

All calculations were done using the Nelder-Mead method.

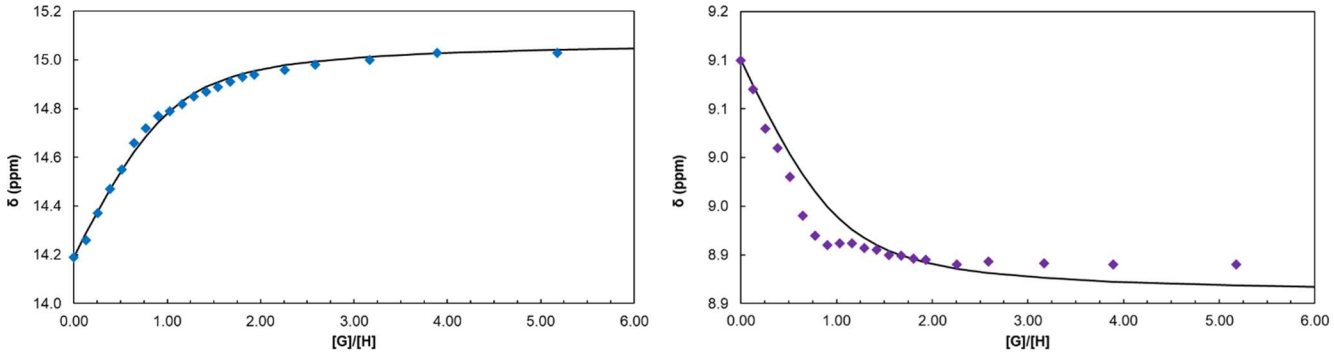


**Figure S38.** Binding isotherm of **1+DXA$^+$** using protons *A* and *B* in DCM-$d_2$ 1:1 (host/guest).

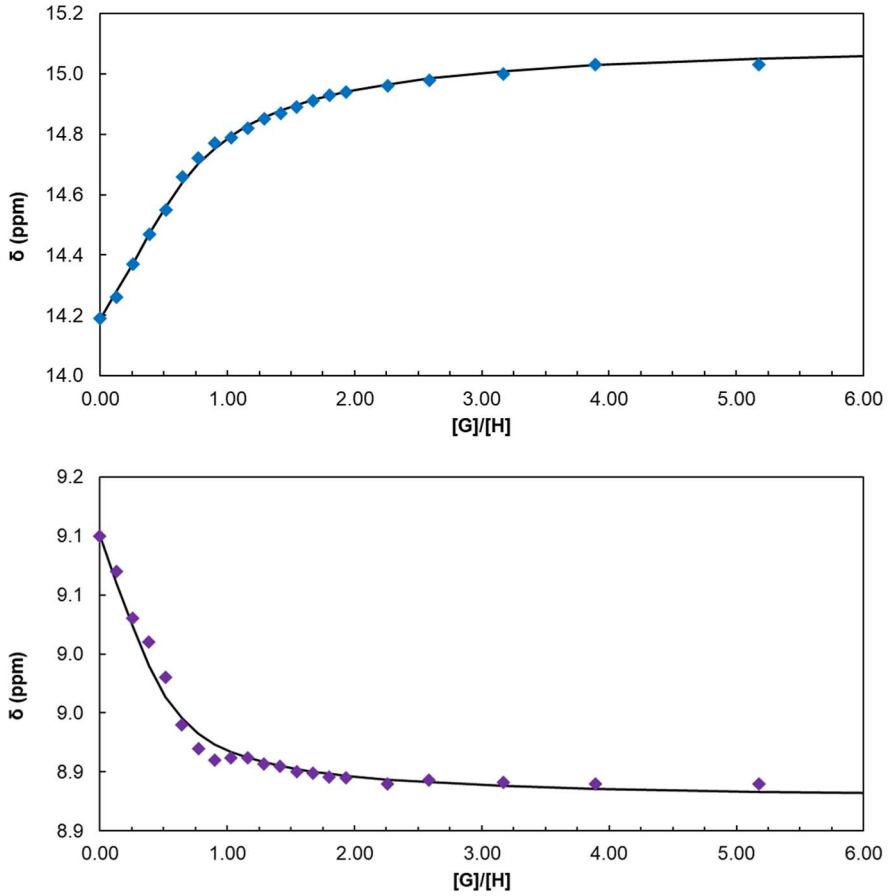


**Figure S39.** Binding isotherm of **1+DPA**$^{+}$ using protons *A* and *B* in DCM-$d_2$ 1:2 (host/guest) non-competitive.

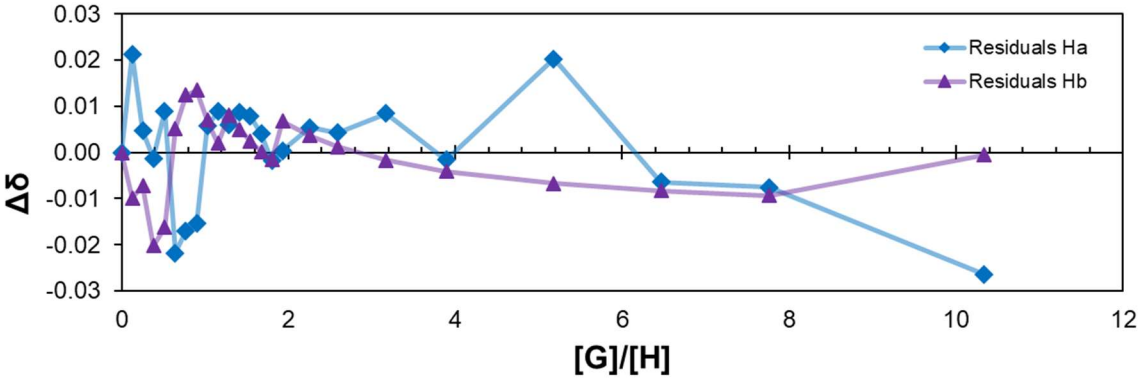


**Figure S40.** Residuals for the binding isotherm of **1+DPA**$^{+}$ using protons *A* and *B* in DCM-$d_2$ 1:2 (host/guest) non-competitive.

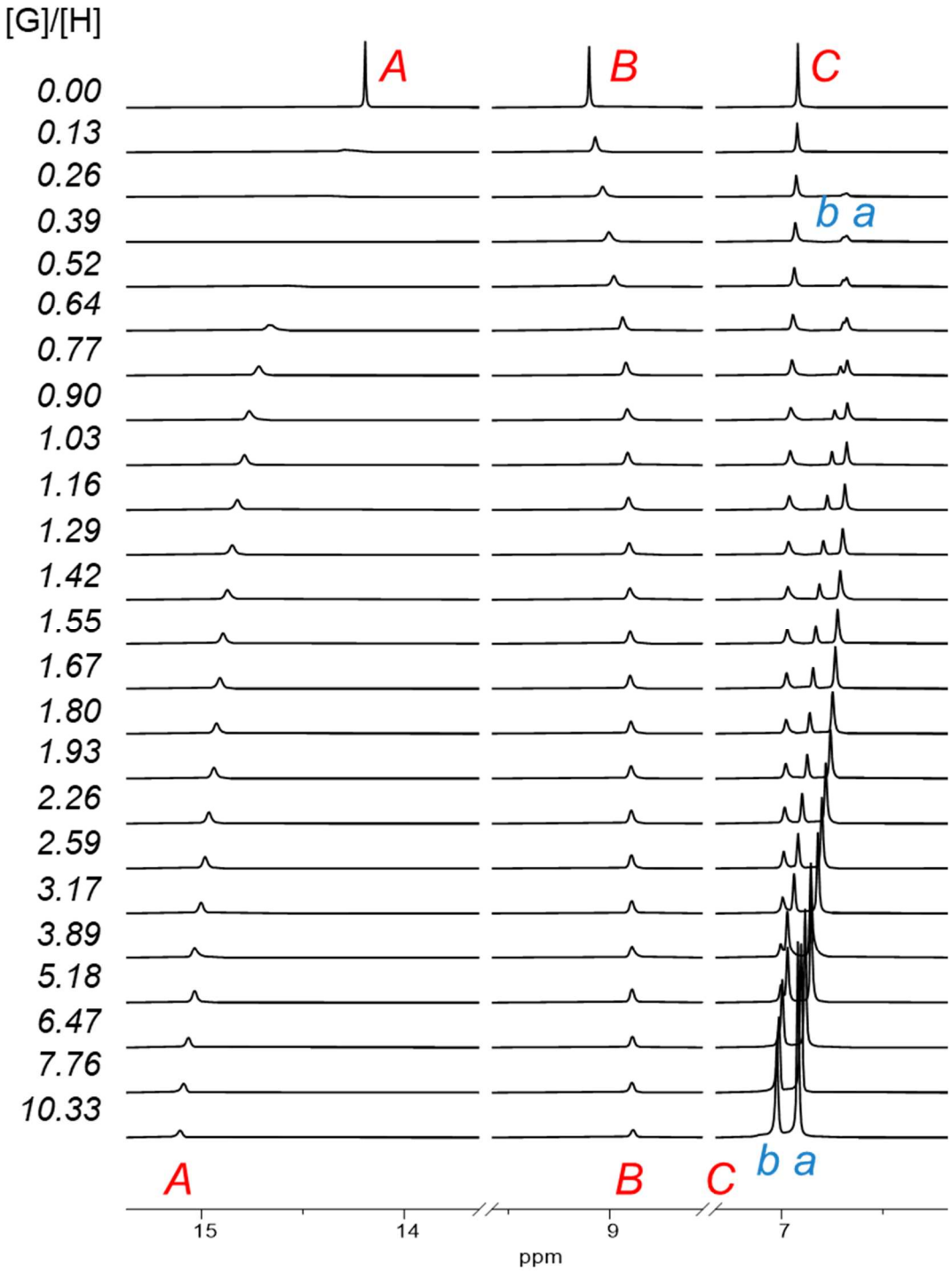


**Figure S41.** Partial stacked $^{1}$H NMR (400 MHz, DCM-$d_2$, 25 °C) showing the titration of **1** with **DXA**$^{+}$.

## *Method of continuous variations*

The method of continuous variation is a common technique used to determine binding stoichiometries (*i.e.* 1:1, 2:1, 3:1, etc.) in host-guest systems. We attempted this method using **1+DPA**$^+$ and **1+DXA**$^+$ in THF-$d_8$ and DCM-$d_2$ but were unable to obtain reliable results due to the low solubility of the host-guest complex and the large solubility differences of **1** and the cationic guest molecules. **1+DPA**$^+$ precipitates over time when DCM-$d_2$ or THF-$d_8$ are used as solvents at concentrations suitable for NMR analysis. Even at very low concentrations (0.1 mM) all complexes precipitated over time.

The corresponding Job plot (Figure S42), obtained by UV-vis spectroscopy, did not show a dominant stoichiometry for **1+DPA**$^+$. While we attempted several conditions to get a reliable result, none of these experiments was successful.

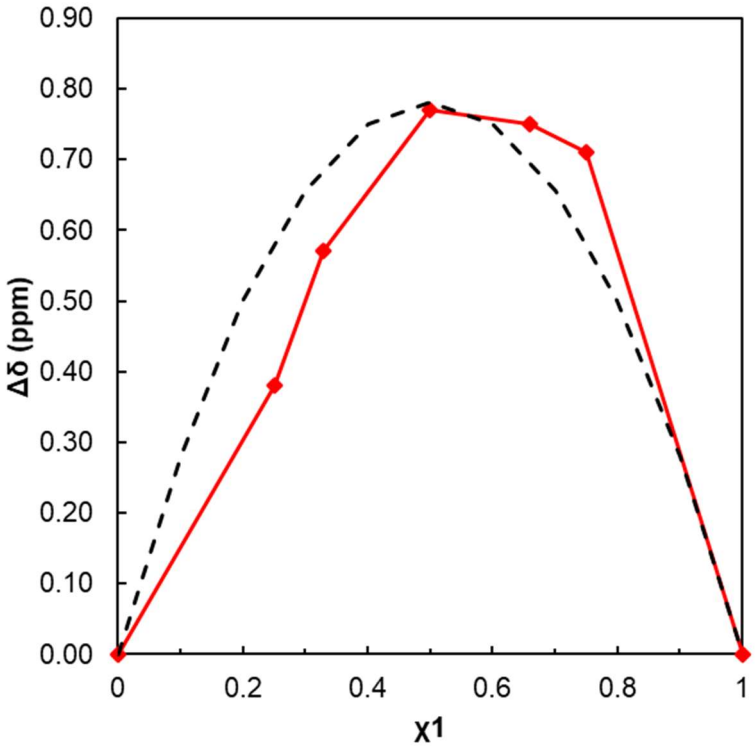


**Figure S42.** Job plot derived from $^1$H NMR data for **1+DPA**$^+$ in THF-$d_8$ (red) and a hypothetical idealized curve for a 1:1 binding isotherm (black dashed).

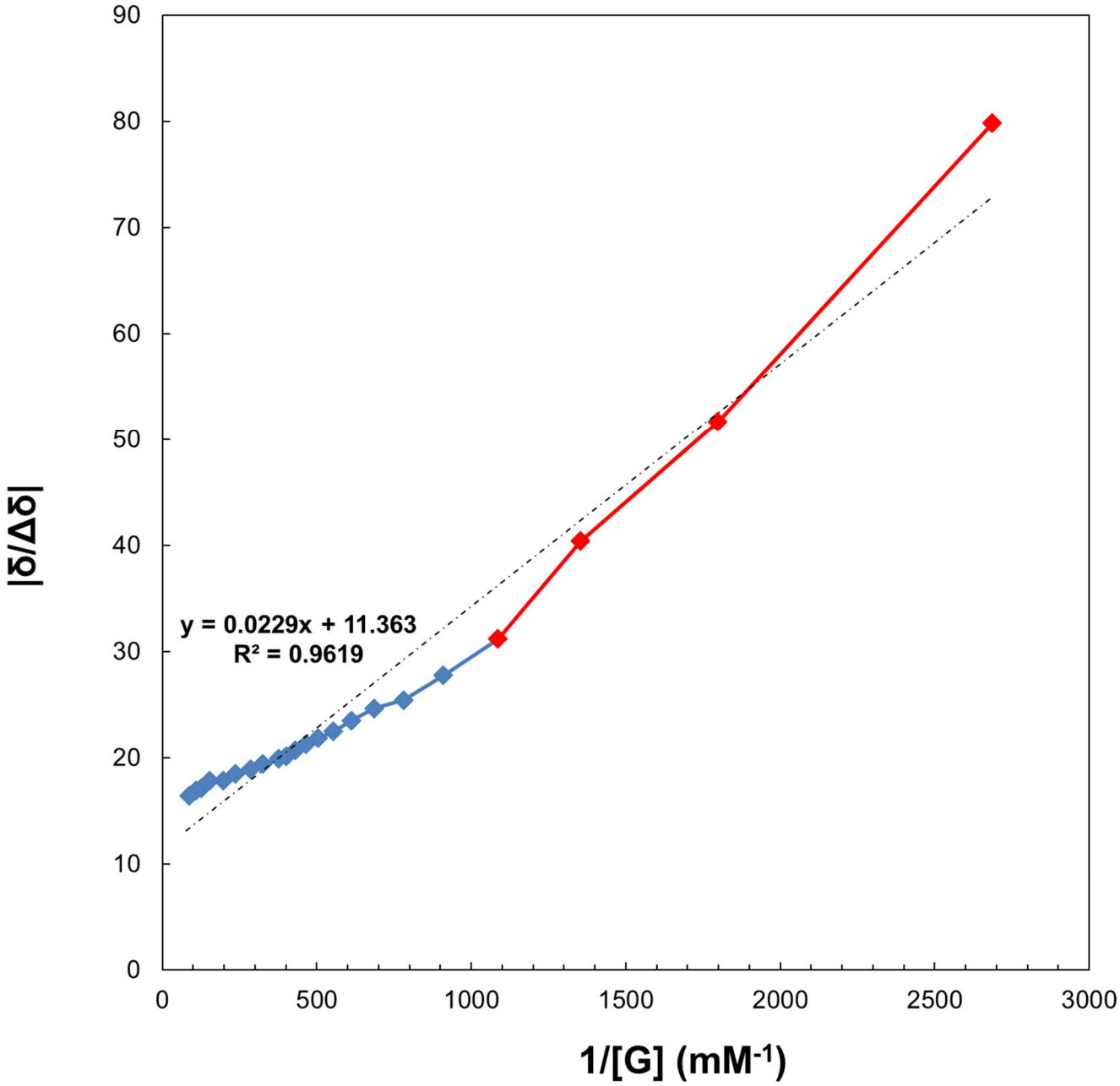


**Figure S43**. Double reciprocal graph for the titration data of **1+DXA⁺**. The data fit reasonably well to a line, which suggests the existence of only one host:guest stoichiometry.

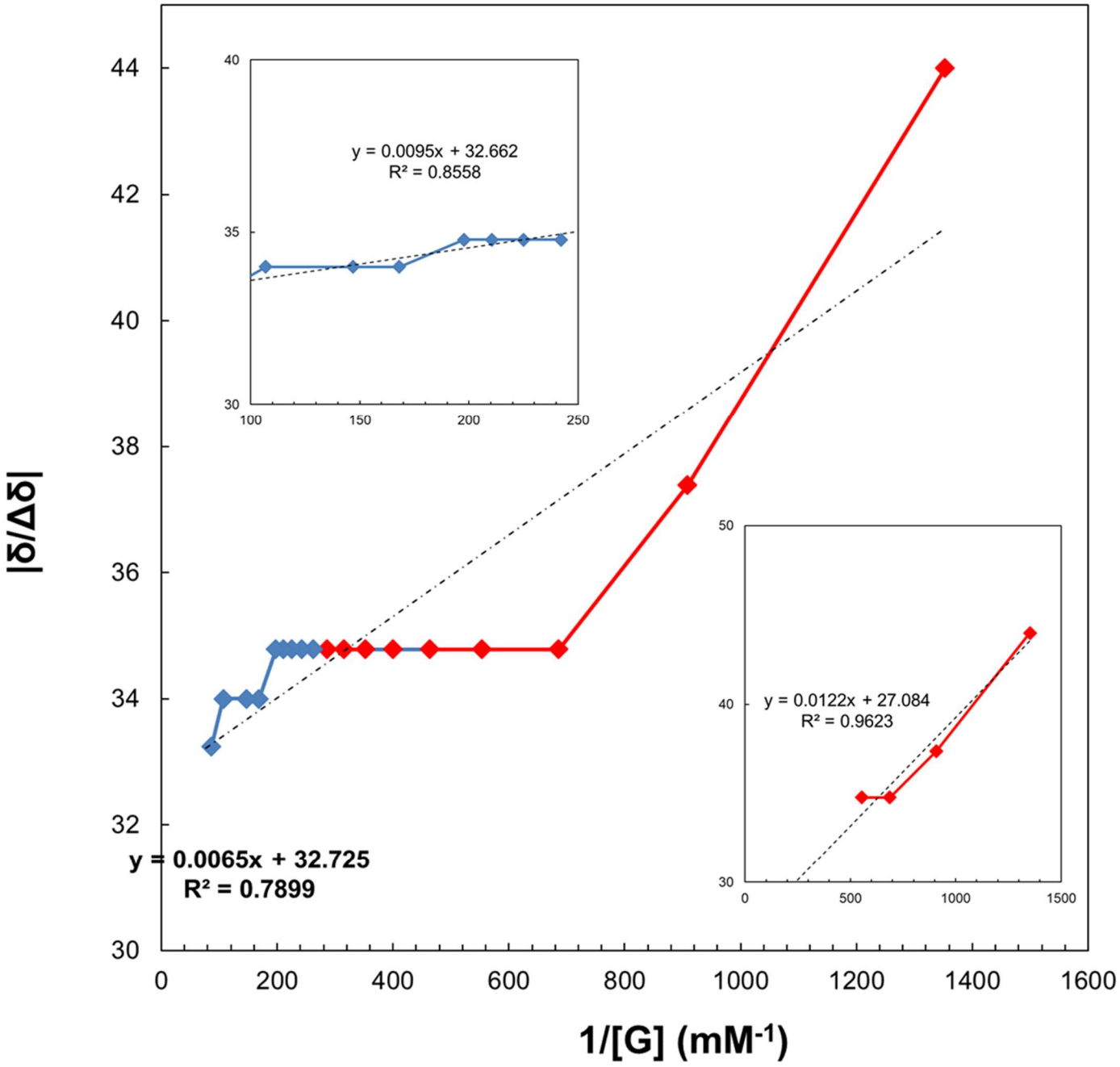


**Figure S44.** Double reciprocal graph for the titration data of **1+DPA$^{+}$**. The data do not fit well to a line, suggesting that more than one complex is present in solution.

## *DBA$^+$ as a template in the formation of Schiff-base macrocycles*

In this section we highlight how the **DBA**$^+$ template reactions were conducted.

**Method for the template assisted synthesis of Schiff-base macrocycle using DBA$^+$**

A stock solution of **DBA**·$PF_6$ was prepared (25 mM, MeCN-$d_3$). Stock solutions of building blocks *o*-phenylenediamine, and **5** were prepared (50 mM, DCM-$d_2$). Compound **5** (36 µL, mmol) was added to an NMR tube, followed by **DBA**·$PF_6$ (7 µL, mmol). The mixture was then diluted with DCM-$d_2$ (228 µL) and MeCN-$d_3$ (293 µL), and finally the amine (36 µL, mmol) was added. The solution immediately turned from yellow to red. The final solution obtained had a DCM-$d_2$/MeCN-$d_3$ ratio of 1:1, v/v, with a final concentration of *ca.* 3 mM, with respect to **5**.

Solutions were stored in the dark at room temperature and analyzed *via* NMR spectroscopy.

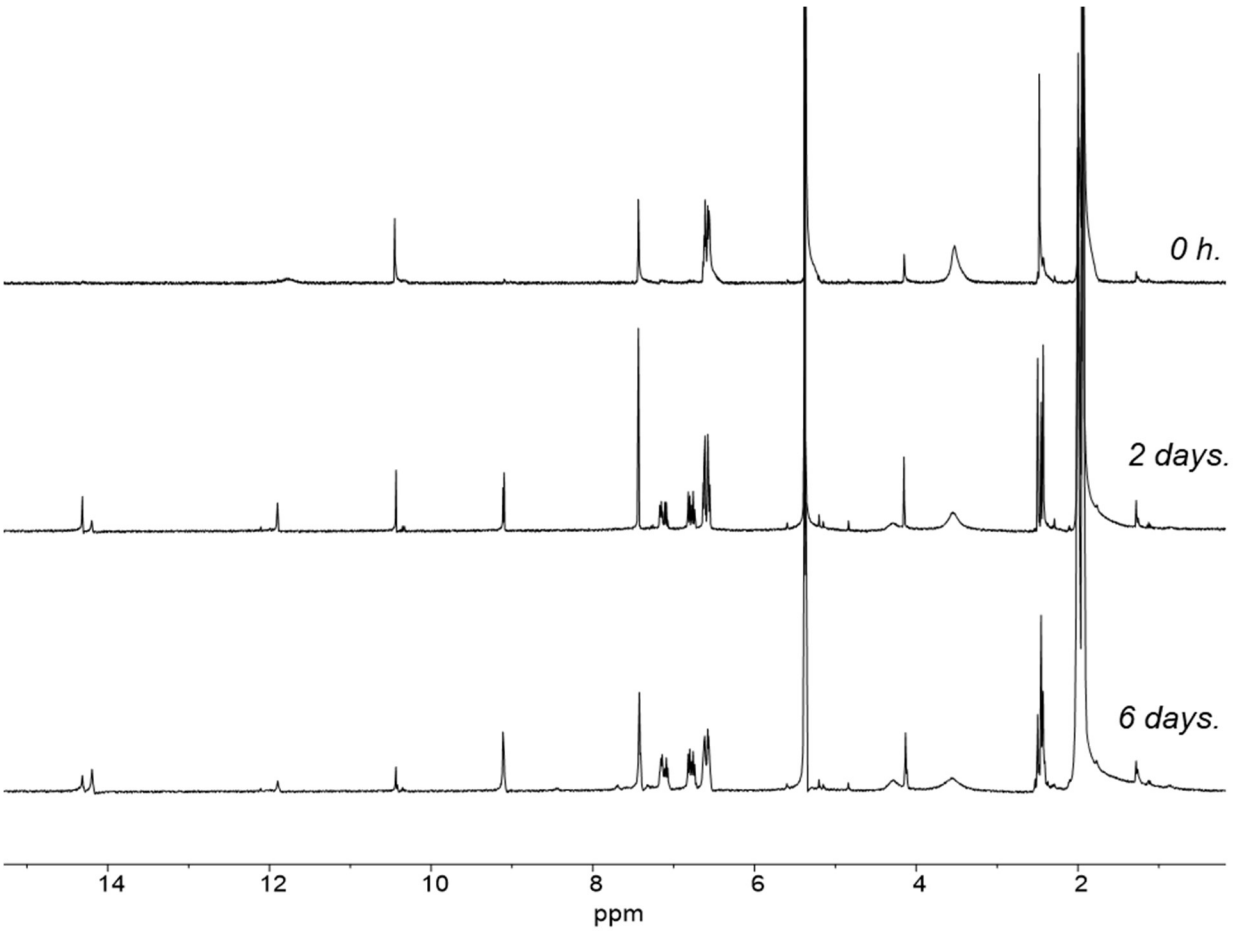


**Figure S45.** Stacked $^1$H NMR spectra (400 MHz, DCM-$d_2$/MeCN-$d_3$, 25 °C) showing the conversion of **5** and *o*-phenylenediamine to give a Schiff base macrocycle in the presence of 10 mol% **DBA**$^+$ over time.

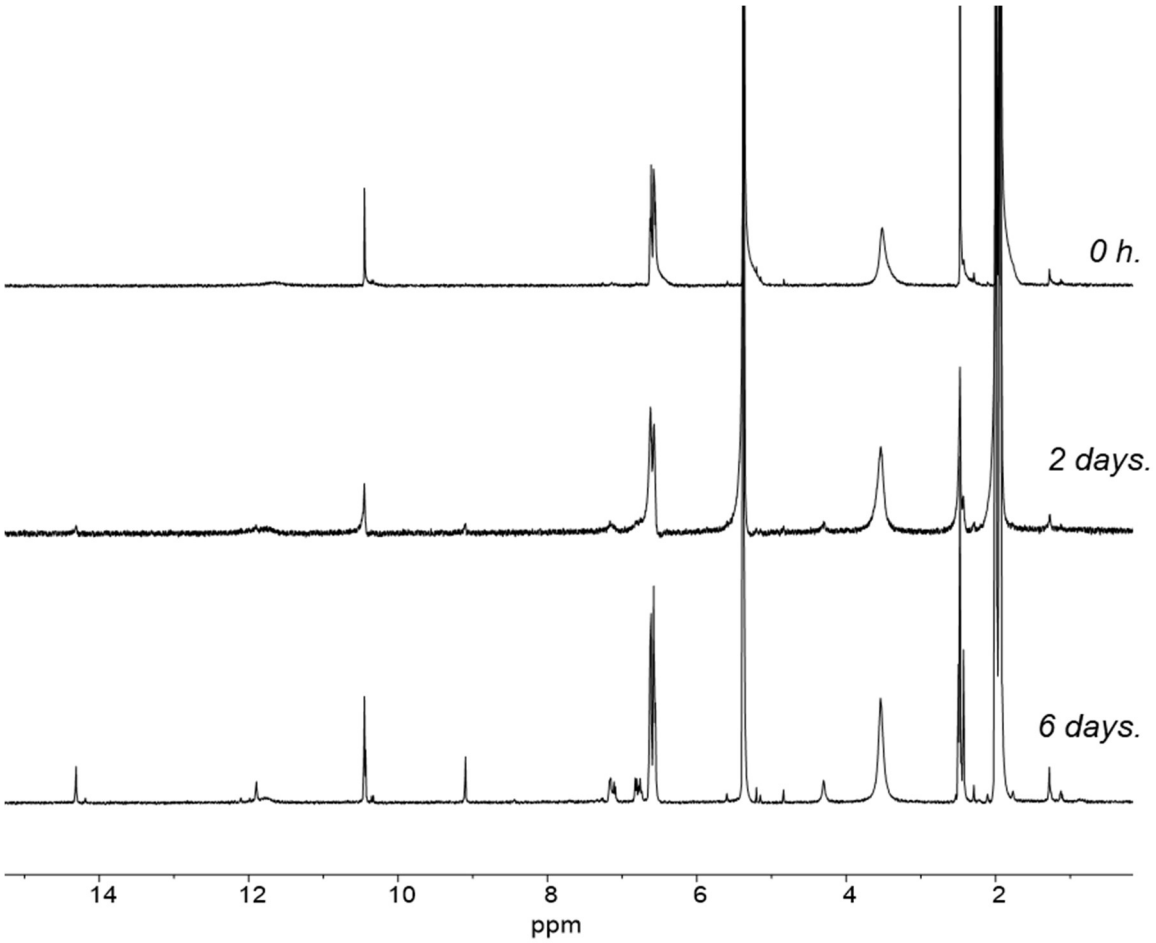


**Figure S46.** Stacked $^1$H NMR spectra (400 MHz, DCM-$d_2$/MeCN-$d_3$, 25 °C) showing the conversion of **5** and *o*-phenylenediamine to a Schiff base macrocycle in the absence of additive (control) over time.

**Template assisted synthesis of 1 using DBA$^+$ (10 mol%) - Mainly DCM-$d_2$*** 

Under an $N_2$ atmosphere, stock solutions of compounds **5** (50 mM, DCM-$d_2$), **6** (50 mM, DCM-$d_2$), and **DBA**·$PF_6$ (25 mM, MeCN-$d_3$) were prepared. Compound **5** (100 µL, 5.84 µmol) was added carefully to a valve-locked NMR tube, followed by **DBA**·$PF_6$ (10 µL, 0.58 µmol). The mixture was diluted with solvent DCM-$d_2$ (500 µL). Finally, compound **6** (100 µL, 5.84 µmol) was added, resulting in a color change from yellow to deep red. The final solution obtained contained predominantly DCM-$d_2$ with minimal MeCN-$d_3$, and had a final concentration of *ca.* 7 mM, with respect to **5**. The NMR tubes were sealed and were stored in the dark at room temperature. $^1$H NMR spectra were recorded after 0 h, 1 h, 3 d, and 7 d. After the 7 d, the mixture was dried *in vacuo*, and the crude product was reanalyzed using DMSO-$d_6$ (600 µL).**

**Aside from DCM-$d_2$ and MeCN-$d_3$, above experiments were also conducted using THF-$d_8$. However, decomposition was seen after several days, making analysis difficult.*

***DMSO-$d_6$ is highly coordinating, and results in no host-guest complexes being detectible, which makes analysis of the conversion of **5** and **6** to **1** much simpler.*

Simultaneously, a control sample was also prepared identical to the above procedure, but with no **DBA**·$PF_6$ added.

**Template assisted synthesis of 1 using $DBA^+$ (10 mol%) - DCM-$d_2$/MeCN-$d_3$, 1:1, v/v**

Stock solutions of compounds **5** (50 mM, DCM-$d_2$), **6** (50 mM, DCM-$d_2$), and **DBA**·$PF_6$ (25 mM, MeCN-$d_3$) were prepared under an atmosphere of $N_2$. Compound **5** (100 µL, 5.84 µmol) was added carefully to a valve-sealed NMR tube, followed by **DBA**·$PF_6$ (10 µL, 0.58 µmol). The mixture was diluted with solvent DCM-$d_2$ (200 µL) and MeCN-$d_3$ (300 µL). Finally, compound **6** (100 µL, 5.84 µmol) was added, resulting in a color change from yellow to deep red. The final solution obtained contained predominantly DCM-$d_2$ with minimal MeCN-$d_3$, and had a final concentration of *ca.* 7 mM, with respect to **5**. The NMR tubes were sealed and brought out of the glovebox. Solutions were stored in the dark at room temperature and analyzed via $^1$H NMR spectroscopy after 0 h, 1 h, 3 d, and 7 d (Figure S45). After the 7 d, the solvent was removed *in vacuo*, and the crude product was reanalyzed using DMSO-$d_6$ (600 µL).

Simultaneously, a control sample was also prepared identical to the above procedure, except without **DBA**·$PF_6$.

**Template assisted synthesis of 1 using $DBA^+$ (100 mol%) - DCM-$d_2$/MeCN-$d_3$, 1:1, v/v**

Stock solutions of compounds **5** (50 mM, DCM-$d_2$), **6** (50 mM, DCM-$d_2$), and **DBA**·$PF_6$ (25 mM, MeCN-$d_3$) were prepared under an atmosphere of $N_2$. Compound **5** (100 µL, 5.84 µmol) was added carefully to a valve-capped NMR tube, followed by **DBA**·$PF_6$ (100 µL, 5.84 µmol). The mixture was diluted with solvent DCM-$d_2$ (100 µL) and MeCN-$d_3$ (200 µL). Finally, compound **6** (100 µL, 5.84 µmol) was added, resulting in a color change from yellow to deep red. The final solution obtained contained predominantly DCM-$d_2$ with minimal MeCN-$d_3$, and had a final concentration of *ca.* 8 mM, with respect to **5**. The NMR tubes were sealed and were stored in the dark at room temperature. $^1$H NMR spectra were collected after 0 h, 1 h, 3 d, and 7 d. After 7 d, the solvent was removed *in vacuo*, and the crude product was reanalyzed using DMSO-$d_6$ (600 µL).

Simultaneously, a control sample was also prepared identical to the above procedure, except without **DBA**·$PF_6$.

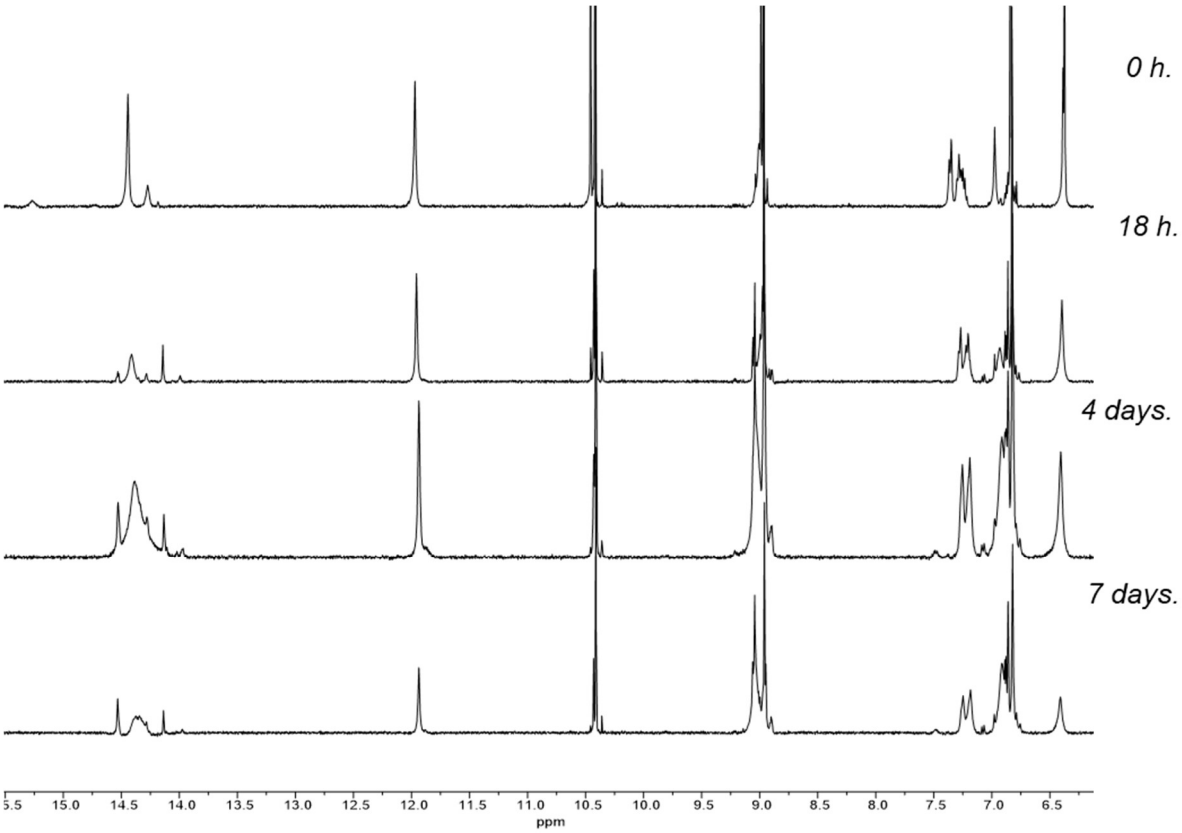


**Figure S47.** Stacked $^{1}$H NMR spectra (400 MHz, DCM-$d_2$/MeCN-$d_3$, 25 °C) showing the conversion of **5** and **6** to **1** in the presence of 10 mol% **DBA**$^{+}$ over time.

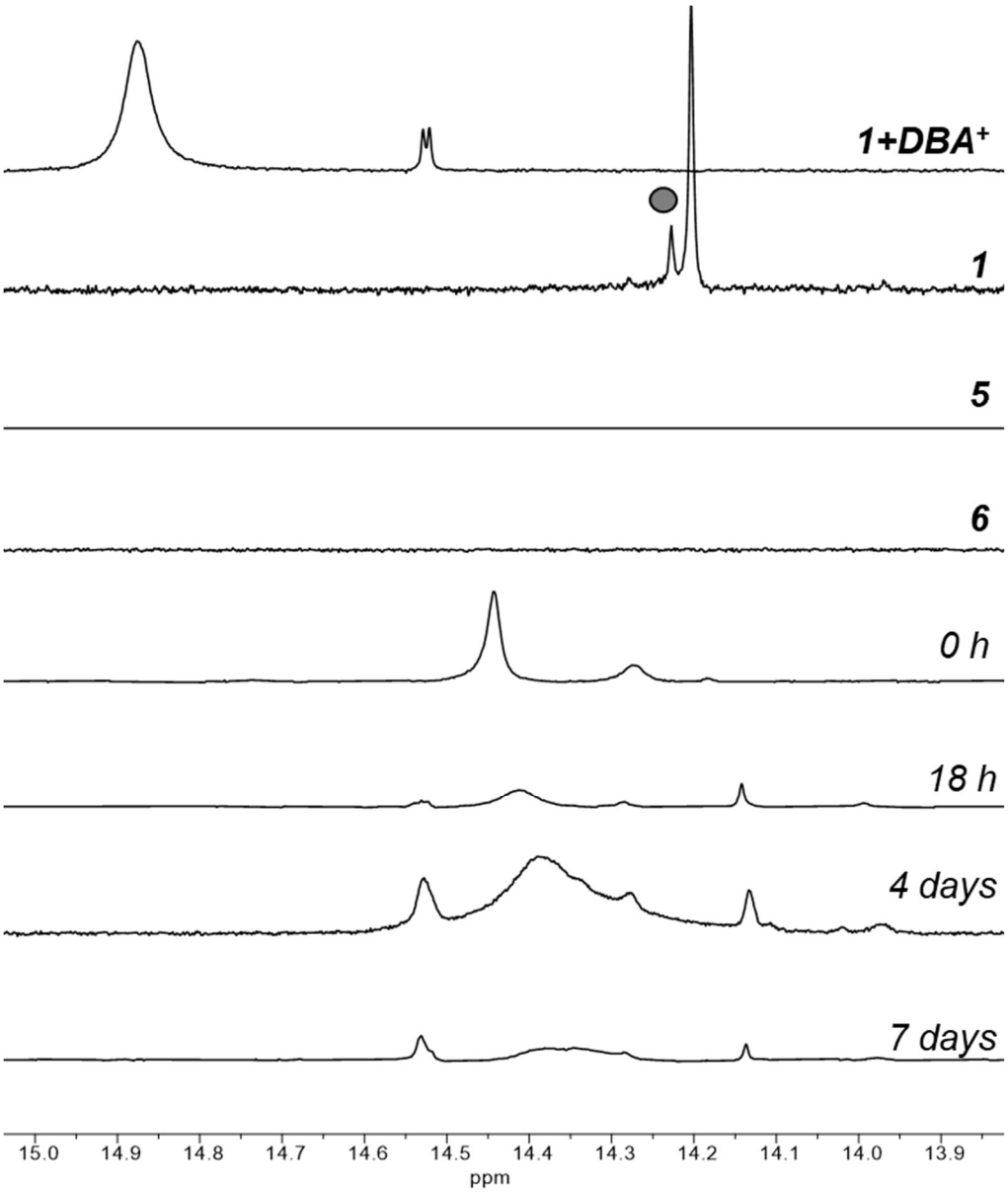


**Figure S48.** Partial stacked $^{1}$H NMR spectra (400 MHz, DCM-$d_2$/MeCN-$d_3$, 25 °C) showing the conversion of **5** and **6** to **1** in the presence of 10 mol% **DBA**$^{+}$ after 0 h, 18 h, 4 days, and 7 days. An impurity is highlighted with a grey circle.

As the reaction progresses, **DBA**$^{+}$ can associate with oligomeric growing chains. Also, as we showed, depending on the ratio of **DBA**$^{+}$ $H_A$ will shift **1+DBA**$^{+}$. Due to these reasons the $^{1}$H NMR spectra becomes very complicated, as illustrated in Figure S47 and Figure S48. In the latter, none of the new signals correspond to **1**, **1+DBA**$^{+}$, or starting materials (**5** and **6**). To circumvent this problem, after 7 d, the solvent was removed *in vacuo* and the sample was redissolved in DMSO-$d_6$, as no host-guest interactions are possible in the highly coordinating solvent. This allows for the determination of conversion from **2** and **3** to **1**.

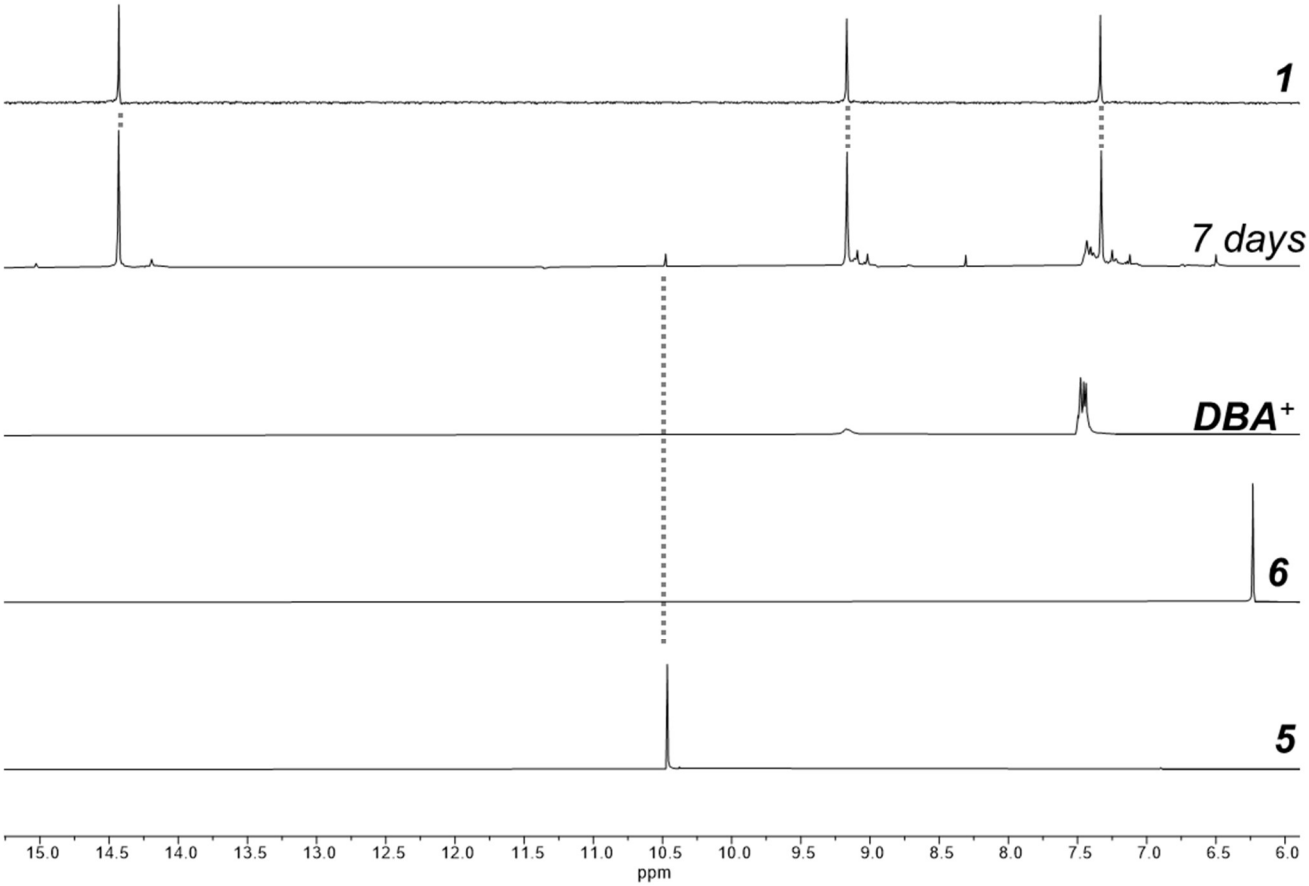


**Figure S49.** Partial stacked $^{1}$H NMR spectra (400 MHz, DMSO-$d_6$, 25 °C) showing the conversion of **5** and **6** to **1** in the presence of 10 mol% **DBA**$^{+}$.

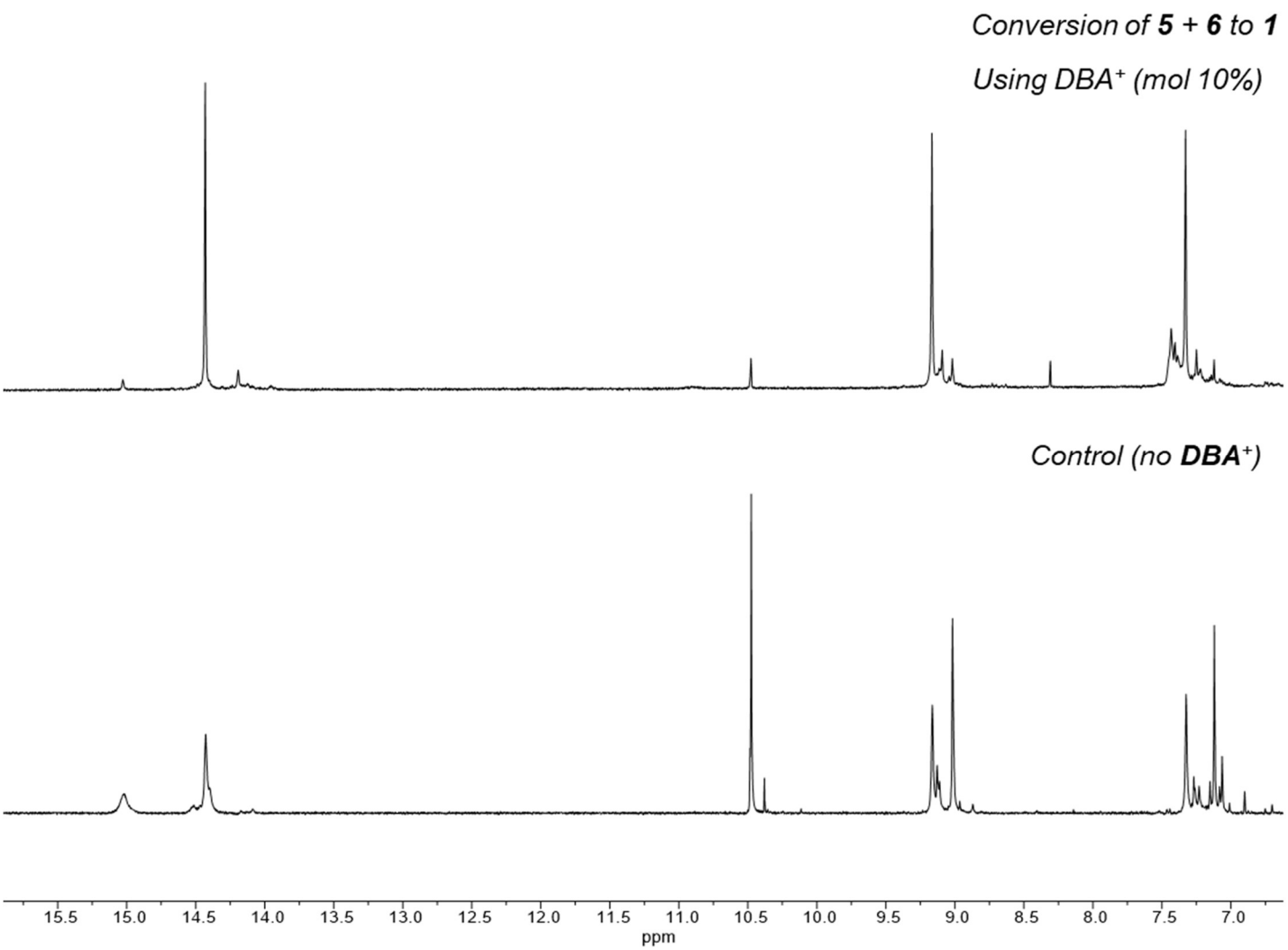


**Figure S50.** Stacked partial $^{1}$H NMR spectra (400 MHz, DMSO-$d_6$, 25 °C) showing the conversion of **5** and **6** to **1** in the presence of 10 mol% **DBA**$^{+}$ (top) and with control sample (bottom).

As highlighted in Figure S49 and Figure S50, the $^{1}$H NMR spectrum of the crude mixture for the template reaction has fewer peaks, owing to no host-guest complexes formed in DMSO-$d_6$.

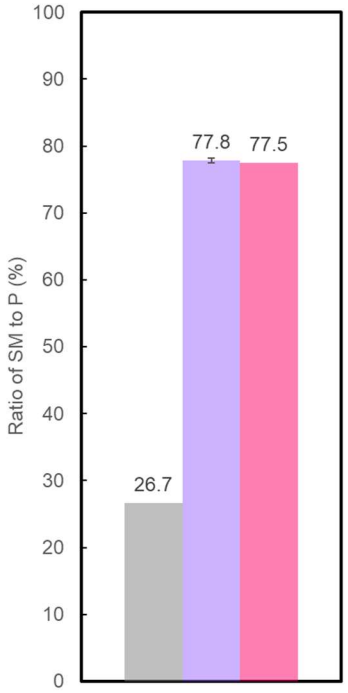


**Figure S51.** Conversion of **5** and **6** to **1** in 1:1 DCM-$d_2$/MeCN-$d_3$ after 7 days, with no additive (grey), 10 mol% (purple), and 100 mol% **DBA**$^+$ (pink).

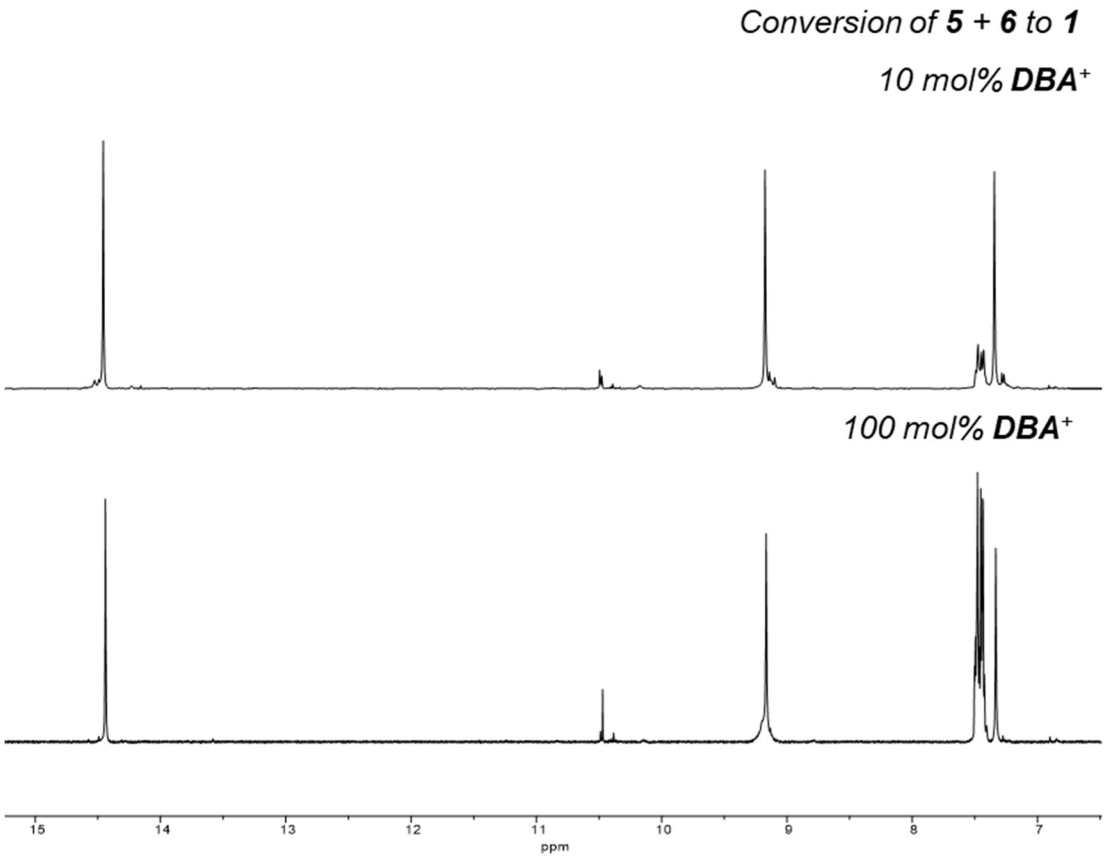


**Figure S52.** Stacked partial $^1$H NMR spectra (400 MHz, DMSO-$d_6$, 25 °C) showing the conversion of **5** + **6** to **1** in the presence of 10 mol% (top) and 100 mol% of **DBA**$^+$(bottom).

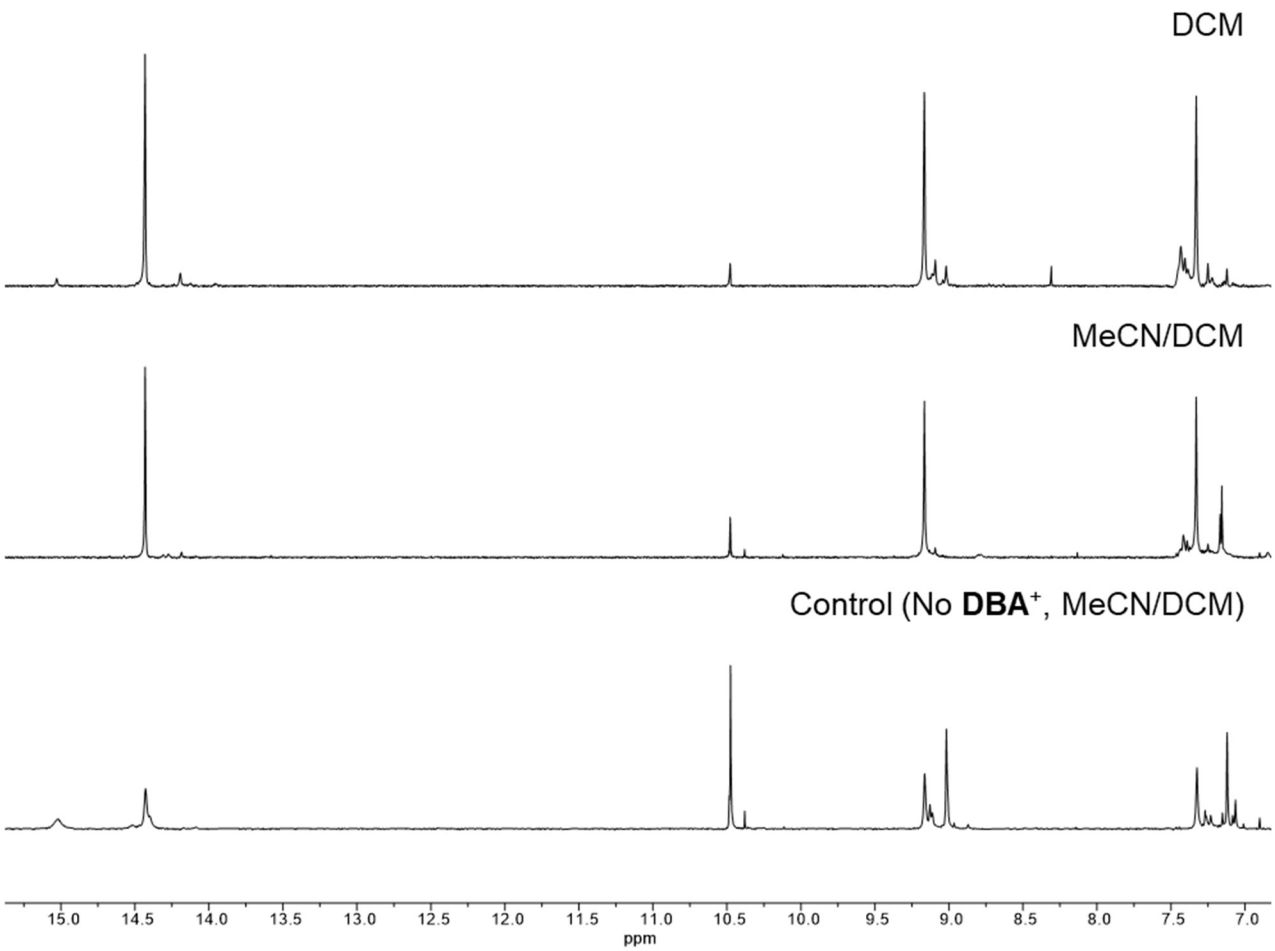


**Figure S53.** Stacked partial $^{1}$H NMR spectra (400 MHz, DMSO-$d_6$, 25 °C) showing conversion of **5** and **6** to **1** with 10 mol% **DBA**$^{+}$ in DCM-$d_2$ (top), 1:1 DCM-$d_2$/MeCN-$d_3$ (middle) after 7 days. Control in 1:1 DCM-$d_2$/MeCN-$d_3$, with no **DBA**$^{+}$ added.

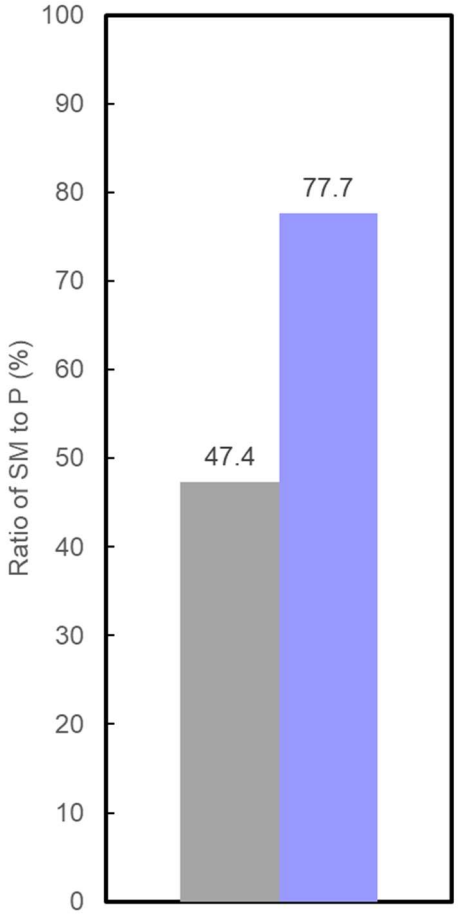


**Figure S54.** Conversion of **5** and *o*-phenylenediamine to modified macrocycle **3** in 1:1 DCM-$d_2$/MeCN-$d_3$ after 6 days, with no additive (grey), 10 mol% **DBA**$^+$ (purple).

## *Computational methods*

The Gaussian suite of program G016.revC0[10] has been used for all geometry and Hessian calculations. Geometries have been computed with M06 meta hybrid GGA xc functional[11] and in case of **$1_{Me}$.DPA** also by the old but widely used B3LYP hybrid xc-functional.[12] Basis set for all atoms were 6-31g(d),[13] 6-311g(d,p),[14] and 6-311+g(d,p).[15] All structures were checked being minima by their Hessian matrix at the same level of theory. All integral has been computed using the "Ultrafine" integration grid. Calculations has been performed in solvent (DCM and in cases of **$1_{Me}$.$DBA^+$** also in THF) using the (Self Consistent Reaction Field) SCRF approach for continuum solvent model simulation included in the Gaussian suite of programs.[16]

**$C_3$ and $C_s$ conformation of free macrocycle $1_{Me}$**

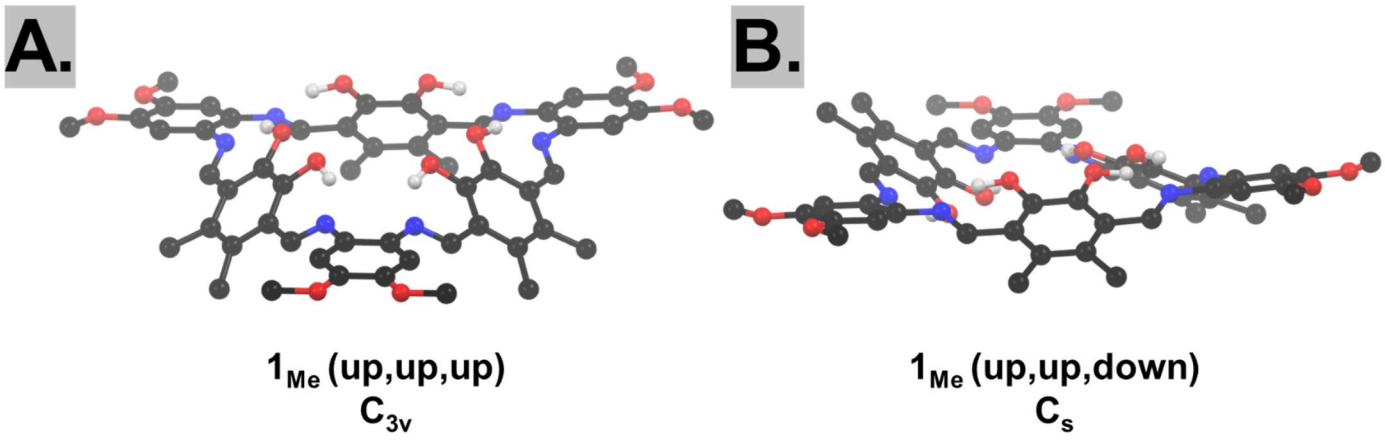


**Figure S55.** A) Cone shaped geometry ($C_{3v}$) of **$1_{Me}$** with catechol rings all pointing up. B) pseudo-planar geometry of **$1_{Me}$** with one catechol ring pointing away from the plane ($C_s$).

The free macrocycle backbone (i.e., without considering the peripheral alkyl and alkoxy substitutions) could belong to three possible point groups; $D_{3h}$ symmetry if **$1_{Me}$** is planar, or $C_{3v}$/$C_s$ if torsion between arene groups causes the macrocycle to form a cone-like geometry. Compared to the average ring plane the possible conformation can then be $C_{3v}$ (up, up, up) or $C_s$ (up, up, down).

**Relative molecular energies of several mixed tautomers of $1_{Me}$+DBA$^+$**

Relative stabilities of different tautomers found in **$1_{Me}$+DBA$^+$**. Numbering scheme is based on the image below (Figure S56 Atom assignment for 1Me.), where oxygen 1 (O1) is hydrogen bonding to the guest.

At higher levels of theory, while the values for certain tautomers change slightly, the overall trend stays the same. Interesting to note , at higher levels of theory the stability of the internal and external complexes switch, with **$1_{Me}$·DBA$^+$** being more stable based on the 6-311g(d,p)/M06/DCM level of theory, and **$1_{Me}$⊃DBA$^+$** more stable at a lower level of theory. At the highest level of theory computed (6-311+g(d)/M06) using DCM or THF as a continuum show very little different in overall molecular energy.

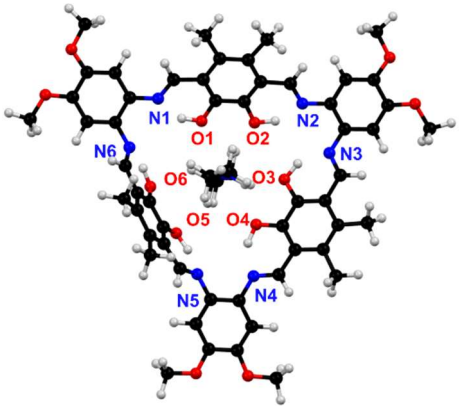


**Figure S56** Atom assignment for **$1_{Me}$**.

**Table S3.** Relative stability of different tautomers of $\mathbf{1}_{Me}$⊃**DBA**$^{+}$. Values computed employing 6-31g(d)/M06 and DCM as a continuum using the Self-Consistent Reaction Field approach

| **Computed tautomer** | ***E* (kJ/mol)** |
|---|---|
| 1,2,3,4,6-NH | 3.6 |
| 1,2,3,4-NH | 7.4 |
| 1,2,3,4,5-NH | 8.8 |
| 1,2,4-NH | 10.0 |
| 1,2-NH | 13.8 |
| 3,4-NH | 14.1 |
| Full keto | 21.3 |
| 1,2,3-NH | 21.6 |
| 2,3,4-NH | 23.1 |
| 2,3,5,6-NH | 27.0 |
| 2,4-NH | 27.0 |
| 1,3-NH | 29.6 |
| 2-NH | 32.0 |
| 5,6-NH | 33.6 |
| 1,4-NH | 35.1 |
| 3-NH | 37.2 |
| 1-NH | 37.6 |
| 2,3-NH | 37.9 |
| 4-NH | 38.6 |
| 5-NH | 46.5 |
| 6-NH | 49.0 |
| Full enol | 45.1 |

**Table S4.** Relative stability of different tautomers of $\mathbf{1}_{Me}$·**DBA**$^{+}$. Values computed employing 6-31g(d)/M06 and DCM as a continuum using the Self-Consistent Reaction Field approach.

| Computed tautomer | *E* (kJ/mol) |
|---|---|
| 1,2,3,4-NH | 0.0 |
| 1,2,4-NH | 4.1 |
| 1,2-NH | 8.7 |
| 3,4-NH | 12.2 |
| Full keto | 12.5 |
| 1,2,3,4,5-NH | 12.8 |
| 1,2,3,4,6-NH | 13.6 |
| 1,2,3-NH | 14.9 |
| 1,3-NH | 19.0 |
| 2,3,4-NH | 22.0 |
| 1,4-NH | 22.8 |
| 1-NH | 27.2 |
| 2,4-NH | 28.9 |
| 2,3,5,6-NH | 29.1 |
| 5,6-NH | 30.0 |
| 3-NH | 30.9 |
| 2-NH | 34.2 |
| 4-NH | 35.5 |
| 2,3-NH | 39.0 |
| Full enol | 41.1 |
| 6-NH | 43.4 |
| 5-NH | 44.0 |

**Table S5.** Relative stability of tautomers of $\mathbf{1}_{Me}$⊃**DBA**$^{+}$ computed at different levels of theory using DCM or THF as a continuum using the Self-Consistent Reaction Field approach.

| Computed tautomer | *E* (kJ/mol) | | |
|---|---|---|---|
| | 6-311g(d,p)/M06 (DCM) | 6-311+g(d,p)/M06 (DCM) | 6-311+g(d,p)/M06 (THF) |
| 1,2,3,4-NH | 0.0 | 0.0 | 0.0 |
| 1,2-NH | 3.0 | 1.7 | 1.4 |
| 1,2,4-NH | 4.2 | 2.3 | 2.4 |
| 1,2,3-NH | 8.0 | 6.9 | 6.9 |
| 1,2,3,4,6-NH | 12.9 | 12.7 | |
| 2,4-NH | 15.4 | 13.5 | |
| Keto | 16.3 | | |
| 1,2,3,4,5-NH | 17.6 | | |
| 2,3,4-NH | 28.9 | | |
| 1,3-NH | 31.1 | | |
| Enol | 37.8 | | |

**Table S6.** Relative stability of tautomers of **1**$_{Me}$**·DBA**$^{+}$ computed at different levels of theory using DCM or THF as a continuum using the Self-Consistent Reaction Field approach.

| **Computed tautomer** | ***E* (kJ/mol)** | | |
|---|---|---|---|
| | 6-311g(d,p)/M06 (DCM) | 6-311+g(d,p)/M06 (DCM) | 6-311+g(d,p)/M06 (THF) |
| 1,2,3,4-NH | 4.5 | 4.7 | 5.0 |
| 1,2,4-NH | 7.3 | 6.7 | 6.9 |
| 1,2-NH | 8.3 | 6.7 | 6.8 |
| 3,4-NH | 11.9 | 11.2 | 11.3 |
| 1,2,3-NH | 17.4 | 16.2 | 16.5 |
| 1,3-NH | 18.8 | 16.8 | 16.9 |
| 1,4-NH | 21.6 | 20.0 | 20.1 |
| 1-NH | 22.6 | 20.1 | |
| 1,2,3,4,5-NH | 23.2 | | |
| 1,2,3,4,6-NH | 24.1 | | |
| 2,3,4-NH | 24.3 | | |
| Keto | 26.8 | | |
| 2,4-NH | 28.1 | | |
| enol | 32.3 | | |

**Table S7.** Relative stability of tautomers of **1**$_{Me}$**⊃DPA**$^{+}$ computed at different levels of theory using DCM as a continuum using the Self-Consistent Reaction Field approach.

| **Computed tautomer** | ***E* (kJ/mol)** | | |
|---|---|---|---|
| | 6-31g(d)/M06 | 6-311g(d,p)/M06 | 6-311+g(d,p)/B3LYP |
| 1,2,3,4-NH | 0.0 | 0.0 | 0.0 |
| 1,2,4-NH | 5.7 | 6.8 | 8.6 |
| 1,2-NH | 12.3 | 7.0 | 8.3 |
| 1,2,3-NH | 19.5 | 14.2 | 15.0 |
| 1,3-NH | 22.9 | 19.9 | |
| 2,4-NH | 22.9 | 19.8 | |
| 1,4-NH | 29.7 | | |
| 2,3-NH | 37.6 | | |
| enol | 58.1 | 30.6 | |

**Table S8.** Relative stability of tautomers of **1**$_{Me}$**·DPA**$^{+}$ computed at different levels of theory using DCM as a continuum using the Self Consistent Reaction Field approach.

| Computed tautomer | *E* (kJ/mol) | | |
|---|---|---|---|
| | 6-31g(d)/M06 | 6-311g(d,p)/M06 | 6-311+g(d,p)/B3LYP |
| 1,2,4-NH | 19.8 | 20.4 | 25.2 |
| 1,2,3,4-NH | 20.0 | 24.1 | 29.2 |
| 1,2-NH | 26.9 | 24.7 | |
| 3,4-NH | 30.5 | 25.9 | |
| 1,2,3-NH | 33.4 | 34.0 | |
| 1,3-NH | 36.6 | 33.2 | |
| 2,4-NH | 41.8 | | |
| 1,4-NH | 44.3 | | |
| Enol | 44.6 | 30.6 | |
| 2,3-NH | 52.7 | | |

**Table S9.** Relative stability of tautomers of **1**$_{Me}$**⊃DXA**$^{+}$ computed with 6-311g(d,p)/M06 and using DCM as a continuum using the Self-Consistent Reaction Field approach.

| Computed tautomer | *E* (kJ/mol) |
|---|---|
| 1,2,3,4-NH | 0.0 |
| 2,4-NH | 19.3 |
| Enol | 32.5 |

**Table S10.** Relative stability of tautomers of **1**$_{Me}$**·DXA**$^{+}$ computed with 6-311g(d,p)/M06 and using DCM as a continuum using the Self-Consistent Reaction Field approach.

| Computed tautomer | *E* (kJ/mol) |
|---|---|
| 1,2,3,4-NH | 3.3 |
| 1,2-NH | 6.9 |
| 1,3-NH | 25.1 |
| enol | 37.3 |

## *References*


1 P. R. Ashton, P. J. Campbell, E. J. T. Chrystal, P. T. Glink, S. Menzer, D. Philp, N. Spencer, J. F. Stoddart, P. A. Tasker and D. J. Williams, Dialkylammonium Ion/Crown Ether Complexes: The Forerunners of a New Family of Interlocked Molecules, *Angew. Chem. Int. Ed.*, 1994, **34**, 1865–1869.

2 M. Horn, J. Ihringer, P. T. Glink and J. F. Stoddart, Kinetic versus Thermodynamic Control During the Formation of[2]Rotaxanes by a Dynamic Template-Directed Clipping Process, *Chem. Eur. J.*, 2003, **9**, 4046–4054.

3 K. E. Shopsowitz, D. Edwards, A. J. Gallant and M. J. MacLachlan, Highly substituted Schiff base macrocycles via hexasubstituted benzene: a convenient double Duff formylation of catechol derivatives, *Tetrahedron*, 2009, **65**, 8113–8119.

4 X. Wang and B. List, Asymmetric counteranion-directed catalysis for the epoxidation of enals, *Angew. Chem. Int. Ed.*, 2008, **47**, 1119–1122.

5 S. M. Hessam Mehr, H. Depmeier, K. Fukuyama, M. Maghami and M. J. MacLachlan, Formylation of phenols using formamidine acetate, *Org. Biomol. Chem.*, 2017, **15**, 581–583.

6 Z. Chen, S. Guieu, N. White, F. Lelj and M. J. MacLachlan, The Rich Tautomeric Behavior of Campestarenes, *Chem. Eur. J.*, 2016, **22**, 17657–17672.

7 J. H. Chong, M. Sauer, B. O. Patrick and M. J. MacLachlan, Highly Stable Keto-Enamine Salicylideneanilines, *Org. Lett.*, 2003, **5**, 3823–3826.

8 A. J. Gallant and M. J. MacLachlan, Ion-Induced Tubular Assembly of Conjugated Schiff□Base Macrocycles, *Angew. Chem. Int. Ed.*, 2003, **42**, 5307–5310.

9 P. Thordarson, Determining association constants from titration experiments in supramolecular chemistry, *Chem. Soc. Rev.*, 2011, **40**, 1205–1323.

10 M. J. Frisch, G. W. Trucks, H. B. Schlegel, G. E. Scuseria, M. A. Robb, J. R. Cheeseman, G. Scalmani, V. Barone, G. A. Petersson, H. Nakatsuji, X. Li, M. Caricato, A. V. Marenich, J. Bloino, B. G. Janesko, R. Gomperts, B. Mennucci, H. P. Hratchian, J. V. Ortiz, A. F. Izmaylov, J. L. Sonnenberg, D. Williams-Young, F. Ding, F. Lipparini, F. Egidi, J. Goings, B. Peng, A. Petrone, T. Henderson, D. Ranasinghe, V. G. Zakrzewski, J. Gao, N. Rega, G. Zheng, W. Liang, M. Hada, M. Ehara, K. Toyota, R. Fukuda, J. Hasegawa, M. Ishida, T. Nakajima, Y. Honda, O. Kitao, H. Nakai, T. Vreven, K. Throssell, J. A. Montgomery Jr., J. E. Peralta, F. Ogliaro, M. J. Bearpark, J. J. Heyd, E. N. Brothers, K. N. Kudin, V. N. Staroverov, T. A. Keith, R. Kobayashi, J. Normand, K. Raghavachari, A. P. Rendell, J. C. Burant, S. S. Iyengar, M. C. J. Tomasi, J. M. Millam, M. Klene, C. Adamo, R. Cammi, J. W. Ochterski, R. L. Martin, K. Morokuma, O. Farkas, J. B. Foresman and D. J. Fox, *Gaussian 16*, Revision B.01, Gaussian, Inc., Wallingford, CT , 2016.

11 Y. Zhao and D. G. Truhlar, The M06 suite of density functionals for main group thermochemistry, thermochemical kinetics, noncovalent interactions, excited states, and transition elements: two new functionals and systematic testing of four M06-class functionals and 12 other function, *Theor. Chem. Acc.*, 2008, **120**, 215–41.

12 A. D. Becke, A new mixing of Hartree-Fock and local density-functional theories, *J. Chem. Phys.*, 1993, **98**, 1372–1377.

13 M. M. Francl, W. J. Pietro, W. J. Hehre, J. S. Binkley, D. J. DeFrees, J. A. Pople and M. S.

Gordon, Self-Consistent Molecular Orbital Methods. 2 3. A polarization-type basis set for 2nd-row elements, *J. Chem. Phys.*, 1982, **77**, 3654–3655.

14 K. Raghavachari, J. S. Binkley, R. Seeger and J. A. Pople, Self-Consistent Molecular Orbital Methods. 20. Basis set for correlated wave-functions, *J. Chem. Phys.*, 1980, **72**, 650–654.

15 M. J. Frisch, J. A. Pople and J. S. Binkley, Self-Consistent Molecular Orbital Methods. 25. Supplementary Functions for Gaussian Basis Sets, *J. Chem. Phys.*, 1984, **80**, 3265–69.

16 G. Scalmani and M. J. Frisch, Continuous surface charge polarizable continuum models of solvation. I. General formalism, *J. Chem. Phys.*, 2010, **132**, 114110.